3 Benzamidines and their Rhenium and Technetium Complexes

In 1982, Beyer et al. explored a new substance class, N-[(dialkylamino)(thiocarbonyl)] benzimidoyl chlorides (R^1R^2bzm-Cl), which were synthesized by the decomposition of the corresponding nickel benzoylthioureato complexes with $SOCl_2$ [54]. Two years later, the same authors reported about reactions of R^1R^2bzm-Cl with ammonia, some of primary amines and the formation of dialkylaminothiocarbonylbenzamidines (HL^0, Scheme 3.1) [55] and the first metal complexes of HL^0 [56]. This opened the door for transition metal complexes with chelators containing a thiourea building block, which have been extensively studied in the following decades. Up to now, numerous ligands (HL^0) have been synthesized, and their coordination chemistry with such transition metal ions as Ni^{2+} [57], Pd^{2+} [58], Pt^{2+} [59], Co^{3+} [60], Cu^{2+} [61], Ag^+ [62] and Au^+ [63] has been extensively explored. With technetium and rhenium, HL^0 act as versatile ligands and stabilize various cores such as $[M{=}O]^{3+}$ [64], $[M{\equiv}N]^{2+}$ [65], and $[M(CO)_3]^+$ (M = Re, Tc) [66]. In most of the structurally characterized complexes, they bind as mononegative, 'N,S' bidentate ligands. More rarely, HL^0 coordinate monodentate via the S donor site of thiourea, as can be found in some Ag^+ and Au^+ complexes, and as bridging ligand in a technetium tricarbonyl complex [66b].

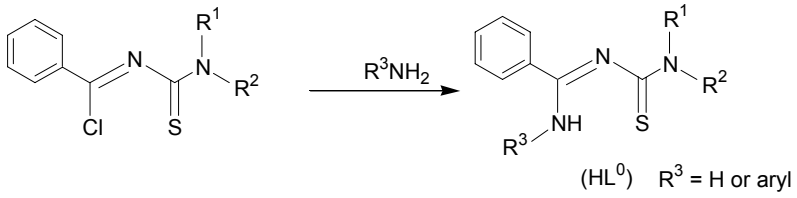

Scheme 3.1 The synthesis of bidentate dialkylaminothiocarbonylbenzamidines.

In principle, the general synthetic procedure of the ligand class HL^0, in which benzimidoyl chlorides react with ammonia or primary aromatic amines shown in Scheme 3.1, should also be well suitable for reactions with other functionalized primary amines. This finally gives access to multidentate benzamidine chelating systems. However, hitherto, only the reactions with a small number of amino acid esters [67], diamines [14], and tris(aminoethyl)amine [62] have been reported. Furthermore, no metal complexes of the potentially tridentate ligands have been isolated and structurally characterized. Only two structural reports of Cu(II) and Ni(II) complexes with tetradentate benzamidinates exist [14].

In the following part of this thesis, new multidentate benzamidine systems and their rhenium and technetium complexes are discussed. Potential applications of these compounds in anti cancer drugs and radiopharmaceuticals are also included.

3.1 Tridentate Benzamidines and their Rhenium and Technetium Complexes

3.1.1 Tridentate N-(N'',N''-Dialkylaminothiocarbonyl)-N'-substituted Benzamidines

3.1.1.1 Reactions of Benzimidoyl Chlorides with Functionalized Primary Amines

Despite the fact that there are several ways to access to multidentate ligand systems containing thiourea building blocks [68], the synthesis via the reaction of N-[N',N'-dialkylamino(thiocarbonyl)]benzimidoyl chlorides with primary amines is the most convenient approach. The coordination behavior of the obtained ligands much depends on the amines used, since the reaction on each amino group results in increasing of the denticity of the ligand by one S donor site in a six-membered chelate ring based on the benzimidine skeleton. Thus, tridentate N-[(N'',N''-dialkylamino)(thiocarbonyl)]-N'-substituted benzamidine ligands can be synthesized from reactions of appropriate R^1R^2bzm-Cl and functionalized primary amines such as 2-aminophenol(H_2L^1), 2-aminomethylpyridine (HL^2) and 2-aminobenzoic acid (H_2L^3).

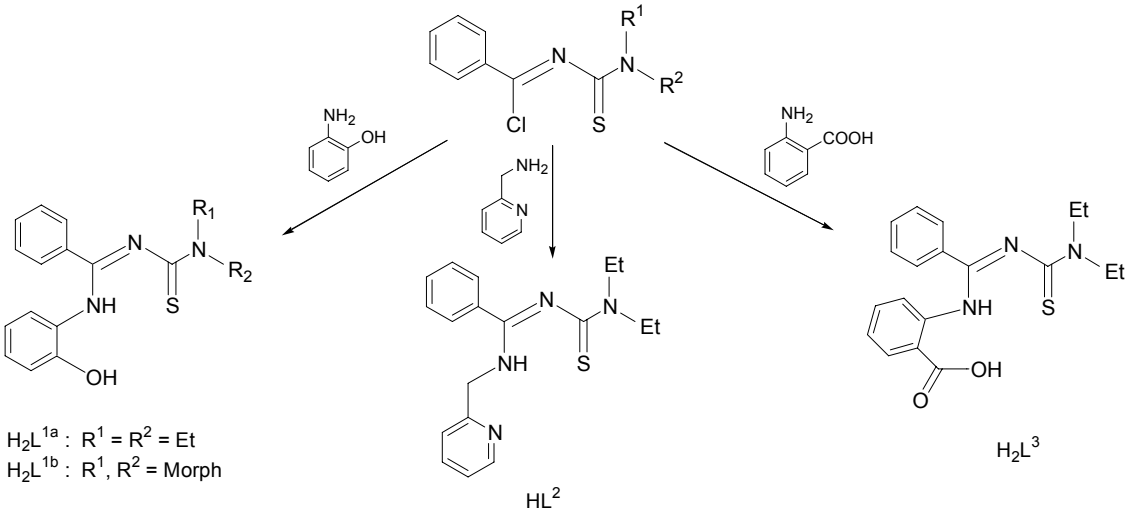

Scheme 3.2 Reactions of R^1R^2bzm-Cl and functionalized primary amines.

The reactions are done in dry acetone in order to prevent R^1R^2bzm-Cl from hydrolysis and the formation of HR^1R^2btu impurities and performed at room temperature in the case of the preparation of H_2L^1 and HL^2 or in warm acetone (40°C) in the case of the synthesis of H_2L^3. Under refluxing conditions, the cyclization and/or oxidative cyclization of the ligands followed by desulfurization/ring transformation to imidazoles happen, what leads to dramatical decrease of the yields [69]. In the presence of the supporting base NEt_3, the formation the desired products proceeds quickly. The progress of the reactions can readily be

checked by thin-layer chromatography on alumina and is indicated by the formation of a colorless precipitate of $NEt_3 \cdot HCl$, which is almost insoluble in acetone. The ligands were obtained as crystalline solids in high yields.

The ligands H_2L^1 and HL^2 are good soluble in methanol and acetone. Their ^1H NMR spectra are characterized by two sets of well separated signals corresponding to their alkyl residues, which is due to the hindered rotation around the C–NEt_2 or C-$N(CH_2)_2O$ bonds. This finding has also been observed with their parent N,N-dialkylbenzoylthioureas [16]. However, the C–NR^1R^2 bonds of N,N-dialkylbenzoylthioureas seem to be more flexible as indicated by broad signals in their ^1H NMR spectra.

The anthranilic acid derivative H_2L^3 is separated as a yellow oil upon concentration of the reaction mixture. This compound, which is analytically pure H_2L^3 according to IR and NMR spectra, can be crystallized from a concentrated MeOH solution stored in a deep freezer. Slightly yellow crystals of the methanol solvate $H_2L^3 \cdot MeOH$ deposit over a period of several days.

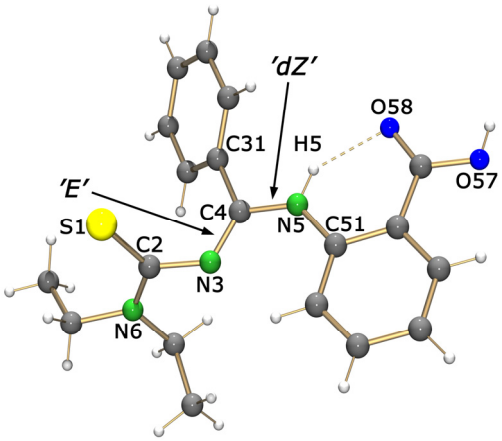

Figure 3.1 Molecular structure of H_2L^3.

Table 3.1 Selected bond lengths and angles in H_2L^3

Bond lengths (Å)					
S1–C2	1.678(3)	N3–C4	1.290(4)	N5–C51	1.402(4)
C2–N6	1.330(4)	C4–C31	1.493(5)	C57–O57	1.305(4)
C2–N3	1.383(4)	C4–N5	1.363(4)	C57–O58	1.220(4)

Hydrogen bond				
D-H…A	d(D-H)	d(H…A)	d(D…A)	<(DHA)
N5-H5…O58	0.86	1.93	2.655(3)	140.8
O(57)-H(57)...O(62)	0.82	1.78	2.568(4)	160.7
O(62)-H(62)...S(1)^{i}#1	0.82	2.66	3.190(3)	124.1

(i) Symmetry transformations used to generate equivalent atoms: #1 -x,-y+2,-z

Figure 3.1 illustrates the molecular structure of H_2L^3 together with the intramolecular hydrogen bond. Additional hydrogen bonds are established between S1 and O57 and co-crystallized solvate MeOH. Selected bond lengths and angles are summarized in Table 3.1. While the C4-N3 bond of 1.290 Å is within the expected range of C=N double bonds, the C4-N5 bond of 1.363 Å has only partial double bond character. This is found in all similar ligands and suggests that the hydrogen atom is mainly located at the N5 atom. The configuration of the H_2L^3 molecule is best described as *E*, *dZ*, which has also been found in some related ligands [59a,70]. The *E*, *dZ* configuration is obtained due to the intramolecular hydrogen bond between N5 and O57, which is more stable than a potential hydrogen bonding between N5 and S1.

3.1.1.2 Reactons of Benzimidoyl Chlorides with Hydrazine Derivatives

Similar to the primary amines, hydrazine derivatives such as 4,4-dialkylthiosemi carbazides or benzoylhydrazine easily react with R^1R^2bzm-Cl compounds in dry acetone under formation of novel tridenate benzamidine ligands H_2L^4 and H_2L^5 in high yields (Scheme 3.3). All the products were isolated as colorless, analytically pure, microcrystalline solids directly from the reaction mixtures.

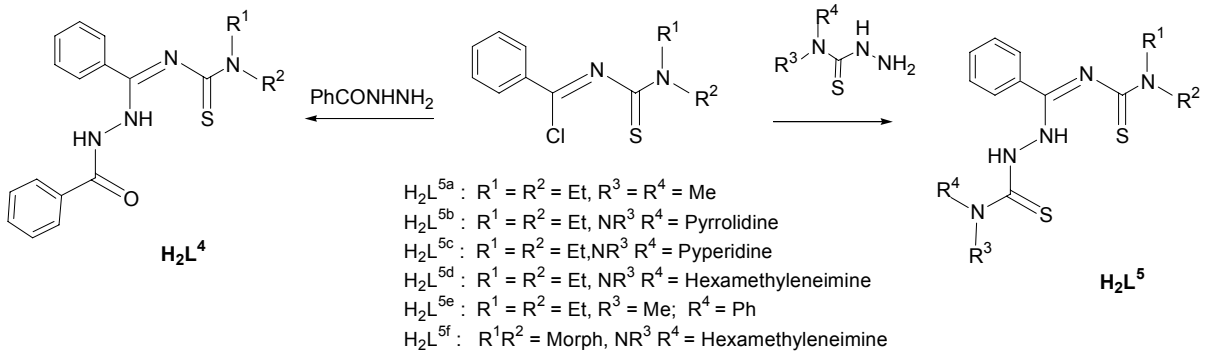

Scheme 3.3 Reactions of R^1R^2bzm-Cl with hydrazine derivatives.

The IR spectrum of H_2L^4 reveals two broad absorptions at 3225 cm^{-1} and 3163 cm^{-1} corresponding to NH stretches and a very strong absorption at 1655 cm^{-1} which can be assigned to the C=O vibration. In the IR spectrum of H_2L^5, NH stretches appear in the 3180 cm^{-1} region and C=N stretches appear as very strong and sharp absorptions at the range between 1625 and 1635 cm^{-1}

The ^1H NMR spectra of H_2L^5 ligands show two sets of well resolved signals corresponding to their ethyl residues, which are due to the hindered rotation around the C–NEt_2 bonds of the

thiourea moiety previously observed for H_2L^{1a} and HL^2. The corresponding signals in the ^1H NMR spectrum of H_2L^4 are less resolved and appear as four singlets. Interestingly, the rotation around the C–NR^1R^2 bonds of thiosemicarbazide sides in H_2L^5 is not restricted as is indicated by the appearance of magnetically equivalent resonances. While the signals of the two NH protons in the ^1H NMR spectra of H_2L^5 appear in a very broad singlet in the region between 9.5 and 10.1 ppm, those in the ^1H NMR spectrum of H_2L^4 is characterized by two broad singlet signals of NH protons at 8.63 and 10.17 ppm.

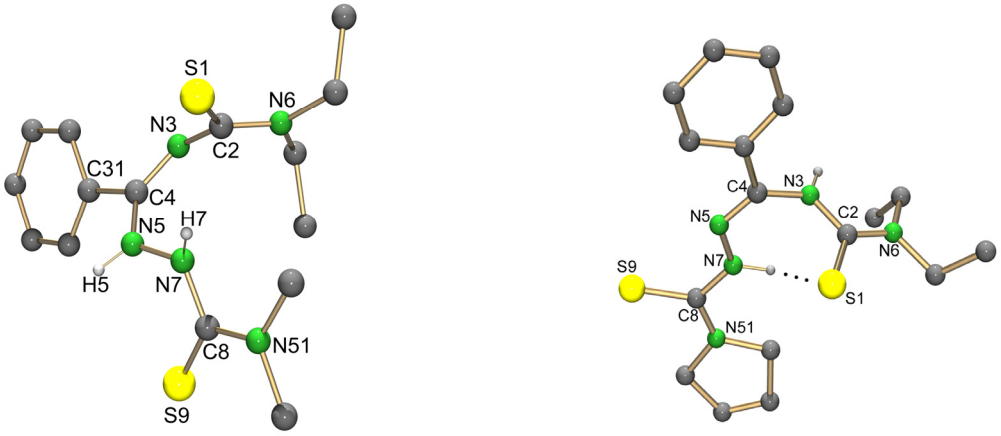

(a) **(b)**

Figure 3.2 Molecular structures of H_2L^{5a} (**a**) and H_2L^{5b} (**b**). Hydrogen atoms bonded to carbons were omitted for clarity.

Table 3.2 Selected bond lengths and angles in H_2L^5

Bond lengths (Å):	$\mathbf{H_2L^{5a}}$	$\mathbf{H_2L^{5b\,(i)}}$		$\mathbf{H_2L^{5a}}$	$\mathbf{H_2L^{5b}}$
S1–C2	1.701(2)	1.692(4) / 1.685(3)	C4–N5	1.348(2)	1.285(4) / 1.281(4)
C2–N6	1.332(2)	1.337(4) / 1.346(4)	N5–N7	1.380(2)	1.374(4) / 1.365(3)
C2–N3	1.367(2)	1.372(4) / 1.372(4)	N7–C8	1.372(2)	1.361(4) / 1.357(4)
N3–C4	1.285(2)	1.417(4) / 1.429(4)	C8–S9	1.669(2)	1.680(3) / 1.683(3)

Hydrogen bonds for $\mathbf{H_2L^{5a}}$

D-H…A	d(D-H)	d(H…A)	d(D…A)	<(DHA)
N7–H7…S1	0.83(2)	2.55(2)	3.1690(15)	132.5(19)
N5–H5…S1$^{(ii)}$#1	0.86(2)	2.69(2)	3.4976(17)	156.8(16)

Hydrogen bonds for $\mathbf{H_2L^{5b\,(i)}}$

N7–H7…S1	0.86 / 0.86	2.88 / 3.05	3.238(3) / 3.389(3)	107.1 / 106.2
N3–H3…S9$^{(ii)}$#2	0.86 / 0.86	2.59 / 2.70	3.378(3) / 3.433(3)	152.1 / 144.6

(i) Values for two crystallographically independent molecules
(ii) Symmetry transformations used to generate equivalent atoms: #1 (-x+1,-y+2,-z) ; #2 (x,y-1,z) / (x,y+1,z)

H_2L^5 were additionally studied by X-ray analysis. Representations of the molecular structures of H_2L^{5a} and H_2L^{5b}, respectively, are given in Figure 3.2. In the structure of H_2L^{5a},

the protonation of the nitrogen atoms N5 and N7 is experimentally justified by the detection of the corresponding hydrogen atoms and the fact that they are involved in hydrogen bonds. Thus, the bonding situation in the solid state of the compound recommends the treatment of H_2L^{5a} as a 'thiosemicarbazide' rather than as as a 'thiosemicarbazone', as is indicated by the mesomeric formula **A** in Chart 3.1. This is also supported by the bond length situation inside the C,N skeleton of the ligand with a C4-N5 bond lengths of 1.348(2) Å, which can be regarded as an (only slightly shortened) single bond. In contrast, a bonding feature of thiosemicarbazone was found for H_2L^{5b} which exhibits a double bond established between C4–N5 with the distance of 1.285(4) /1.281(4) Å together a typical single bond N3–C4 (1.417(4) / 1.429(4) Å). This is consistent with the finding of hydrogen atoms on N3 and N7 from peaks of electron density in the final Fourier map and they are also suitable to make hydrogen bonds. It is interesting to note that both structures reveal the same molecular arrangement, that means a configuration, which allows an intramolecular hydrogen bond between the atoms N7 and S1. The remaining acidic proton can then be located either on N3 or N5, which most probably is controlled by the possibility of the formation of intermolecular hydrogen bonds. Thus, H_2L should finally be treated as between 'thiosemicarbazide' and 'thiosemicarbazone', and the solid state structures of the compounds do not represent a suitable tool to predict the situation in metal complexes of the compounds.

Nevertheless, in solution and in metal complexes of H_2L^4 and H_2L^5 the other mesomeric forms should also be considered, particularly when chelate formation establishes an extended system of delocalized π-electron density.

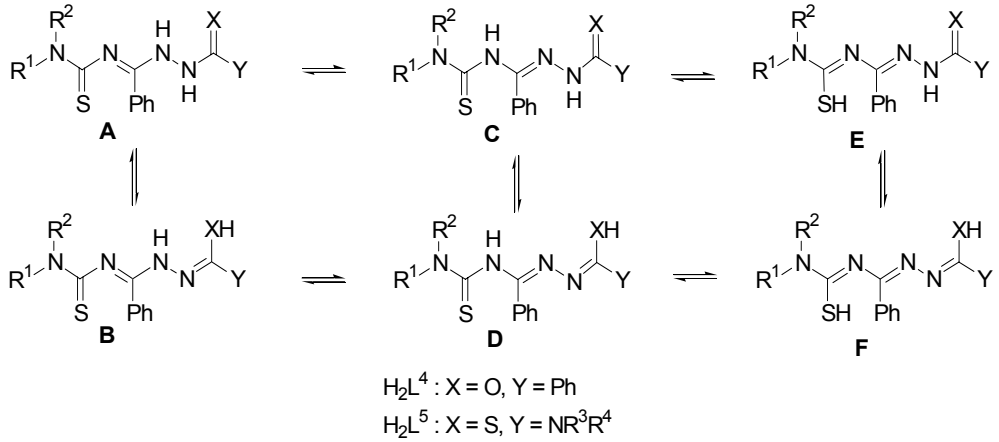

Chart 3.1 Possible conformations of H_2L^4 and H_2L^5.

3.1.2 Re and Tc Complexes with N'-(2-Hydroxyphenyl)benzamidine (H_2L^1)

3.1.2.1 Re^VO and Tc^VO Complexes with H_2L^1

Reactions of H_2L^1 with the common rhenium(V) and technetium(V) precursors $(NBu_4)[MOCl_4]$ in methanol at room temperature yield without addition of supporting base red solids of the composition $[ReOCl(L^1)]$ (**14**) and $[TcOCl(L^1)]$ (**15**) in excellent yields. Corresponding reactions with a rhenium phosphine containing precursor like $[ReOCl_3(PPh_3)_2]$ also give the products **14** , but with significantly lower yields. This is mainly due to the formation of side-products with remaining PPh_3 ligands, which cause difficulties during the isolation of the products. The complexes **14** and **15** are well soluble in solvents such as $CHCl_3$ or CH_2Cl_2, sparingly soluble in alcohols and acetone and almost insoluble in pentane or hexane.

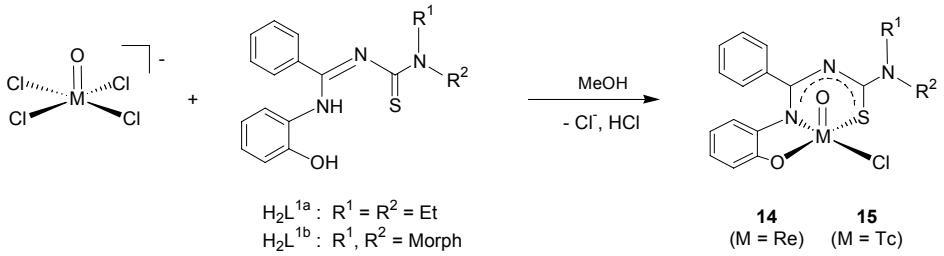

Scheme 3.4 Reactions of H_2L^1 with $(NBu_4)[MOCl_4]$.

Infrared spectra of the complexes **14** and **15** exhibit a strong bathochromical shift of the $\nu_{C=N}$ stretches from the range between 1610 and 1620 cm^{-1} of the non-coordinated benzamidines bands to the 1525 cm^{-1} region. This indicates chelate formation with a large degree of π-electron delocalization within the chelate rings. The absence of absorptions in the regions around 3350 cm^{-1} and 3150 cm^{-1}, which correspond to ν_{NH} and ν_{OH}, respectively, in the uncoordinated H_2L^1, indicates the expected double deprotonation of the ligands during complex formation. The absorptions of the Re=O vibrations in **14** appear between 991 and 995 cm^{-1}, while the intense absorptions at 972 cm^{-1} are assigned for Tc=O stretches in **15** [37].

The NMR spectra of the complexes **14** and **15** are very similar. Two expected triplet signals of the methyl groups are observed in the ^1H NMR spectrum of **14a**. Furthermore, the ^1H NMR spectrum reflects the rigid structure of the tertiary amine nitrogen atom. The appearance of four proton signals of the methylene groups shows that they are magnetically not equivalent with respect to their axial and equatorial positions. This leads to complex coupling patterns in the proton spectra of these compounds. The ^{13}C NMR spectra of complexes **14** exhibit a pattern similar to the spectra of the non-coordinated ligands, in which each couple of signals for the CH_2

and CH_3 groups appears. Deprotonation of the aromatic C_{ar}-NH and C_{ar}-OH groups during the complex formation of the H_2L^1 ligands results in a strong shift of their respective ^{13}C NMR chemical shifts of 145 ppm and 165 ppm, respectively. Mass spectra of **14** do not show the molecular peak, but the most intense peaks belong to the $[M - Cl^- + MeOH]^+$ fragment. This reflects the lability of the chloro ligands of these compounds.

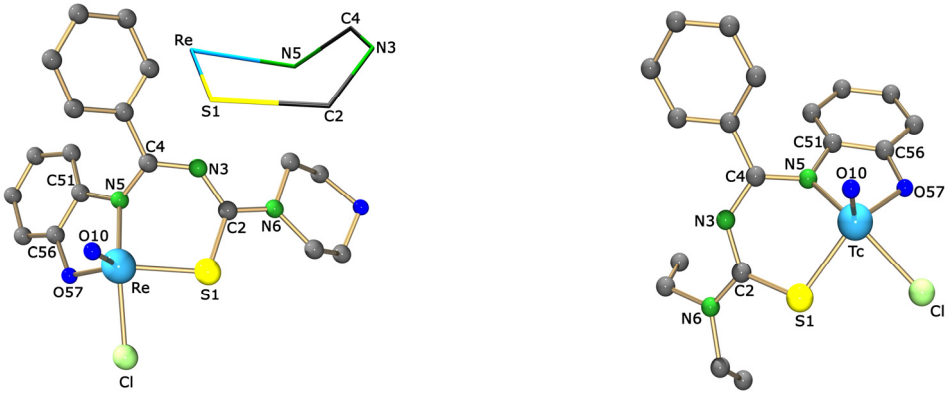

Figure 3.3 Molecular structure of [ReOCl(L^{1b})] (**14b**) (left) and [TcOCl(L^{1a})] (**15a**) (right). Hydrogen atoms were omitted for clarity.

Table 3.3 Selected bond lengths and angles in ReOCl(L^{1b})] **14b** and [TcOCl(L^{1a})] **15a**

	14b	**15a**		**14b**	**15a**
Bond lengths (Å)					
M–O10	1.665(7)	1.642(6)	M–O57	1.957(6)	1.994(4)
M–Cl	2.344(2)	2.351(2)	S1–C2	1.786(9)	1.758(8)
M–S1	2.289(2)	2.296(2)	C4–N5	1.37(1)	1.386(8)
M–N5	1.999(7)	1.991(5)	C2–N6	1.33(1)	1.321(9)
Angles (°)					
O10–M–Cl	104.4(3)	106.1(2)	O10–M–N5	106.1(3)	104.8(2)
O10–M–S1	108.6(3)	111.2(2)	O10–M–O57	114.8(3)	114.0(2)

Figure 3.3 depicts the molecular structure of compound **14b** and **15a** as prototype compounds for this type of complexes. Selected bond lengths and angles are compared in Table 3.3 The metal atoms exhibit a distorted square-pyramidal environment with the oxo ligand in the apical position. The square plane defined by the donor atoms of the tridentate ligand and the chloro ligand is slightly distorted, with a main deviation of about 0.124 Å from a mean least-square plane for atom O57. The metal atoms are situated by 0.671(3) Å for **14b** and 0.691(2) Å for **15a** above this plane towards the oxo ligands. All O10–M–X angles (X = equatorial donor atom) fall in the range between 104 and 114°. This is in agreement with the typical bonding situation in $Re^{V}O$ and $Tc^{V}O$ complexes with square-pyramidal geometry [71]. The Re-O10 distance of 1.665(7) Å and the Tc-O10 distance of 1.642(6) Å are within the

expected ranges of rhenium–oxygen and technetium–oxygen double bonds [33]. Despite the fact that the six-membered chelate ring is not planar (see also the wire-frame model of the chelate ring for **14b** in Figure 3.3), a considerable delocalization of π-electron density is indicated by the observed bond lengths. The C–S and C–N bonds inside the chelate ring fall within the range between carbon–sulphur and carbon–nitrogen single and double bonds. This bond length equalization is even extended to the C2-N6 bond of about 1.330 Å, which is significantly shorter than expected for a single bond. The partial transfer of electron density into this bond strongly agrees with the ^{1}H NMR spectrum of the compounds, which indicates a rigid arrangement of the morpholine ring in the complex.

When the reaction of H_2L^1 with $(NBu_4)[ReOCl_4]$ or $[ReOCl_3(PPh_3)_2]$ is undertaken in MeOH under reflux and in the presence of a supporting base like Et_3N, red solids of the composition $[ReO(OMe)(L^1)]$ (**16**) are isolated in excellent yields. The same products are formed by the addition of Et_3N to the refluxing CH_2Cl_2 – MeOH solution of **14**. This has exemplarily been demonstrated with H_2L^{1a} and the corresponding rhenium complex **14a**. The formation of **16a** reveals that the chloro ligand in the coordination sphere of compound **14a** is reasonably labile and can easily be solvolized under basic condition (Scheme 3.5).

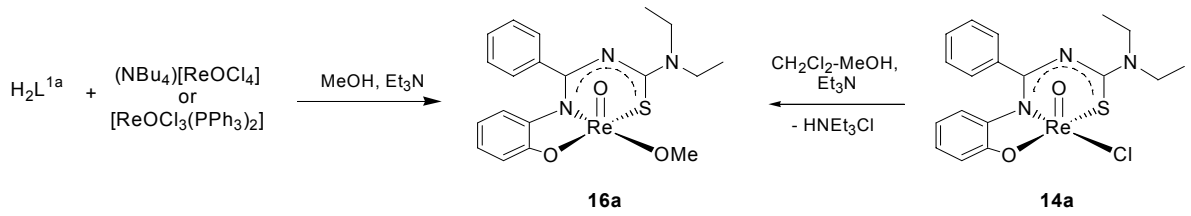

Scheme 3.5 Formation of $[ReO(OMe)(L^{1a})]$ (**16a**).

The IR spectrum of **16a** has a pattern similar to that of **14a** except of slightly hypsochromic shifts of absorptions corresponding to the C=N and Re=O vibrations by about 8 cm^{-1} and 4 cm^{-1} with respect to those in **14a**. The ^{1}H NMR spectrum of **16a** reveals an additional signal of coordinated $\{MeO\}^-$ at 3.32 ppm. Other chemical shifts in the ^{1}H NMR spectrum of **16a** appear at almost the same positions as those in **14a** but are less resolved.

The molecular structure of **16a** was studied by X-ray diffraction and is shown in Figure 3.4**.** The coordination sphere of the rhenium atom is similar to that discussed for **14a** except that a methoxo ligand occupies the position of the chloro ligand. The rhenium atom is placed by 0.678(2) Å above the equatorial plane, which is defined by the donor atoms of $\{L^{1a}\}^{2-}$ and $\{MeO\}^-$ ligands, towards the oxo ligand. This means that the methoxo ligand is cis to the oxo ligand which is an uncommon feature for oxo/alkoxo rhenium complexes. In most of the hitherto structurally studied oxo/alkoxo complexes of rhenium, *trans* coordination is

established and stabilized by the transfer of electron density from the Re=O double bond to the Re-OR bond. This results in a significant shortening of the latter bond. The Re-O20 bond distance of 2.000(6) Å in **16a** is much longer than the Re-OR bond of 1.795(7) in the *trans* alkoxo complex **3c**. The Re-O10 bond length of 1.682 Å is in the expected range for rhenium-oxygen double bonds. Other selected bond lengths are presented in Table 3.4.

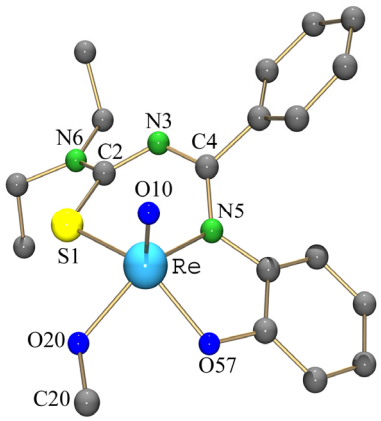

Figure 3.4 Molecular structure of [ReO(OMe)(L^{1a})] (**16a**). Hydrogen atoms were omitted for clarity.

Table 3.4 Selected bond lengths and angles in [ReO(OMe)(L^{1a})] (**16a**)

Bond lengths (Å)					
Re-O10	1.693(5)	Re-O57	1.967(5)	C2-N6	1.321(8)
Re-S1	2.291(1)	Re-O20	2.000(6)	C4-N5	1.360(8)
Re-N5	2.017(6)	S1-C2	1.750(7)	C20-O20	1.24(1)
Angles (°)					
O10-Re-O20	107.4(3)	O10-Re-N5	107.6(3)	N5-Re-O20	144.7(2)
O10-Re-O57	113.1(2)	O10-Re-S1	108.5(2)	S1-Re-O57	138.3(2)

The addition of a base such as Et_3N to the solution of **14a** in CH_2Cl_2 results in a color change from bright red to dark red. The dimer of the composition [{ReO(L^{1a})}$_2$O] (**17a**) was isolated from this solution. The compound **17a** is most probably formed via the hydroxo complex, which has not been isolated but should be the product of a hydrolysis of **14a** or **16a**.

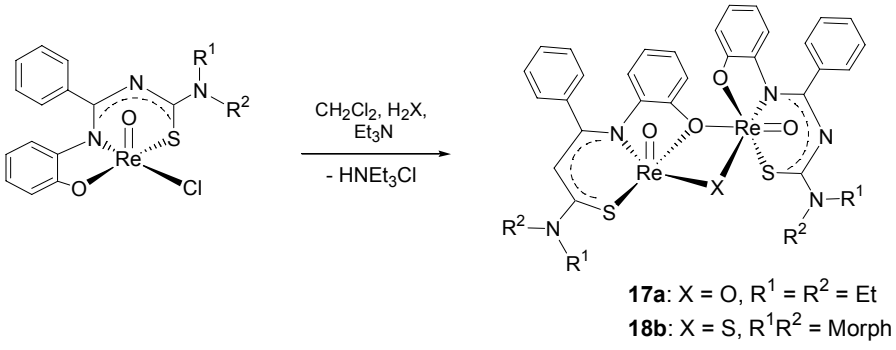

Scheme 3.6 Formation of [{ReO(L^{1a})}$_2$O] (**17a**) and [{ReO(L^{1b})}$_2$S] (**18b**).

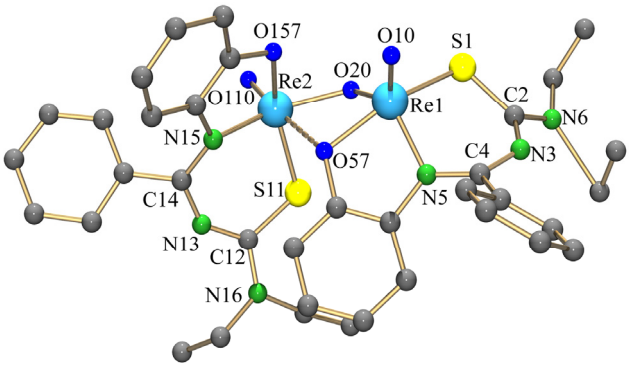

Figure 3.5 Molecular structure of [{ReO(L^{1a})}$_2$O] (**17a**). Hydrogen atoms were omitted for clarity.

Table 3.5 Selected bond lengths and angles in [{ReO(L^{1a})}$_2$O] (**17a**)

Bond lengths (Å)			
Re1-O10 / Re2-O110	1.676(1) / 1.66(1)	Re1-O20 / Re2-O20	1.87(1) / 1.991(9)
Re1-S1 / Re2-S11	2.316(4) / 2.30(5)	S1-C2 / S11-C12	1.75(1) / 1.73(1)
Re1-N5 / Re2-N15	1.98(1) / 1.99(1)	C2-N6 / C12-N16	1.32(1) / 1.32(1)
Re1-O57 / Re2-O157	2.032(9) / 1.97(1)	C4-N5 / C14-N15	1.38(1) / 1.34(1)
Re2-O57	2.52(1)		
Angles (°)			
O10-Re1-O20 / O110-Re2-O20	123.6(6) / 108.1(5)	O110-Re2-O57	173.3(4)
O10-Re1-O57 / O110-Re2-O157	103.1(5) / 103.8(5)	Re1-O20-Re2	118.2(5)
O10-Re1-N5 / O110-Re2-N15	111.6(6) / 105.9(5)	Re1-O57-Re2	92.9(4)
O10-Re1-S1 / O110-Re2-S11	101.0(4) / 101.8(5)		

Figure 3.5 depicts the molecular structure of the dimeric complex **17a**. Each oxorhenium core is meridionally coordinated by a tridentate $\{L^{1a}\}^{2-}$ ligand as was discussed for **14a** and connected to the other by an oxygen bridge in the remaining position of the equatorial plane. Their equatorial coordination planes are almost perpendicular to each other and the Re1-O20-Re2 angle of 118.2(5) ° strongly deviates from the angle for ideal linear oxygen-bridged dimers. Such a situation goes along with a lower double bond character in the bent oxo bridge compared to a linear one, which is also reflected by the Re1-O20-Re2 bond lengths. The rhenium atom Re1 is coordinated in a way that its phenolato oxygen (O57) is directed to the vacant coordination position *trans* to the oxo ligand of the rhenium atom Re2 and acts as the second bridging oxygen atom. However, the distance between Re2 and O57 of 2.522(11) Å is very long and reflects only a weak interaction. Thus, in this bonding situation, the Re1 atom has a square-pyramidal environment and Re2 reveals an octahedral arrangement. Consequently, the Re1 atom is placed 0.646(7) Å above the equatorial plane

towards the oxo ligand, while this distance for Re2 is only 0.547(7) Å. The bond distance Re1-O20 of 1.875(11) Å is shorter by 0.112 Å than the distance Re2-O20. Other selected bond lengths are presented in Table 3.5.

The IR spectrum of **17a** shows a bathochromic shift of 20 cm^{-1} for the C=N band compared to that in **14a.** The absorption of Re=O stretch in **17a** appears as a strong band at 975 cm^{-1} and can, thus, readily be distinguished from that in linear dimeric {O=Re-O-Re=O} complexes which is normally absent or appears as a weak band in the region between 900 cm^{-1} and 1000 cm^{-1}.

In addition to compound **17a**, some crystals of [{ReO(L^{1b})}$_2$S] (**18b**), which has an analogous structure to **17a** but with a bridging sulfur atom, were isolated from the reaction of (NBu_4)[$ReOCl_4$] with an excess amount of H_2L^{1b} in a CH_2Cl_2 – Me_2CO solution with the addition of Et_3N. The formation of the bridging sulfur atom is explained by the reaction of **14b** with S^{2-} which may be generated by the decomposition of H_2L^{1b}. Similar decomposition of dialkylthiocarbonyl benzamidines and the formation of a sulfido-bridged dimer has been reported recently for phenylimido rhenium(V) complexes under similar conditions [72]. In order to prove this suggested reaction pathway, the reaction of **14b** with a slight excess of Na_2S in CH_2Cl_2 – Me_2CO was undertaken. The color of reaction mixture did not change after heating on reflux for 2h. However, beside other oily red products, which were not characterized, compound **18b** could be isolated with about 15 % yield by recrystallization of the reaction mixture from CH_2Cl_2/n-hexane.

In comparison to the IR spectrum of **14b**, the absorption of $\nu_{C=N}$ in **18b** is almost not changed, while the Re=O stretch is bathochromically shifted by about 20 cm^{-1}. The mass spectrum reveals the molecular peak at 1116.0760 (calcd. 1116.0817) with the typical isotopic distribution pattern for a dimeric rhenium compound. The ^{1}H NMR spectrum of **18b** shows two magnetically equivalent rhenium units. The rigid structure of the morpholinyl residue is reflected by multiplet signals corresponding to eight magnetically nonequivalent protons. Four of them are well resolved and appear at 3.58, 3.21, 3.29 and 3.44 ppm and the remaining four signals overlap in the range between 3.6 ppm and 3.8 ppm.

The molecular structure of **18b**, which is shown in Figure 3.6, reveals an analogous bonding pattern as was discussed for **17a**. The bond length between the rhenium atom and the bridging sulfur in the square-pyramidal unit is shorter by about 0.13 Å than that in the octahedral unit. This brings the phenolic oxygen close to the other rhenium atom. However, replacement of the bridging oxygen in **17a** by sulphur in **18b** lengthens the Re2-O56 distance to 2.673(5) Å. The interactions between Re2 and O56 are not strong enough to maintain this

arrangement in solution. This means, in the solution, the two units rotate around the Re1-S20-Re2 bond and are magnetically equivalent. Other selected bond lengths of **18b** are listed in Table 3.6.

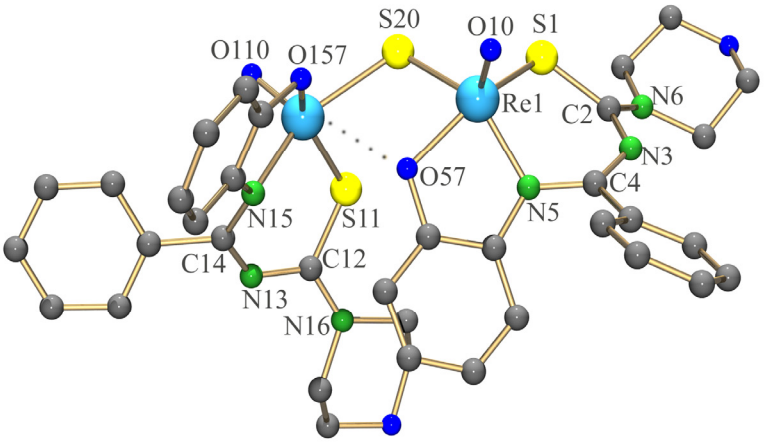

Figure 3.6 Molecular structure of [{ReO(L^{1b})}$_2$S] (**18b**). Hydrogen atoms were omitted for clarity.

Table 3.6 Selected bond lengths and angles in [{ReO(L^{1b})}$_2$S] (**18b**)

Bond lengths (Å)			
Re1-O10 / Re2-O110	1.677(8) / 1.650(8)	Re1-S20 / Re2-S20	2.282(3) / 2.415(3)
Re1-S1 / Re2-S11	2.300(3) / 2.287(3)	S1-C2 / S11-C12	1.73(1) / 1.75(1)
Re1-N5 / Re2-N15	2.022(8) / 2.029(7)	C2-N6 / C12-N16	1.31(1) / 1.32(1)
Re1-O57 / Re2-O157	2.012(6) / 1.973(7)	C4-N5 / C14-N15	1.38(1) / 1.35(1)
Re2-O57	2.673(5)		
Angles (°)			
O10-Re1-S20 / O110-Re2-S20	110.0(3) / 99.8(3)	O110-Re2-O57	167.3(1)
O10-Re1-O57 / O110-Re2-O157	107.5(3) / 106.9(4)	Re1-S20-Re2	104.9(1)
O10-Re1-N5 / O110-Re2-N15	112.5(4) / 107.8(3)	Re1-O57-Re2	104.4(1)
O10-Re1-S1 / O110-Re2-S11	107.2(3) / 104.5(3)		

3.1.2.2 '3+2' Mixed-ligand Complexes of Re and Tc Containing H_2L^1

In general, the labile chloro ligand in the coordination sphere of compounds such as **14** or **15** will allow further ligand exchange or hydrolysis under physiological conditions. This makes the *in vivo* distribution of the compounds uncontrollable and is not acceptable with regard to potential use in radiopharmaceutical applications. Replacement of the chloro ligand by other organic ligands which strongly bind to the metal atom and form mixed-ligand

complexes is mostly recommended. Additionally, following the mixed ligand approach, the ligand sphere can easily be varied, which gives access to a smooth tuning of the complex properties and, thus, of their biological behavior.

When the chloro ligands of **14** and **15** are replaced by each one other monodentate, a so-called '3+1' mixed-ligand complex is obtained. Hitherto , many '3+1' systems, which are neutral complexes with a $[MO]^{3+}$ core and a mixed-ligand set of a dianionic tridentate ligand containing one or more sulfur donor atoms, such as [SSS], [SOS], [SNS], [SNN], or [ONS], and a monodentate thiolate have been studied [73]. However, it was found that many of them were relatively unstable *in vitro* and *in vivo* due to a ready substitution of the labile monothiolate RS^- by physiological thiols such as cysteine or glutathione [74]. Generally, this can be explained by the 16 valence electron nature of the five-coordinate '3+1' complexes. Replacement of the labile monothiolate by bidentate ligands results in so-called '3+2' systems with a closed-shell electron configuration and a higher stability is expected [75]. Thus, several '3+2' mixed-ligand complexes with ligands carrying different donor sets such as [SNS]/[PO] [75], [NOS]/[NO] [76], [NOS]/[NN] [77], [NON]/[OO] [78], [NOS]/[SN] [79], or [ONO]/[PO] were studied[80]. Some of them show interesting properties, which encourages further studies and the introduction of previously not regarded ligand systems such as H_2L^1 in such considerations.

Thus, the reaction of **14a** with glycine, Hgly, in a CH_2Cl_2/MeOH mixture yields the dark red mixed-ligand complex $[ReO(L^{1a})(gly)]$ (**19**) in good yields. The same product is formed in a one-pot reaction starting from $(NBu_4)[ReOCl_4]$ and one equivalent of HL^{1a} in a CH_2Cl_2/MeOH mixture followed by the addition of a slightly excess of Hgly. In both cases, addition of a base such as NEt_3 supports the deprotonation of glycine.

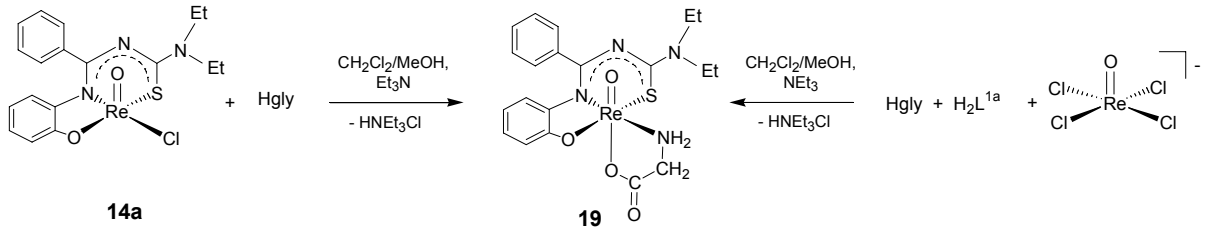

14a **19**

Scheme 3.7 Reaction of **14a** with glycine.

The infrared spectrum of **19** shows a medium broad band at 3425 cm^{-1} and a strong absorption at 1651 cm^{-1}, which can be assigned to ν_{NH} and ν_{CO} stretches of the chelating glycinate ligand. While the absorption of the Re=O vibration shifts to longer wavelengths by about 20 cm^{-1} with respect to **14a**, the absorption of the C=N stretch moves to the shorter wave region by about 15 cm^{-1}. The chelate formation of the glycinate ligand is indicated by

the detection of magnetically unequal protons of methylene and amino groups in the NMR spectrum of the compound. Thus, two multiplet signals for each proton of the CH_2 group are observed due to the combination of the geminal coupling and the vicinal coupling with the adjacent NH_2 group. One of them is well resolved at 3.50 ppm and the other is partially covered by the NCH_2 signals of the L^{1a} ligand in the range between 3.9 ppm and 4.1 ppm. Two broad signals of the NH_2 protons appear at 5.87 ppm and 6.85 ppm.

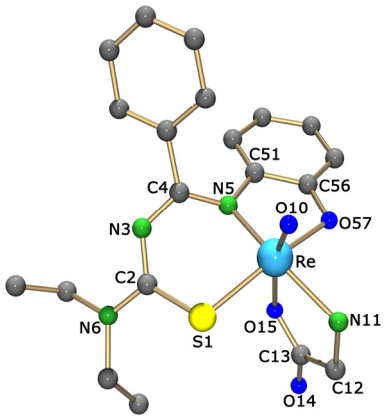

Figure 3.7 Molecular structure of [ReO(L^{1a})(gly)] (**19**). Hydrogen atoms were omitted for clarity.

Table 3.7 Selected bond lengths and angles in [ReO(L^{1a})(gly)] (**19**)

Bond lengths (Å)					
Re–O10	1.680(5)	Re –O15	2.120(5)	N3–C4	1.304(8)
Re–S1	2.348(2)	Re –N11	2.189(6)	C4–N5	1.353(8)
Re–N5	1.989(5)	S1–C2	1.760(7)	C13–O14	1.210(9)
Re–O57	2.029(5)	C2–N6	1.328(9)	C13–O15	1.300(8)
Angles (°)					
O10–Re –Sl	98.44(18)	O10–Re–N5	104.7(2)	O10–Re–O15	164.6(2)
O10–Re–N11	90.5(2)	O10–Re–O57	100.3(2)	O57–Re–S1	161.3(1)

The molecular structure of **19** is depicted in Figure 3.7. The solid state structure confirms the results of the spectroscopic studies. The rhenium atom is placed in a distorted octahedral coordination environment, which is formed by the oxo oxygen, an equatorially coordinated $(L^{1a})^{2-}$ ligand and a bidentate glycinate. The amino group occupies the remaining equatorial position, whereas the carboxylate group coordinates *trans* to the oxo ligand. With respect to the structure of the five-coordinate **14a**, the rhenium atom expectedly drops towards the equatorial plane. While the Re-O10 distance is slightly lengthened, all C–N and C–S bonds in the chelate ring are slightly shortened. This is in agreement with the IR spectroscopic results. Nevertheless, the Re-O10 bond length of 1.680 Å falls into the typical range of Re=O double bonds. The Re-N11 (2.189 Å) and Re-O15 (2.120 Å) bond lengths are about 0.1 Å longer

than the Re-N5 and Re-O57 bonds, which reflects the coordination of the NH_2 group as an amine and the *trans* influence of the oxo ligand. Selected bond lengths of **16** are given in Table 3.7.

More examples for the '3+2' mixed-ligand complexes containing H_2L^1 are the $[MO(L^1)(R^1R^2btu)]$ {M = Re (**20**), Tc (**21**)} compounds. As shown in Scheme 3.8, complexes of the type **20** can be synthesized by four alternative routes. The first approach (**A**) is a two-step synthesis using the compounds $[ReO(L^1)Cl]$ (**14**) as intermediate complexes. The labile square-pyramidal complexes are subsequently reacted with equivalent amounts of the benzoylthioureas in warm CH_2Cl_2/MeOH. The mixed-ligands complexes are formed in high yields following this procedure. They are readily soluble in CH_2Cl_2 and only sparingly soluble in MeOH. Single crystals of good quality were obtained by slow evaporation of the reaction mixtures.

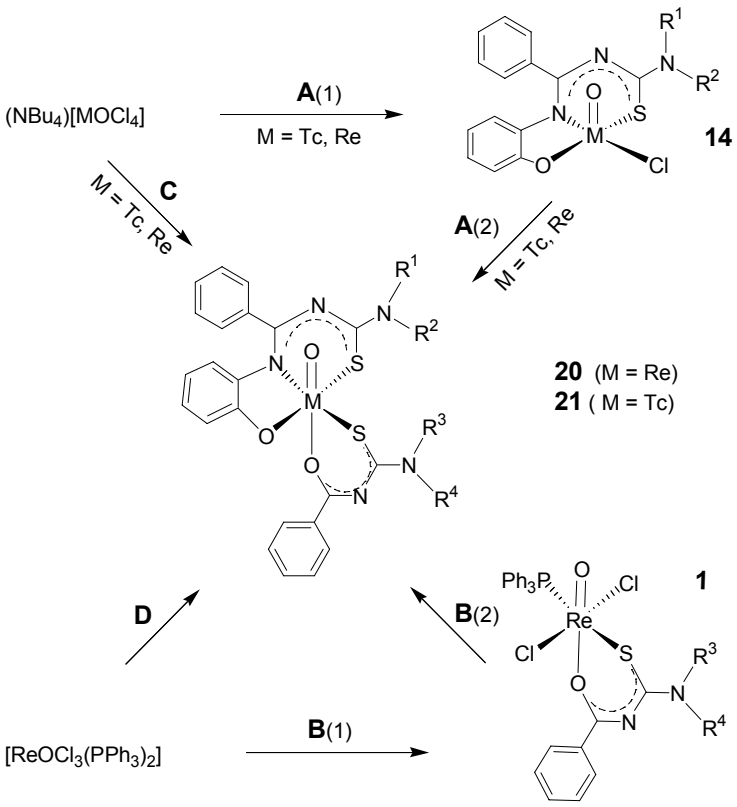

Scheme 3.8 Synthetic approaches for the [3+2] mixed-ligand complexes under study. Approach **A**: (1) H_2L^1, MeOH, rt; (2) HL^2 , Et_3N, CH_2Cl_2-MeOH, 35°C. Approach **B**: (1) HL^2, CH_2Cl_2, rt; (2), H_2L^1, Et_3N, CH_2Cl_2, reflux. Approach **C:** H_2L^1, HL^2, Et_3N, CH_2Cl_2-MeOH, 35°C. Approach **D:** H_2L^1, HL^2, Et_3N, CH_2Cl_2, rt.

The second two-step synthesis (approach **B**) starts from a common precursor, $[ReOCl_3(PPh_3)_2]$. In the first step, $[ReOCl_3(PPh_3)_2]$ is treated with a slight excess of the corresponding benzoylthiourea in CH_2Cl_2 to give monosubstituted $[ReOCl_2(R^1R^2btu)(PPh_3)]$ complexes (**1**). In the second step, the compounds **1** are exposed to equivalent amounts of

H_2L^1 in refluxing CH_2Cl_2 until the initial green-yellow colour changes to clear red. The yields of analytically pure mixed-ligand complexes from this synthetic approach are significantly lower than those using $[ReO(L^1)Cl]$ as starting materials. This is most probably the result of incomplete substitution and/or further reduction of the $\{ReO\}^{3+}$ core by released PPh_3 under the conditions applied. Such side-reactions, which finally yield rhenium(III) complexes are common, when phosphines are present [33].

The mixed-ligand complexes can also be prepared in good yields in one-pot reactions starting from $(NBu_4)[ReOCl_4]$ or $[ReOCl_3(PPh_3)_2]$ and stoichiometric amounts of the tridentate benzamidines and benzoylthioureas. Reactions starting from $(NBu_4)[ReOCl_4]$ (approach **C**) are best done in CH_2Cl_2/MeOH mixtures, while CH_2Cl_2 should be used for the reactions starting from $[ReOCl_3(PPh_3)_2]$ (approach **D**). The yields of such reactions are not significantly lower than those following **A**. However, a supporting base such as NEt_3 should be added in such reactions a few minutes after the addition of the ligands in order to complete the reaction and to avoid rapid hydrolysis of the precursors.

Infrared spectra of the oxorhenium mixed-ligands complexes **20** show no absorptions in the region above 3100 cm^{-1}, which would correspond to ν_{NH} and ν_{OH} vibrations in the uncoordinated H_2L^1 and HR^1R^2btu and indicate the expected double deprotonation of the benzamidines and deprotonation of benzoylthioureas during the complex formation. Additionally, the sharp intense absorptions in the range between 1620-1690 cm^{-1} assigned to the $\nu_{C=N,}$ $\nu_{C=O}$ stretches in the spectra of the non-coordinated benzamidines and thioureas shift to the range between 1500 and 1540 cm^{-1} and appear as broad bands. An unambiguous assignment of the two bands either to the thiocarbamoylbenzamidine or benzoylthiourea stretches have not been done. Despite the fact that these absorptions are about 30 cm^{-1} higher than the corresponding bands in the infrared spectra of both **1** and **14**, the bathochromic shifts of about 100 cm^{-1} with respect to H_2L^1 and HR^1R^2btu indicate for both ligands a chelate formation with a large degree of π-electron delocalization within the chelate rings. Intense bands appear between 964 and 980 cm^{-1}, which can be assigned to the Re=O stretches [33].

The NMR spectra of complexes **20** provide additional evidence for the proposed composition and the molecular structures of the complexes. The hindered rotation around the C-NR_2 bonds results in magnetic inequivalence of the two residues R. Thus, two triplet signals of the methyl groups in -NEt_2 residue are observed in the ^{1}H-NMR spectrum of $[ReO(L^{1a})(Ph_2btu)]$ (**20a**) measured at room temperature. However, the proton signals of the two methylene groups, which should consequently be two quartet signals, appear as four sextet resonances with ABX_3 coupling pattern, where J_{AB} is approximately $2 \cdot J_{AX}$ including

two overlapped signals at 3.79 ppm and two well separated signals at 3.97 ppm and 4.05 ppm. This splitting pattern of methylene signals can be explained by the rigid structure of the tertiary amine group, which makes the methylene protons magnetically inequivalent with respect to their axial and equatorial positions. More interestingly, the ^{1}H-NMR spectrum of [ReO(L^{1a})(morphbtu)] (**20b**) shows rigidity for the whole morpholinyl moiety of $\{L^{2b}\}^{-}$, which results in eight magnetically inequivalent protons in this unit. This is indicated by five well resolved multiplet signals with ABXY splitting pattern at 4.02, 4.20, 4.37, 4.42 and 4.62 ppm corresponding to four different CH_2-O protons and one CH_2-N proton. Three other CH_2-N protons appear together with two CH_2-N protons of the NEt_2 residue of $\{L^{1a}\}^{2-}$ as a broad multiplet at 4.00 ppm. A similar magnetic behaviour of the morpholinyl moieties, but less resolved, is observed in the ^{1}H-NMR spectrum of [ReO(L^{1b})(morphbtu)] (**20c**). The ^{13}C-NMR spectra of the complexes are easier to explain, since their patterns are only influenced by hindered rotation around the C-NR_2 bonds. Consequently, two separated signals for each CH_2 and CH_3 carbon atoms in NEt_2 groups and/or CH_2-N and CH_2-O atoms in the morpholinyl units appear. The chemical shifts of aromatic carbon atoms, which can not be unambiguously assigned, are in the range from 117 – 136 ppm, with the exception of the C_{ar}-N and C_{ar}-O resonances, which clearly appear at lower field (145 ppm and 165 ppm, respectively). This is due to deprotonation of the imino and phenol groups during the complex formation of the H_2L^1 ligands. The low intense resonances of carbon atoms of the C=X (X = N, O, S) groups are in the range from 163 ppm to 187 ppm. The closely related structures of the benzoylthioureas and thiocarbamoylbenzamidines produce some difficulties in the assignment of the C=X signals in the ^{13}C-NMR of complexes **20**. Nevertheless, with regard to the analogous coordination spheres of **20a** and **20b**, the chemical shifts of C=X signals of $\{L^{1a}\}^{2-}$ in these complexes should be similar. Thus, the comparison of the chemical shift values give hints for a detailed assignment of the C=X signals (see experimental section). While the chemical shift of the C=S resonances of the benzoylthiourea ligands in the mixed-ligand complexes are in the same range as those of the precursors **1**, the corresponding C=O resonances are shifted to higher field by about 5 ppm. Both C=N and C=S resonances of the $\{L^{1}\}^{2-}$ ligand appear at lower field by about 6 ppm compared to the values in the spectra of **14**.

FAB^{+} mass spectra of the mixed-ligand complexes show intense peaks of the molecular ions with the expected isotopic patterns. Interestingly, the fragments which result from loss of $R^1R^2NC{\equiv}N$ residues from benzoylthiourea ligands appear in all spectra as very intense

signals. The loss of complete $\{R^1R^2btu\}^-$ ligands is also observed in the mass spectra of all complexes of the type **20**.

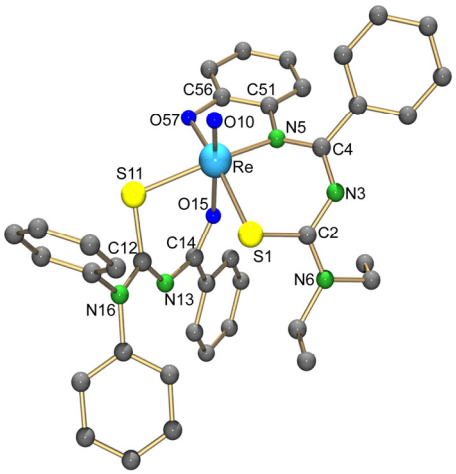

Figure 3.8 Molecular structure of [ReO(L^{1a})(Ph_2tbu)] (**20a**). Hydrogen atoms were omitted for clarity.

Table 3.8 Selected bond lengths in [MO(L^{1a})(R^1R^2btu)]

	20a	**20b**	**21b**
Bond lengths (Å)			
M–O10	1.662(4)	1.681(2)	1.641(4)
M–S1	2.360(2)	2.354(1)	2.344(2)
M–N5	2.009(6)	2.028(2)	2.048(4)
M–O57	1.988(5)	1.996(2)	1.998(4)
M–O15	2.196(4)	2.158(2)	2.200(4)
M–S11	2.399(2)	2.408(1)	2.414(1)
S1–C2 / S11–C12	1.741(7) /1.754(8)	1.748(2) / 1.750(3)	1.748(6) / 1.749(6)
C2–N3 / C12–N13	1.348(9) / 1.335(9)	1.342(3) / 1.343(3)	1.323(7) / 1.333(7)
N3–C4 / N13–C14	1.298(9) / 1.346(9)	1.311(3) / 1.335(3)	1.308(7) / 1.333(7)
C4–N5 / C14–O15	1.367(9) / 1.252(8)	1.355(3) / 1.261(3)	1.357(8) / 1.268(6)
C2–N6 / C12–N16	1.328(8) / 1.340(9)	1.331(3) / 1.334(3)	1.338(8) / 1.342(7)

The structures of complexes **20a** and **20b** have been studied by X-ray diffraction. As a representative for this type of complexes, the molecular structure of **20a** is shown in Figure 3.8. Since the structure of **20b** is identical with the exception of the residues of the benzoylthiourea ligand, no extra Figure is shown. Table 3.8 contains selected bond lengths and angles for both compounds. In both complexes, the rhenium atoms possess a distorted octahedral coordination environment. Axial positions are occupied by the oxo ligands and the oxygen atoms of the bidentate ligands. The tridentate benzamidine ligands occupy three positions in the equatorial coordination sphere, which is completed by the sulphur atoms of $\{L^2\}^-$. The metal atoms are located slightly above the mean least-square plan formed by S1,

N5, O57 and S12 toward the oxo ligand. The Re=O distances of 1.662(4) and 1.681(2) Å are in the expected range of rhenium-oxygen double bonds [33].

A remarkable structural feature is the coordination of the benzoylic oxygen atoms *trans* to the oxo ligand. The Re1-O15 bonds fall in the range from 2.158(2) to 2.196(4) Å This is significantly longer than the corresponding Re-O bonds in the complexes **1**, while the corresponding C14-O15 bonds are only shorter than in the complexes **1** with the same benzoylthioureas by about 0.03 Å. The Re-O15 bong lengths in **20** are at the upper limit of *trans*-O=Re-O single bond distances in Re(V) oxo complexes. Similar values have previously only been reported for some complexes with small monodentate neutral ligands such as H_2O, MeOH or Me_2CO [49]. This means that an electron transfer from the Re=O double bond to a trans-Re-O single bond, which is frequently observed for alkoxo-type ligands, does not apply for the compounds under study [35].

The Re-S11 and C12-S11 bond lengths are in the typical range of Re-S single bonds and C-S bonds with partial double bond character, as has been dicussed for other benzoylthiourea complexes of rhenium previously. In the benzamidine moiety, the Re-S1 and Re-N5 bonds are lengthened by about 0.03 – 0.06 Å with respect to the bonds in the complexes **14**. Nevertheless, the Re-S1 bond lengths are still about 0.06 Å shorter than the Re-S11 bonds in the co-coordinated benzoylthiourea ligands. The atoms S11, C12, N13, C14 and O15 lie almost in a plane with a maximum deviation from a mean least-square plan of only 0.175(5) Å for C12 in **20a** and 0.097(2) Å for C14 in **20b.** The six-membered chelate rings, however, which are formed from these atoms and the Re atoms are dramatically distorted with distances of the metal atoms to the mean least-square plane of 1.157(7) Å and 1.093(3) Å, respectively for **20a** and **20b**. The six-membered chelate rings of the ligands $\{L^1\}^{2-}$ are only slightly distorted with maximum deviations from a mean least-square plane of about 0.30 Å. A considerable delocalization of π-electron density is found inside all chelate rings. This is indicated by similar lengths of all C-N bonds, which fall within the range between C-N single and double bonds. These bond length equalizations are also extended to the C2-N6/C12-N16 bonds (1.33 -1.34 Å). The partial transfer of electron density into these bonds well agrees with the ^{1}H NMR spectrum of the compounds, which indicates a rigid arrangement of the -NR^1R^2 moiety.

The synthetic approaches **B** and **D** to the mixed-ligand complexes (Scheme 3.7) are restricted to rhenium, since a compound of the composition '$[TcOCl_3(PPh_3)_2]$' does not exist due to the ready reduction of technetium by phosphines under formation of Tc(IV) and Tc(III) compounds. It is consequently not possible to prepare a complex of the composition

'[$TcOCl_2(L^2)(PPh_3)$]'. Nevertheless, synthesis of the corresponding technetium mixed-ligand complexes succeeded following the approaches **A** and **C**. Figure 3.9 shows the molecular structure of one of these complexes, [$TcO(L^{1b})$(morphbtu)] (**21b**), which was isolated as a green crystalline solid in high yields from both synthetic pathways.

The IR spectrum of **21b** exhibits the $\nu_{(Tc=O)}$ frequency at 957 cm^{-1} and the spectral features described above for the compounds **20**, such as the strong bathochromic shift of the C=O and the C=N bands, also apply for the Tc complex. The presence of two rigid morpholinyl residues in the molecule leads to a complicated pattern of the methylene region of the ^1H NMR spectrum of **21b**. However, three multiplet signals of three CH_2-O protons with a typical ABXY splitting pattern can clearly be resolved at 4.35, 4.53 and 4.75 ppm.

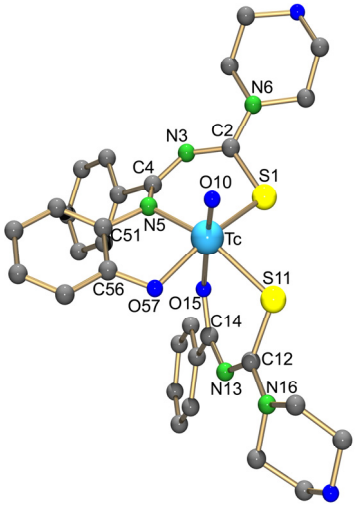

Figure 3.9 Molecular structure of [TcO)(L^{1b})(morphbtu] (**21b**). Hydrogen atoms were omitted for clarity.

All main structural features of compound **21b** are similar to the facts discussed for the complexes **20** and shall not be repeated in detail. The corresponding bond lengths and angles are compared to those of the structurally characterized rhenium mixed-ligand complexes in Table 3.8. However, the orientation of the tridentate ligand is different from those observed in the analogous rhenium compounds. This can easily be seen at the phenyl ring at the atom C4. It directs away from the oxo ligand in **21b**, while it is positioned above the equatorial coordination plan in the complexes **20a** and **20b**, and is probably caused by the fluctuation of the whole molecule.

Compound **21b** readily reacts with an excess of PPh_3 in CH_2Cl_2 under formation of a red crystalline technetium (III) complex of the composition [$Tc(PPh_3)(L^{1b})(R^1R^2btu)$] (**22b).** This reaction proceeds in high yields even at room temperature, and it should be mentioned that similar reactions with the corresponding rhenium complexes **20** could not be observed. The reduction of oxotechnetium(V) complexes by phosphines is not uncommon and can be

explained by the formation of an intermediate $\{Tc\text{-}OPPh_3\}^{3+}$ complex, and the subsequent abstraction of $OPPh_3$ from the coordination sphere [41]. Indeed, released $OPPh_3$ could be detected by ^{31}P-NMR in the reaction mixture between **21b** and PPh_3. The resulting technetium(III) product is stable as solid, while in solution a slow oxidation by air is observed. It is accompanied by a change of the colour from red to yellow-green. Recrystallization of **22b** from a CH_2Cl_2/MeOH mixture must be performed under unaerobic condition or in the presence of an extra amount of PPh_3 in order to avoid ongoing oxidation.

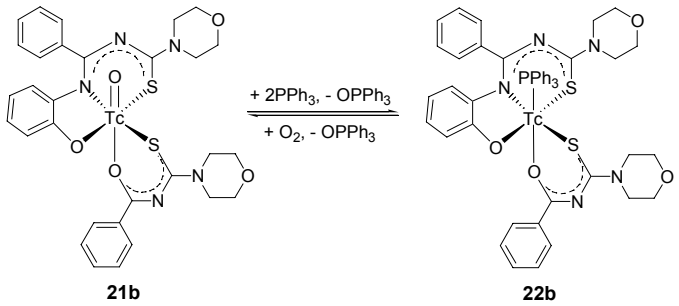

Scheme 3.9 Reaction of [TcO(L^{1b})(morphbtu)] (**21b**) with PPh_3.

The infrared spectrum of complex **22b** confirms the reduction of the metal atom by the absence of a typical $\nu_{Tc=O}$ stretch between 900 and 1000 cm^{-1}. The $\nu_{C=O}$ and/or $\nu_{C=N}$ bands are slightly shifted to longer wavelengths compared to **21b** and appear at 1497 cm^{-1} as a strong broad band.

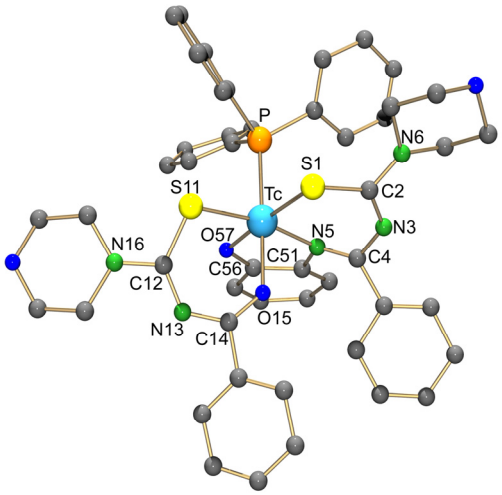

Figure 3.10 Molecular structure of [Tc(PPh_3)(morphbtu)(L^{1a})] (**22b**). Hydrogen atoms were omitted for clarity.

Figure 3.10 shows the molecular structure of **22b**. Selected bond lengths and angles are contained in Table 3.9. The coordination environment of the metal atom is best described as a distorted octahedron with *trans* angles between 168.4(3) and 178.8(3)°. The ligand $\{R^1R^2btu\}^-$ coordinates to technetium as a common S,O bidentate ligand with its oxygen atom *trans* to the PPh_3 ligand. The three remaining positions in the coordination sphere are occupied by the

planar tridentate $(L^{1b})^{2-}$ ligand. The Tc-O15 bond length of 2.072(9) Å falls in the range of typical Tc-O single bonds. The Tc-S1 and Tc-S11 bond lengths are almost equal and in the same range of those in other Tc(III) benzoylthioureato complexes such as $[TcCl(PPh_3)(Ph_2btu)_2]$ **7a** and $[Tc(Ph_2btu)_3]$ **8a**.

Table 3.9 Selected bond lengths and angles in $[Tc(PPh_3)(morphbtu)(L^{1a})]$ (**22b**)

Bond lengths (Å)					
Tc–P	2.413(4)	Tc –O15	2.072(9)	C4–N5	1.28(2)
Tc–S1	2.346(4)	Tc –S11	2.341(4)	C14–O15	1.26(1)
Tc–N5	2.09(1)	S1–C2	1.75(1)	C2–N6	1.36(1)
Tc–O57	2.048(8)	S11–C12	1.74(1)	C12–N16	1.37(2)
Angles (°)					
P–Tc–O15	178.8(3)	S11–Tc–N5	168.4(3)	O57–Tc–S1	174.0(3)
N5–Tc–S1	92.3(3)	S11–Tc –O15	88.4(3)	S1–Tc–S11	96.0(1)

The redox behaviour of **22b** as described above reveals some interesting features, which makes it interesting to study its electrochemistry. Thus, the cyclic voltammetry measurement of the compound was undertaken in dry CH_2Cl_2 under Ar atmosphere. The complex **22b** shows no reduction process from -1.2 V to 0.0 V, but two almost reversible oxidations at 0.218 V (ΔEp = 98 mV) and 1.078 V (ΔEp = 85 mV) (Figure 3.11)corresponding one-electron transfer processes (Chart 3.2).

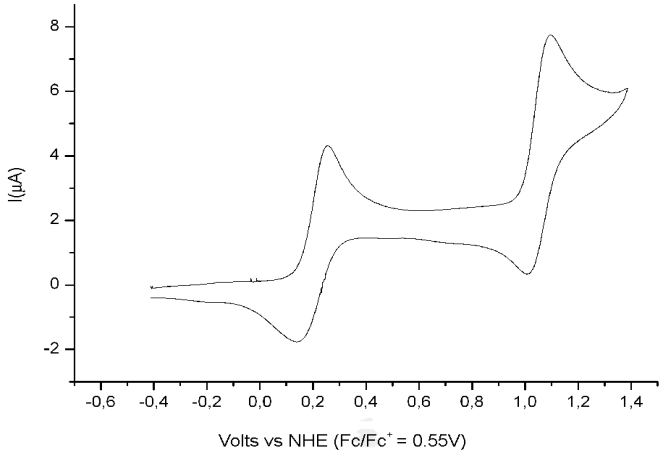

Figure 3.11 Cyclic voltammogram of **22b** in 0.2M $[NBu_4][PF_6]$-CH_2Cl_2 at a scan rate of 100 mV/s.

$$[Tc^{III}(PPh_3)(L^{1b})(L^{2b})] \underset{+e}{\overset{-e}{\rightleftharpoons}} [Tc^{IV}(PPh_3)(L^{1b})(L^{2b})]^{+} \underset{+e}{\overset{-e}{\rightleftharpoons}} [Tc^{V}(PPh_3)(L^{1b})(L^{2b})]^{2+}$$

Chart 3.2

It is necessary to quote that at the same condition the ΔEp value of Fc/Fc^+ couple is 83 mV. The low potential of the first oxidation process is well in agreement with the observed oxidation of **22b** under aerobic conditions. It is understood that in the timescale of the applied CV, the $[Tc^V(PPh_3)(L^{1b})(morphbtu)]^{2+}$ species is sufficiently kinetically inert to undergo the backward reduction. However, in the oxidation reaction of **22b** in the air, the oxo complex **21b** is the thermodynamically more stable product.

3.1.2.3 Re^VN and Tc^VN Complexes with H_2L^1

H_2L^1 readily reacts with rhenium(V) and technetium(V) nitrido precursors like $[M(N)Cl_2(PPh_3)_2]$ in CH_2Cl_2 at ambient temperature with the addition of a supporting base (Et_3N) under formation of red crystalline complexes of the composition $[M(N)(L^1)(PPh_3)]$ {M = Re (**23**), Tc (**24**)} in high yields. The products have poor solubility in alcohols and can be recrystallized from CH_2Cl_2-MeOH solutions.

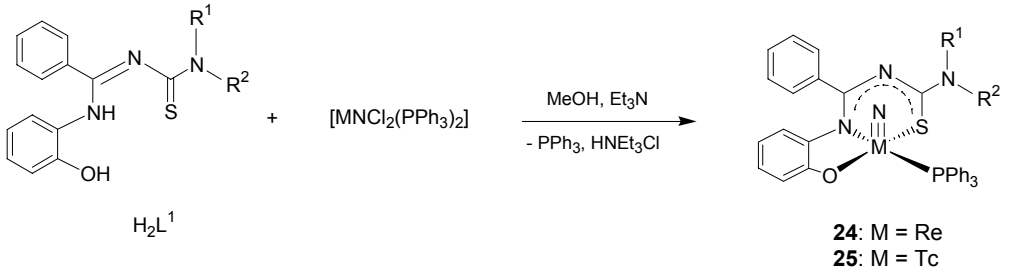

H_2L^1

24: M = Re
25: M = Tc

Scheme 3.10 Reactions of $[M(N)Cl_2(PPh_3)_2]$ (M = Re, Tc) with H_2L^1.

Figure 3.12 illustrates the molecular structure of **23b**. The structure of the analogous rhenium complex **24b** is not presented. The metal atoms show a distorted square-pyramidal coordination sphere with a nitrido ligand in apical position. The ligand H_2L^1 coordinates equatorially to the metal atoms as a tridentate dianionic ligand as in the oxo complexes **15** and the remaining position in the basal plane is occupied by a triphenylphosphine ligand. The metal atoms lie above the equatorial plane by 0.537 Å towards the nitrido ligand and the N10–M–X angles (X = equatorial donor atom) fall in the range between 92.6 and 111.5°. The Re-N10 distance of 1.645(6) Å and the Tc-N10 distance of 1.619(5) Å are within the expected range of rhenium–nitrogen and technetium-nitrogen triple bonds [33]. All the bonds M-O, M-N and M-S are slightly longer than those in the corresponding oxo complexes. The other selected bond lengths of **23b** and **24b** are compared in Table 3.10.

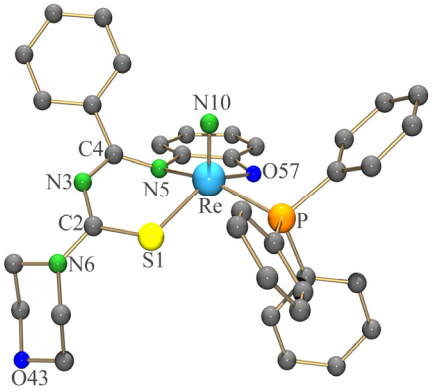

Figure 3.12 Molecular structure of [TcNCl(L^{1b})(PPh_3)] (**24b**). Hydrogen atoms were omitted for clarity.

Table 3.10 Selected bond lengths and angles in [ReNCl(L^{1b})(PPh_3)] (**23b**) and [TcNCl(L^{1b})(PPh_3)] (**24b**)

	23b	**24b**		**23b**	**24b**
Bond lengths (Å)					
M–N10	1.645(6)	1.619(5)	M–O57	2.026(4)	2.029(4)
M–P	2.418(1)	2.436(1)	S1–C2	1.764(6)	1.758(6)
M–S1	2.316(1)	2.330(1)	C4–N5	1.354(7)	1.327(8)
M–N5	2.084(4)	2.091(4)	C2–N6	1.336(8)	1.330(8)
Angles (°)					
N10–M–P	92.6(2)	93.32(17)	N10–M–N5	107.8(2)	107.7(2)
N10–M–S1	104.7(2)	104.9(2)	N10–M–O57	111.5(2)	112.0(2)

The $^{31}P\{H\}$ NMR spectra of **23** and **24** reveal single resonances in the 29 ppm region corresponding to coordinated triphenylphosphine. The ^{1}H NMR spectra of the nitrido complexes generally have the same pattern of those corresponding to oxo complexes but the chemical shifts of the alkyl residues in the -NR^1R^2 moieties and the aromatic protons of the PhOH ring appear at higher field.

3.1.3 A Rhenium Complex with N'-Picolylbenzamidine

Treatment of [$ReOCl_3(PPh_3)_2$] with HL^2 in CH_2Cl_2/acetone at room temperature results in the immediate formation of a green solution, which slowly changes to a brown color when an alcohol is added. Up to now, each of our attempts to isolate crystalline products from such solutions failed.

However, the green color of the solution described above immediately turns to violet after addition of a base such as NEt_3. From this solution, the crystalline violet complex [{ReOCl(L^2)}$_2$O] **25** was isolated in high yields. The same compound can be prepared from

$(NBu_4)[ReOCl_4]$, but with lower yields. The formation of an oxo-bridged dimer is not unexpected with this monoanionic, tridentate ligand, and is frequently observed when traces of water are present. Furthermore, charge compensation more favorably allows the formation of a neutral dimeric rhenium oxo complex rather than a complex cation [28].

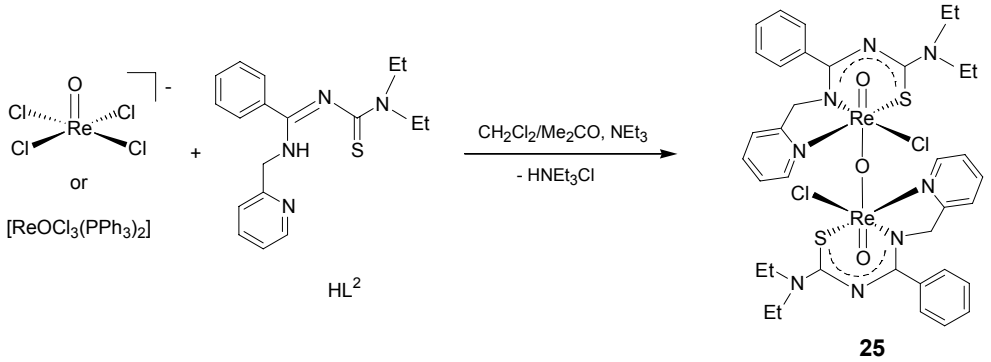

Scheme 3.11 Reactions of $[ReOCl_3(PPh_3)_2]$ and $(NBu_4)[ReOCl_4]$ with HL^2.

The IR spectrum of **25** exhibits a strong bathochromic shift of the C=N vibration of about 120 cm^{-1} and the absence of the medium broad N-H stretch band at 3217 cm^{-1} with respect to the IR spectrum of the uncoordinated HL^2. Moreover, the formation of an oxo-bridged dimeric compound is strongly indicated by a weak absorption of the Re=O stretch at 949 cm^{-1} and a strong absorption of the Re–O–Re' unit at 683 cm^{-1} [39]. In the ^{1}H-NMR spectrum of **25**, the protons of the ethyl residues expectedly show similar patterns as observed in **14a**. The two methylene protons at C6 of the $(L^2)^-$ ligand are magnetically non-equivalent. FAB^+ mass spectra show no evidence of the molecular ion peak. Preferably, the Re-O-Re bond is cleaved as evidenced by peaks corresponding to the $[ReO_2(L^2)]^+$ (m/z = 544) and/or $[ReO(L^2)]^+$ (m/z = 528) fragments.

X-ray quality single crystals of **25** were obtained by slow evaporation of a CH_2Cl_2/acetone solution. Figure 3.13 depicts the molecular structure of **25** showing a dimer with O20 as a center of inversion. The coordination sphere of the metal atom is best described as a slightly distorted octahedron with *trans* angles between 168.9(1) and 172.1(1)°. The tridentate organic ligand is singly deprotonated and coordinates equatorially to the Re center. The established six-membered and five-membered chelate rings are almost planar and show a maximum deviation from planarity for atom S1 (0.182 Å). The Re atom is only slightly (0.098 Å) shifted out of the mean least-square plane which is formed by the atoms S1, N5, N52 and Cl. The described coordination mode leaves less space for an 'in-plane' arrangement of the phenyl ring. Consequently, the plane of this ring stands almost perpendicular to the plane of the adjacent chelate ring and conjugation of π-electron density between these rings is

prevented as can be seen in the relatively long C4-C31 bond length of 1.502(8) Å. More bond lengths and angles of **25** are given in Table 3.11.

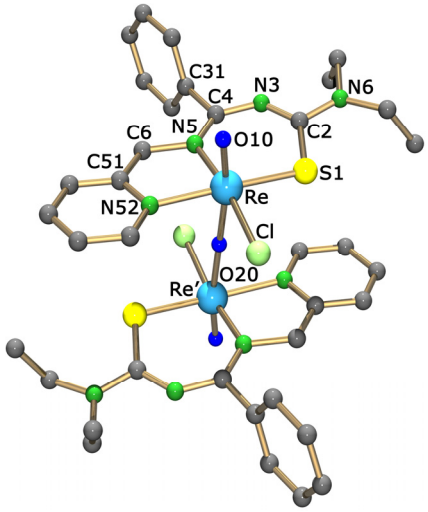

Figure 3.13 Molecular structure of [{ReOCl(L^2)}$_2$O] (**25**). Hydrogen atoms were omitted for clarity.

Table 3.11 Selected bond lengths and angles in **25**

Bond lengths (Å)					
Re-O10	1.692(4)	Re-S1	2.332(2)	S1-C2	1.745(6)
Re-N52	2.156(5)	Re-Cl	2.458(2)	C4-N5	1.329(7)
Re-N5	2.038(5)	Re-O20	1.916(3)	C4-C31	1.502(8)
Angles (°)					
O10-Re-N52	88.3(2)	O10-Re-N5	94.7(2)	O10-Re-S1	98.2(2)
O10-Re-Cl	91.0(2)	N5-Re-S1	94.8(1)	N52-Re-N5	80.0(2)
O10-Re-O20	168.9(1)	N52-Re-S1	172.1(1)	N5-Re-Cl	171.5(2)

3.1.4 A Rhenium Complex with N'-(2-Carboxyphenyl)benzamidine

The reaction of $(NBu_4)[ReOCl_4]$ with an equivalent amount of H_2L^3 in methanol results in ligand exchange and the formation of an oxorhenium(V) complex of the composition $[ReOCl(L^3)]_2$ (**26**), which can be isolated as green, microcrystalline solid directly from the reaction mixture.

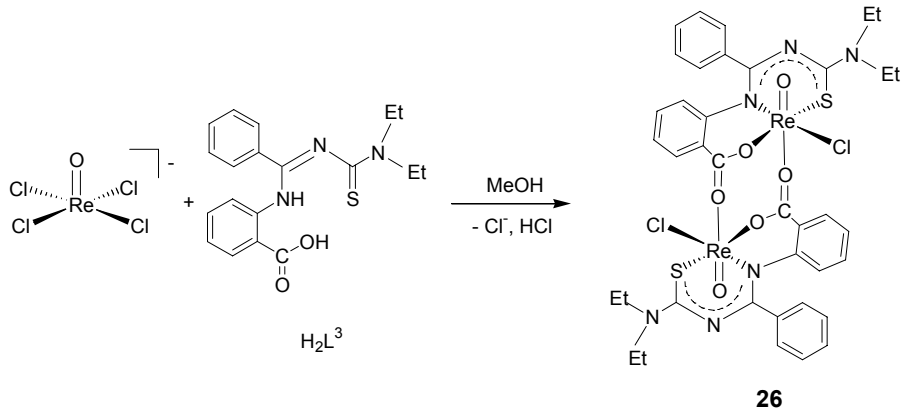

Scheme 3.12 Reactions of $(NBu_4)[ReOCl_4]$ with H_2L^3.

The IR spectrum of **26** shows the disappearance of a broad band at 3163 cm^{-1} due to the O-H vibration in H_2L^3, and a very strong shift of the C=O stretch from 1683 cm^{-1} in the uncoordinated H_2L^3 to 1542 cm^{-1} in the complex. This is commonly observed when carboxylato ligands coordinate to metal centers via both oxygen atoms [81]. A strong band at 1002 cm^{-1} is assigned as the Re=O stretching band. The poor solubility of **26** in organic solvents, even in DMSO, causes difficulties in the elucidation of its structure by spectroscopic methods. The ^1H NMR spectrum of **26** in DMSO-d_6 is less intense and the signals are not sufficiently resolved to allow a detailed analysis of the coupling patterns. Nevertheless, all protons of the ligand can be assigned and integrated in the required ratio.

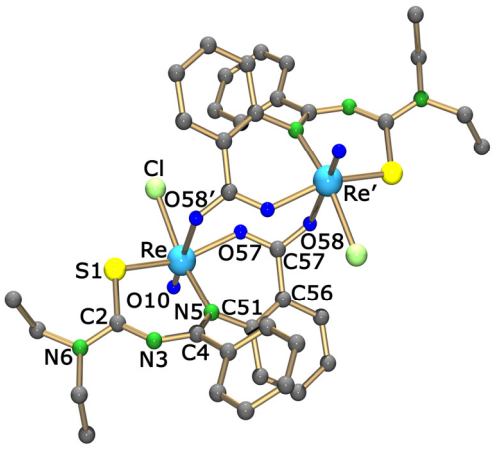

Figure 3.14 Molecular structure of $[\{ReOCl(L^3)\}_2]$ (**26**). Hydrogen atoms were omitted for clarity.

Table 3.12 Selected bond lengths and angles in [{ReOCl(L^3)}$_2$] (**26**)

Bond lengths (Å)					
Re-O10	1.655(8)	Re-N5	2.040(8)	S1-C2	1.75(1)
Re-Cl	2.376(3)	Re-O57	2.051(7)	C4-N5	1.34(1)
Re-S1	2.295(3)	Re-O58’	2.271(7)	C2-N6	1.33(1)
Angles (°)					
O10-Re-Cl	96.4(3)	O10-Re-N5	97.4(4)	O10-Re-O57	88.5(3)
O10-Re-S1	101.6(3)	O10-Re-O58’	175.8(3)	C57-O58-Re’	122.1(6)

Symmetry operation: (’) –x, 1-y, -z

Green blocks of **26** are stable in the air and could be studied by X-ray diffraction without noticeable decomposition. Figure 3.14 illustrates the dimeric structure of the compound. Selected bond lengths and angles are summarized in Table 3.12. Each of the organic ligands establish a tridentate equatorial coordination at one ReO unit. The remaining position in the basal plane of the resulting square pyramid is occupied by a chloro ligand. Dimerization is achieved by coordination of the oxygen atom O58 of a second {ReO(L^3)Cl} unit *trans* to the oxo oxygen. Thus, each of the rhenium atoms has a distorted octahedral environment and the resulting dimeric molecule possesses inversion symmetry. The ‘Re…Re’ distance is 5.324 Å and binding interactions between the metal atoms can be excluded. Such a bridging coordination of a carboxylic group in a rhenium complex with the transition metal in one of its high oxidation states is without precedent. Most of the hitherto structurally characterized rhenium complexes with bridging carboxylate coordination establish metal-metal bonds [82], or contain the tricarbonylrhenium(I) core [83].

3.1.5 Re and Tc Complexes with N’-(Benzamido)benzamidines (H_2L^4)

3.1.5.1 Re^VO and Tc^VO Complexes with H_2L^4

The reaction of H_2L^4 with the common technetium(V) precursor (NBu_4)[$TcOCl_4$] in methanol at room temperature gives a red solid of the composition [TcOCl(L^4)] (**28**), which precipitates directly from the reaction mixture within a few minutes. Under the same condition, H_2L^4 reacts with (NBu_4)[$ReOCl_4$] much slower and an analogous red solid, [ReOCl(L^4)] (**27**) can be isolated. Addition of a base like NEt_3 supports the formation and precipitation of the products but results in some impurities due to solvolysis of **27**.

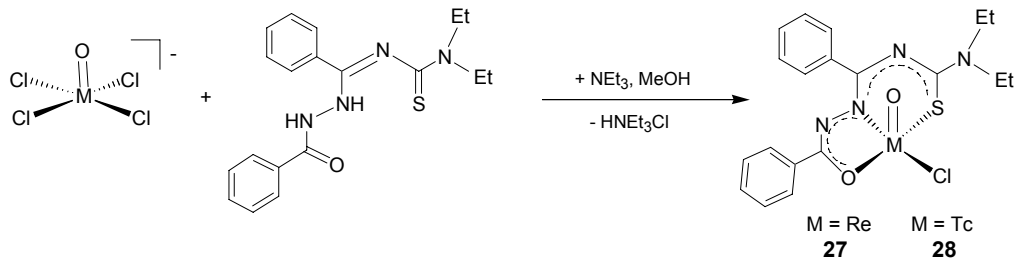

Scheme 3.13 Reactions of $(NBu_4)[MOCl_4]$ (M = Re, Tc) with H_2L^4.

Infrared spectra of complexes **27** and **28** exhibit strong bathochromic shifts of about 150 cm^{-1} of the $\nu_{C=O}$ bands together with the disappearance of absorptions in the region above 3150 cm^{-1}, which correspond to ν_{NH} stretches, in the uncoordinated H_2L^4. This indicates chelate formation with a large degree of π-electron delocalization within the chelate rings and the expected double deprotonation of the ligands. Intense bands appearing at 991 cm^{-1} for **27** and 976 cm^{-1} for **28** can be respectively assigned to the Re=O and Tc=O vibrations [33,41]. ^1H NMR spectra show the hindered rotation around the C–NEt_2 bonds, which is reflected by two sets of well resolved signals corresponding to the ethyl groups. Furthermore, the rigid structure of the tertiary amine nitrogen atom results in magnetic nonequivalence of the methylene protons with respect to their axial and equatorial positions. Thus, four overlapping multiplet signals with ABX_3 coupling patterns of CH_2 protons appear in the region between 3.9 and 4.1 ppm. In the ^{13}C NMR spectrum of **2,** the separated signals of two ethyl groups are also observed due to the hindered rotation. The resonances assigned to C=N, C=S and C=O, respectively, appear at 166.69, 172.70 and 173.73 ppm.

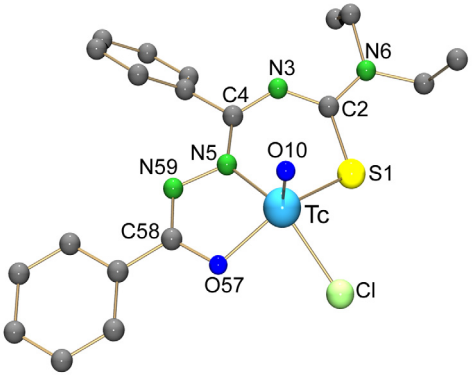

Figure 3.15 Molecular structure of $[TcOCl(L^4)]$ (**28**). Hydrogen atoms were omitted for clarity.

Figure 3.15 depicts the molecular structure of compound **28** as a prototype compound for this type of complexes. Selected bond lengths and angles of **27** and **28** are compared in Table 3.13. The coordination environment of the metal atoms are distorted square-pyramids with oxo ligands in the apical positions and square planes formed by the donor atoms of the tridentate ligands and the chloro ligands. The metal atoms are situated by 0.691(1) Å for **27**

and 0.713(3) Å for **28** above the basal plane towards the oxo ligands. All O10–M–X angles (X = equatorial donor atom) fall in the range between 107° and 112°. This corresponds to the typical bonding situation of square-pyramidal $Re^{V}O$ and $Tc^{V}O$ complexes [71]. The M=O distances of around 1.645 Å are within the expected range of rhenium–oxygen and technetium-oxygen double bonds [33,41].

Table 3.13 Selected bond lengths and angles in [ReOCl(L^4)] (**27**) and [TcOCl(L^4)] (**28**)

Bond lengths (Å)	**27**	**28**	Bond lengths (Å)	**27**	**28**
M–O10	1.644(1)	1.647(9)	M–O57	1.970(1)	1.967(7)
M–Cl	2.336(1)	2.349(3)	S1–C2	1.756(2)	1.74(1)
M–S1	2.288(1)	2.276(3)	C4–N5	1.351(3)	1.36(1)
M–N5	1.994(1)	1.972(9)	C2–N6	1.333(3)	1.34(1)
Angles (°)					
O10–M–Cl	108.0(1)	110.0(4)	O10–M–N5	107.08(7)	107.9(5)
O10–M–S1	108.6(1)	108.1(3)	O10–M–O57	111.92(7)	112.5(4)
S1–M–O57	139.5(1)	139.4(2)	N5–M–Cl	144.63(5)	141.2(3)

3.1.5.2 '3+2' Mixed-ligand $Re^{V}O$ Complexes Containing H_2L^4

Similar to the complexes **14**, compounds **28** have one labile chloro ligand, which can be substituted by a bidentate ligand such as HR^1R^2btu. The mixed-ligand complexes [ReO(L^4)(R^1R^2btu)] (**29**) can be synthesized either from reactions of **28** with HR^1R^2btu or directly from reactions of $(NBu_4)[ReOCl_4]$ and a stoichiometric mixture of H_2L^4 and HR^1R^2btu (Scheme 3.14). The yields obtained from both reaction pathways are very similar. However, a supporting base should be provided a few minutes after addition of ligands for both approaches.

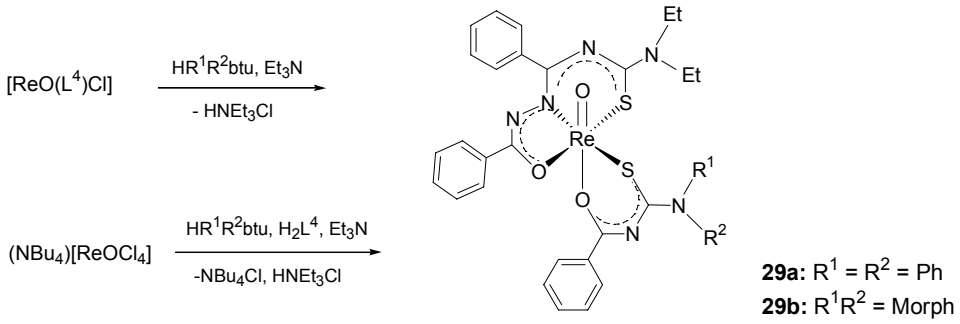

Scheme 3.14 Synthesis of the complexes [ReO(L^4)(R^1R^2btu)] (**29**).

Infrared spectra of the complexes **29** do not show any absorption in the regions above 3100 cm^{-1}, which correspond to ν_{NH} and ν_{OH} in the uncoordinated H_2L^4 and HR^1R^2btu. This indicates the expected double deprotonation of benzamidine and single deprotonation of benzoylthiourea ligands during complex formation. Additionally, the sharp intense absorptions in the range between 1620-1690 cm^{-1} assigned to the $\nu_{C=N,}$ $\nu_{C=O}$ stretches in the spectra of the non-coordinated benzamidines and thioureas shift to the range between 1500 and 1540 cm^{-1} and appear as broad bands. Intense bands appear at 972 cm^{-1} region and can be assigned to the Re=O stretch [33]. This value is about 20 cm^{-1} lower than the corresponding absorption in **28**.

Because of the hindered rotation around the C-NR_2 bonds and the rigidity of both benzamidine and benzoylthiourea ligands, ^{1}H NMR spectra of **29** are quite complicated**.** Especially for complex **29b,** the rigidity of the morpholinyl moiety in the coordinated morphbtu ligand results in a pattern with each of the eight protons being magnetically nonequivalent. This is indicated by four well resolved multiplet signals with ABXY splitting pattern at 4.29, 4.34, 4.46, 4.58 ppm of four different CH_2-O protons and four CH_2-N protons appearing as two multiplet signals at 3.74 and 3.89 ppm. The ^{13}C-NMR spectra of **29** are easier to understand since they are only influenced by hindered rotation around the C-NR^1R^2 bonds. Consequently, two separated signals for each CH_2 and CH_3 carbon atoms in the NEt_2 groups and/or CH_2-N and CH_2-O atoms in the morpholinyl moiety are observed. The chemical shifts of the aromatic carbon atoms, which can not unambiguously be assigned, are in the range between 127 ppm and 136 ppm. The low intense resonances of carbon atoms of the C=X (X = N, O, S) groups are in the range from 163 ppm to 187 ppm.

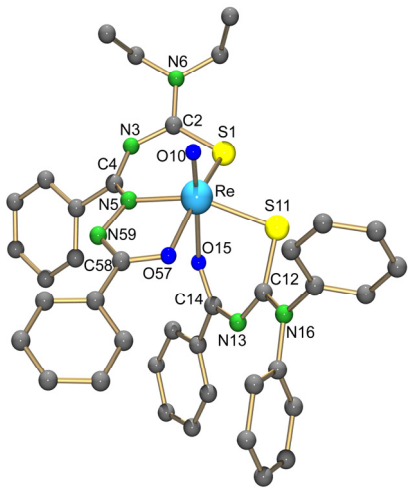

Figure 3.16 Molecular structure of [ReO(Ph_2btu)(L^2)] (**29a**). Hydrogen atoms were omitted for clarity.

Table 3.14 Selected bonds and angles in [ReO(L^4)(Ph_2btu)] **29a**

Bond lengths (Å)					
Re–O10	1.659(7)	Re –O15	2.249(6)	C4–N5	1.32(1)
Re–S1	2.313(2)	Re –S11	2.391(2)	C14–O15	1.26(1)
Re–N5	2.041(7)	S1–C2	1.75(1)	C2–N6	1.36(1)
Re–O57	2.043(5)	S11–C12	1.77(1)	C12–N16	1.35(1)
Angles (°)					
O10–Re –Sl	103.3(3)	O10–Re–N5	102.1(3)	O10–Re–O15	172.1(3)
O10–Re–S11	101.6(3)	O10–Re–O57	95.7(3)	O57–Re–S1	160.8(2)

Figure 3.16 depicts the molecular structures of the mixed-ligand complex **29a** as a representative of this type of complexes. Selected bond lengths and angles are given in Table 3.14. The rhenium atom exhibits a distorted octahedral coordination environment. Axial positions are occupied by an oxo ligand and the oxygen atom of the bidentate R^1R^2btu ligand. The tridentate benzamidine ligand occupies three positions of the equatorial coordination sphere and the remaining position accommodates the sulphur atom of the R^1R^2btu ligand. The Re atom is located slightly above [0.410 (2) Å] the mean least-square plane formed by the atoms S1, N5, O57 and S12 toward the oxo ligand. The Re=O distance of 1.659(7) Å is in the expected range of rhenium-oxygen double bonds. The remarkably long Re-O15 bond indicates a low degree of electron transfer from the oxo ligand in *trans* position. Similar observations have been made for mixed-ligand complexes of the type **20**.

3.1.6 Re and Tc Complexes with Benzamidines Derived from 4,4-Dialkylthiosemicarbazide (H_2L^5)

Thiosemicarbazones, which form stable complexes with many main group and transition metals [84], constantly attract the interest of chemists and pharmacists due to their remarkable biological and pharmacological properties such as antibacterial, antiviral, antineoplastic or antimalarial activities [85]. Modifications of the thiosemicarbazone framework, in order to find new compounds with higher activities and/or to tune their biological behavior, have been extensively studied, and relationships between the biological activity and chelate formation are evident in a number of cases [86]. This makes structural studies more interesting, which are the rational base for structure-activity relationships (SAR).

For that purpose, ligands of the class H_2L^5 were synthesized (Scheme 3.3 or 3.15). The ligands H_2L^5 can easily be modified by different substituents R^1 and R^2 of the thiosemicarbazide moiety. Additionally, variation of the dialkylamino group of the thiourea building block is possible and allows a smooth tuning of the molecular properties. Modification of the metal core (ReO^{3+} vs. ReN^{2+}) as well as of the ligand sphere gives other opportunities to study SAR's.

3.1.6.1 $Re^{V}O$ and $Tc^{V}O$ Complexes with H_2L^5

Surprisingly less is known about thiosemicarbazone complexes with rhenium and technetium. Particularly in the chemistry of the high oxidation states of these metals, the reducing capacity of thiosemicarbazones frequently makes reactions uncontrollable and ligand decomposition is observed. Hitherto, only one stable rhenium(V) oxo complex with 2-pyridine formamide thiosemicarbazone is structurally characterized [87].

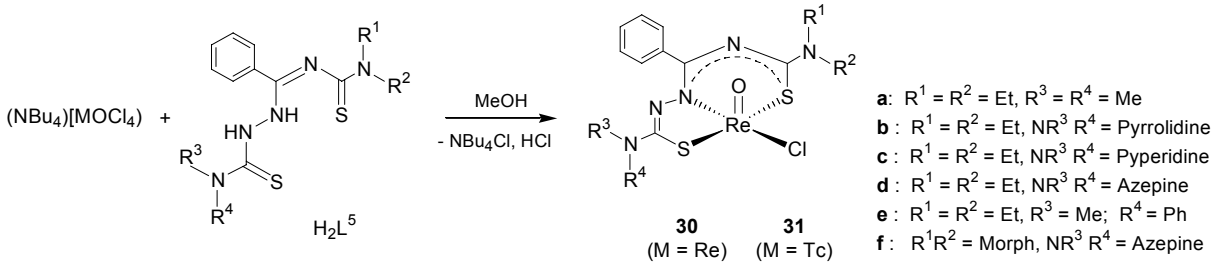

Scheme 3.15 Reactions of $(NBu_4)[MOCl_4]$ (M = Re, Tc) with H_2L^5.

Treatment of $(NBu_4)[MOCl_4]$ (M = Re, Tc) with an equivalent amount of H_2L^5 in methanol at room temperature affords red solids of the composition $[ReOCl(L^5)]$ (**30**) and $[TcOCl(L^5)]$ (**31**) in excellent yields (Scheme 3.15). The compounds are stable both in solution and in the solid state. Infrared spectra of complexes exhibit strong bathochromic shifts of the $\nu_{C=N}$ stretches of H_2L^5 to the region near 1520 cm^{-1}, which indicates chelate formation with a large degree of π-electron delocalization within the chelate rings. The absence of ν_{NH} bands indicates the expected double deprotonation of the ligands during complex formation. Intense bands appearing in the range between 957 and 983 cm^{-1} can be assigned to the Re=O and Tc=O vibrations [33,41]. ^1H NMR spectra of the complexes show, similar to the spectra of the uncoordinated thiosemicarbazones, two well-separated sets of signals for the ethyl groups or morpholine moiety of the thiourea unit and no hindered rotation effects for the C-NR^1R^2 moieties of thiosemicarbazide side. Mass spectra of the complexes do not show the molecular ion peak. The exchange of labile chloro ligands by the

solvent MeOH is observed in all spectra and intense peaks corresponding to the [M- HCl + MeOH +Na]$^+$ cations appear.

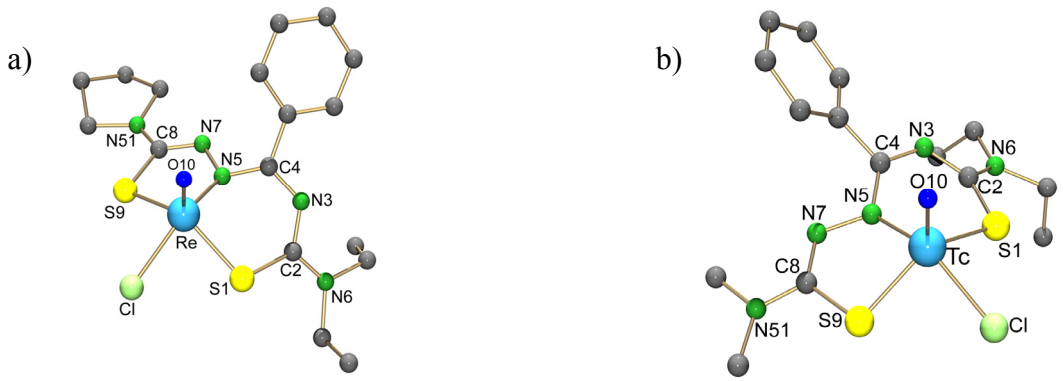

Figure 3.17 Molecular structures of a: [ReOCl(L^{5b})] (**30b**) and b: [TcOCl(L^{5a})] (**31a**). Hydrogen atoms were omitted for clarity.

Table 3.15 Selected bond lengths and angles of [ReOCl(L^{5b})] (**30b**) and [TcOCl(L^{5a})] (**31a**).

	30b	**31a**		**30b**	**31a**
Bond lengths (Å)					
M–O10	1.652(7)	1.646(3)	S1–C2	1.76(1)	1.749(5)
M–S1	2.307(2)	2.303(1)	C4–N5	1.36(1)	1.365(5)
M–N5	2.000(6)	1.996(3)	C2–N6	1.30(1)	1.324(6)
M–S9	2.283(2)	2.276(1)	N7–C8	1.27(1)	1.290(5)
M–Cl	2.364(2)	2.373(1)	C8–S9	1.778(9)	1.773(4)
Angles (°)					
O10–M–S1	111.8(3)	112.5(1)	O10–M–S9	112.8(3)	113.4(1)
O10–M–N5	106.4(3)	105.9(2)	O10–M–Cl	105.7(3)	105.6(1)
S1–M–S9	135.3(1)	133.9(1)	N5–M–Cl	147.7(2)	148.3(1)

Figure 3.17 represents the molecular structure of **30b** and **31a** as prototype compounds of the [MOCl(L^5)] complexes. Selected bond lengths and angles for these compounds are compared in Table 3.15. The coordination environments of the metal atoms are best described as distorted square-pyramids with the oxo ligands in apical positions. The basal planes are defined by the donor atoms of the tridentate ligands and a remaining chloro ligand. The metal atoms are situated by 0.715(2) for **30b** and 0.727(1) Å for **31a** above this plane towards the oxo ligands. All O10-M-X angles (X = equatorial donor atom) fall in the range between 103 and 113°. The M-O10 distances in the compounds are around 1.65 Å, which is within the expected range for a rhenium–oxygen and technetium-oxygen double bonds [33,41]. In the five-membered rings, the C8-N7 bonds, which fall into the range between 1.272(11) Å and 1.286(12) Å, have more double bond character than those in the uncoordinated thiosemicarba-

zones/thiosemicarbazides. While the C-S distances in H_2L^5 are almost equal, the C8-S9 bonds are a little longer than C2-S1 distances in the complexes. This accompanies the fact that the Re-S9 bond lengths are slightly shorter than Re-S1 distances. Nevertheless, the bonding situation of the ligands in the complexes is best discussed to be a borderline case between 'thiosemicarbazide-type' and 'thiosemicarbazone-type'.

The chloro ligand in the coordination spheres of the compounds of **30** is sufficiently labile to allow further ligand exchange. Thus, reactions of **30** with HR^1R^2btu, in CH_2Cl_2/MeOH mixtures under reflux afford the purple-red mixed-ligand complexes of the composition $[ReO(L^5)(R^1R^2btu)]$ (**32**) in excellent yields. The addition of a base such as NEt_3 supports the deprotonation of the benzoylthioureas. This is exemplarily demonstrated for the reactions with HPh_2btu (Scheme 3.16).

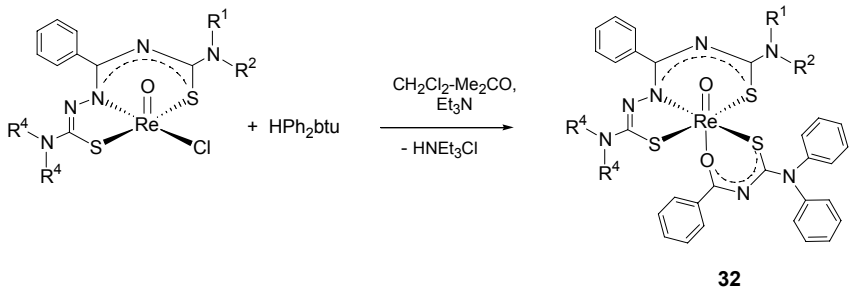

Scheme 3.16 Reactions of $[ReOCl(L^5)]$ 30 with HPh_2btu.

The IR spectra of **32** show bathochromic shifts of about 25 cm^{-1} for the Re=O bands. Mass spectra show the expected molecular ion peaks without any exchange and dissociation of ligands.

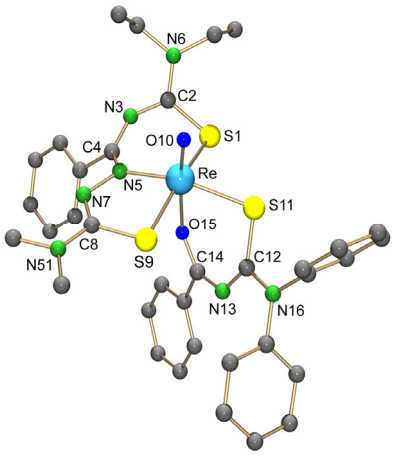

Figure 3.18 Molecular structure of $[ReO(L^{5a})(Ph_2btu)]$ (**32**). Hydrogen atoms were omitted for clarity.

Figure 3.18 depicts the molecular structure of $[ReO(L^{5a})(Ph_2btu)]$ (**32a**). The rhenium atom reveals a distorted octahedral coordination environment with an apical oxo ligand. The arrangement around the rhenium atom in **32a** is similar to that discussed for **20,** except that

the ligand $\{L^5\}^{2-}$, instead of $\{L^1\}^{2-}$, is accommodated in the equatorial plane. The remarkably long Re-O15 bond results from the *trans* influence of O^{2-} ligand and is also observed in **32a**. While the Re-S1 and Re-S9 bond lengths are almost equal, the Re-S11 bond distance is about 0.08 Å longer. The Re-O10 bond of 1.649(6) Å is in the expected range of rhenium-oxygen double bonds.

Table 3.16 Selected bond lengths and angles [ReO(L^{5a})(Ph_2btu)] (**32**)

Bond lengths (Å)					
Re–O10	1.649(6)	Re–S11	2.439(2)	N7–C8	1.29(1)
Re–S1	2.361(3)	Re–O15	2.221(6)	C8–S9	1.770(9)
Re–N5	2.025(7)	S1–C2	1.74(1)	S11–C12	1.75(1)
Re–S9	2.357(2)	C4–N5	1.36(1)	C14–O5	1.26(1)
Angles (°)					
O10–Re –Sl	99.4(3)	O10–Re–N5	103.5(3)	O10–Re–O15	172.9(3)
O10–Re–S11	95.6(2)	O10–Re–S9	97.5(2)	S9–Re–S1	163.0(1)

3.1.6.2 $Re^{V}N$ Complexes with H_2L^5

All complexes of the type **30** are distinguished by the substituents R^3 and R^4 of the thiosemicarbazide side or the R^1 and R^2 of the thiourea residues (**30f**). The replacement of the oxo ligand "O^{2-}" by a nitrido ligand "N^{3-}", however, gives access to a completely new class of rhenium(V) complexes with the novel ligands, and thus the opportunity to study the biological properties of the ligands in another coordination environment.

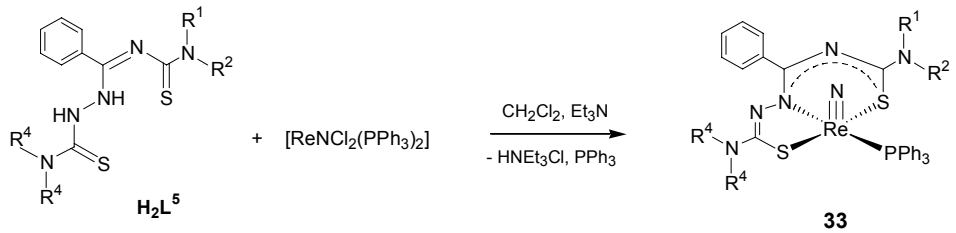

Scheme 3.17 Reactions of $[ReNCl_2(PPh_3)_2]$ with H_2L^5.

$[ReNCl_2(PPh_3)_2]$ is a common Re(V) nitrido starting material (Scheme 3.17). The compound is sparingly soluble in organic solvents. However, it slowly dissolves under formation of deep red solutions, when solutions of H_2L^5 in CH_2Cl_2 are stirred at room temperature. The addition of a supporting base like Et_3N accelerates the consumption of

$[ReNCl_2(PPh_3)_2]$ and yields products of the composition $[Re(N)(L^5)(PPh_3)]$ (**33**). The complexes were studied by common spectroscopic methods. The IR spectra of the products reveal strong bathochromic shifts of the $\nu_{C=N}$ bands and the absence of ν_{NH} absorptions, which indicates the expected formation of dianionic ligands. ^{1}H NMR spectra of **33** have the same patterns as discussed for the corresponding complexes **30**, except that additionally poorly resolved resonances of triphenylphosphine ligands are present. The presence of coordinated PPh_3 is also confirmed by singlets in the region around 33 ppm in the $^{31}P\{H\}$ NMR spectra. The mass spectra of **33** exhibit intense molecular ion peaks with the expected isotopic patterns for $^{185/187}$Re.

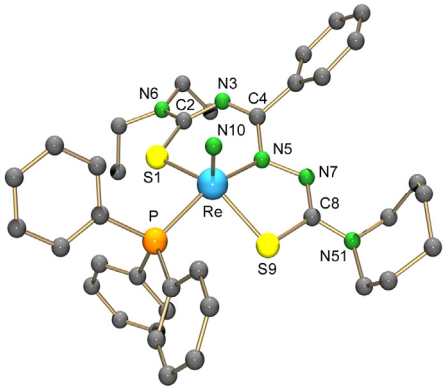

Figure 3.19 Molecular structure of $[Re(N)(L^{5d})(PPh_3)]$ (**33d**). Hydrogen atoms were omitted for clarity.

Table 3.17 Selected bond lengths and angles in $[Re(N)(L^{5d})(PPh_3)]$ (**33d**)

Bond lengths (Å)					
Re–N10	1.658(5)	Re–S9	2.330(1)	C4–N5	1.326(7)
Re–S1	2.339(1)	Re–P	2.397(1)	N7–C8	1.291(7)
Re–N5	2.082(4)	S1–C2	1.752(6)	C8–S9	1.779(6)
Angles (°)					
O10–Re–S1	108.6(2)	O10–Re–S9	109.5(2)	S1–Re–S9	141.9(1)
7O10–Re–N5	106.9(2)	O10–Re–P	97.4(2)	N5–Re–P	155.4(1)

Single crystals of **33d**, which were suitable for X-ray structure analysis, were obtained by slow evaporation of a CH_2Cl_2/MeOH solution of the compound. Figure 3.19 illustrates the molecular structure of **33d**. Selected bond lengths and angles are presented in Table 3.17. The rhenium atom is coordinated in a distorted square-pyramidal environment with a nitrido ligand in the apical position. The tridentate ligand $(L^{5d})^{2-}$ is arranged in the equatorial plane and binds to the rhenium atom via the atoms S1, N5 and S9, as has been observed in the oxo complexes **30**. The remaining equatorial coordination position is occupied by a PPh_3 ligand. The Re atom lies about 0.615(1) Å above this plane towards the nitrido ligand. The Re-N10 bond distance of 1.658(5) Å is in the expected range of Re≡N triple bonds. The bonding

situation of the chelate ring of $(L^{5d})^{2-}$ in **33d** is similar to that discussed for the complexes of type **30**. All Re–S and Re–N bonds in **33d** are slightly longer than those in the corresponding oxo complex **30d**, indicating that the transfer of electron density from the organic ligand to the metal ion is slightly less in the nitrido species than in the oxo compounds. This is not unexpected in the light that the nitrido ligand is a stronger π donor than the oxo ligand.[33]

3.1.6.3 Biological Activity Tests for Re Complexes with H_2L^5

With the novel thiosemicarbazones H_2L^5, their oxo complexes [ReOCl(L^5)] (**30**), the mixed ligand complexes [ReOCl(L^5)(Ph_2btu)] (**32**) and corresponding nitrido complexes [ReN(L^1)(PPh_3)] (**33**), there exists a series of familiar compounds, which is worth to be studied for their biological activity. In order to obtain a first overview about the influence of the individual residues in the molecular framework of the thiosemicarbazones, we have first modified R^1 and R^2 (compounds H_2L^{5d} and H_2L^{5f}). Since first tests showed a similar behaviour for such representatives, a larger number of compounds were prepared under modification of the residues R^3 and R^4 (compounds H_2L^{5a} to H_2L^{5e}) and their corresponding rhenium complexes. The use of different coordination environments in the metal complexes may allow an insight into the mechanism of potential activity.

Table 3.18 Cytotoxic effects of H_2L^5 and complexes [ReOCl(L)] against MCF-7 breast cancer cells

					IC_{50} [μM]	
	R_1	**R_2**	**R_3**	**R_4**	**Ligand**	**[ReOCl(L)]**
H_2L^{5a}	Et	Et	CH_3	CH_3	0.23	0.15
H_2L^{5b}	Et	Et	$(CH_2)_4$		2.19	2.50
H_2L^{5c}	Et	Et	$(CH_2)_5$		0.14	1.12
H_2L^{5d}	Et	Et	$(CH_2)_6$		2.43	1.25
H_2L^{5e}	Et	Et	CH_3	C_6H_5	0.85	0.40
H_2L^{5f}	morpholinyl		$(CH_2)_6$		0.73	4.41

Thiosemicarbazones exhibit various biological activities and have therefore attracted considerable pharmaceutical interest. Several mechanisms of antitumor action were proposed and compelled the interest of an SAR study. Furthermore, it is well known that the cytotoxic properties of the compounds are influenced by the chelation. In many cases, an increased activity of the metal complexes is observed, which is assumed to be an effect of a metal-assisted transport, while complex dissociation inside the cell releases the thiosemicarbazones

as the biologically active species [86d]. Thus, the antiproliferative effects of the ligands H_2L^5 were investigated in relation to their rhenium complexes in a time responds as well as in a concentration responds assay. From the first study the responds of the cells to the compounds can be estimated, while the latter allows the calculation of IC_{50} values (Table 3.17).

The thiosemicarbazone H_2L^{5a} causes a strong reduction of the cell growth. The maximum activity was already detected after an incubation time of 48h (Figure 3.20). At the concentrations of 1.25 to 10 µM cytocidal effects were determined. The rising recuperation of the cells at lower concentrations is characteristic for developed resistance. The time responds curve of cisplatin is quite different, with a maximum cytotoxicity appearing not before an incubation time of more than 100 h. All compounds H_2L^5 show this interesting behaviour and comparable time responds curves, which allowed the comparison of IC_{50} values (after an incubation time of 48h, see Table 3.18).

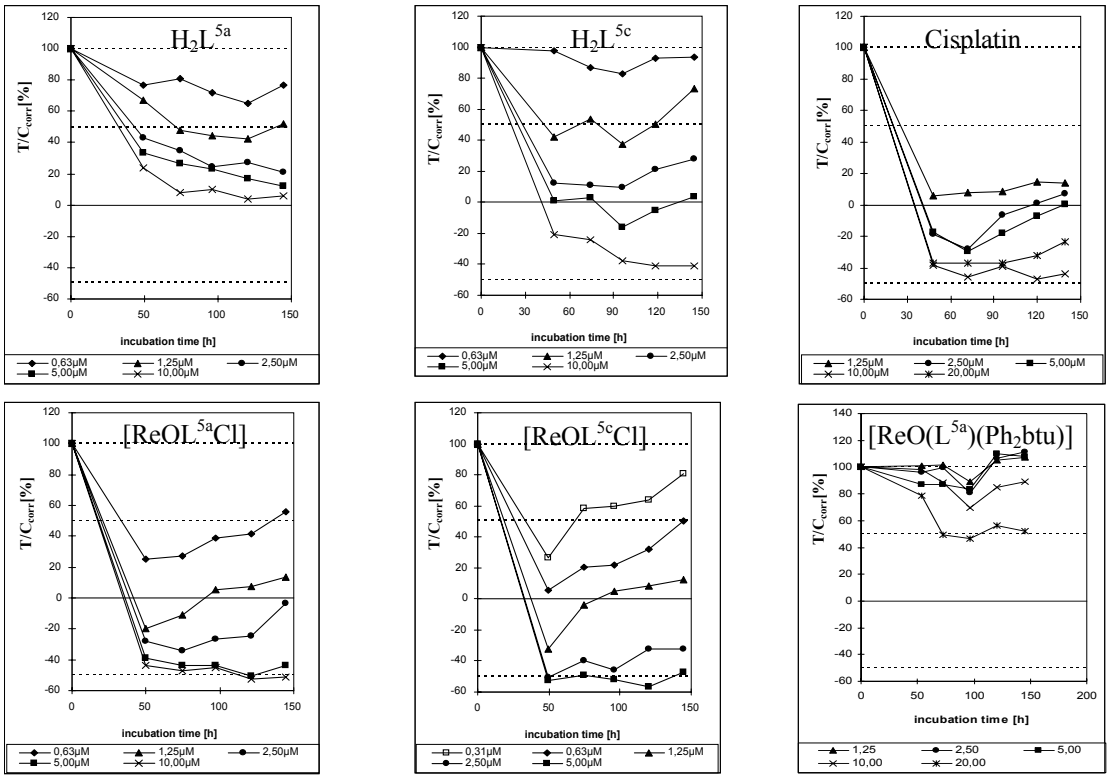

Figure 3.20. Cytotoxic effects of selected ligands and complexes.

The degree of cytotoxicity can be influenced by the variation of the peripheral substituents R^1 and R^2 as well as R^3 and R^4. The IC_{50} value of H_2L^{5a} amounts to 0.23 µM. The exchange of an N-methyl group by R^4 = phenyl (H_2L^{5e}: IC_{50} = 0.85 µM) or the exchange of the N,N-dimethyl group by pyrrolidine (H_2L^{5b}: IC_{50} = 2.19 µM) reduced the cytotoxicity. Interestingly, the ring size (5-membered ring to 7-membered ring) determined the antiproliferative effects. The IC_{50} value of the piperidine derivative H_2L^{5c} (0.14 µM) is lower than that of H_2L^{5b} and

H_2L^{5a}, while that of the azepine derivative H_2L^{5d} was comparable to H_2L^{5b}. Finally, the exchange of the N,N-diethyl moiety of H_2L^{5d} by morpholine increased the cytotoxicity (H_2L^{5f}: IC_{50} = 0.73 μM).

After coordination of the ligands to an oxorhenium(V) centre, no clear trend in biological activity was observed. All [ReOCl(L^5)] complexes show significant toxic effects. In the case of [ReOCl(L^{5a})], and [ReOCl(L^{5d})], the cytotoxicities increased with respect to those of the non-coordinated thiosemicarbazones, while that of ReOCl(L^{5b}) remained essentially unchanged. The effects of [ReOCl(L^{5c})] and [ReOCl(L^{5f})], however, were lower than that of the corresponding thiosemicarbazones.

A participation of the metal on the antiproliferative effect can not be unequivocally deduced from these data. On the one hand, a simple dissociative mechanism, where the antiproliferative activity is mainly determined by the released thiosemicarbazones and the previous coordination has only a marginal influence can be excluded with regard to the biological behaviour of the nitridorhenium(V) complexes **33** and mixed ligand complexes **32**. The exchange of the "O^{2-}" by a nitrido "N^{3-}" ligand and the chloro ligand by a triphenylphosphine completely terminated the cytotoxicity of the complexes, which should not be expected after rapid intracellular dissociation. The complexes **33** were even inactive at the highest concentration used (20 μM). A steric repulsion from possible targets due to the voluminous triphenylphosphine ligand can not be excluded. More interestingly, the substitution of labile chloro ligand by a ligand, which is strongly bonded to the rhenium center like the bidentate HPh_2btu also reduced the cytotoxicity of the complexes **32** significantly (Figure 3.20). This means the chloro ligand in the ligand sphere of complexes **30** plays a key role for their cytotoxicity. We suppose that in the extracellular, the labile chloro ligands of the compounds **30** are firstly exchanged by functional groups of compartment proteins which lead to a strong protein bonding. These metal loaded proteins are carried through the cell membrane by protein transporters. The different mechanisms of transportation of free ligands H_2L^5 and rhenium complexes **30** into the cell can explain the unclear relationship of their cytotoxicities.

3.1.7 Summary and Conclusions

Various tridentate benzamidines, which are potential dianionic ligands such as H_2L^1, $H_2L^{3\text{-}5}$ or a monoanionic ligand like HL^2, have been successfully synthesized from reactions of N,N dialkylaminothiocarbonyl benzimidoyl chlorides and functionalized primary amines as well as hydrazine derivatives.

The dianionic ligands (H_2L^1, H_2L^4 and H_2L^5) are suitable to stabilize both monooxo and nitrido cores of rhenium and technetium, and to form complexes of the general composition $[MO(L^{1,4,5})Cl]$ and $[MN(L^{1,4,5})PPh_3]$. In all cases, the organic ligands are favourably equatorially coordinated to metal cores. The chloro ligand in the coordination sphere of complexes $[MO(L^{1,4,5})Cl]$ is labile and can be solvolized (hydrolysed) or exchanged by bidentate ligands such as Hgly or HR^1R^2btu under formation of mixed ligand complexes.

The ligand H_2L^3 prefers the formation of a dimeric compound **26** via the additional donor oxygen atom of carboxylic group, while the formation of the dimeric complex **25** of H_2L^2 is due to charge compensation.

The ligands H_2L^5 and their rhenium(V) oxo complexes **30** show high cytotoxicity against breast cancer cell. However, the activities of the corresponding mixed ligand complexes **32** are significantly decreased and the nitrido complexes **33** do not show any cytotoxic activities.

3.2 Tetradentate Benzamidines and Their Rhenium and Technetium Complexes

Tetradentate ligands are known as common chelator systems in the radiopharmaceutical chemistry of the elements rhenium and technetium. They form thermodynamically stable and kinetically inert complexes with common metal cores such as M^V=O [88], M^V=NR [89] and M^V≡N [90]. Thus, we find for example tetradentate chelators such as the hexamethyl-propylene amineoxime (HMPAO) ligand [8], the ethylene-bridged ethylcysteinate dimer (ECD) [6] or mercaptoacetyl triglycinate (MAG-3) [6] in standard kits of commercial technetium radiopharmaceuticals for brain (HMPAO, ECD) or kidney imaging (Scheme 3.18).

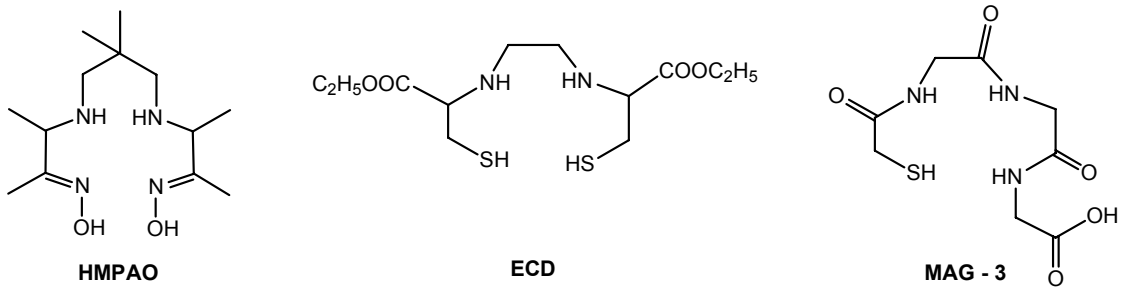

Scheme 3.18 Some chelator systems used in commercial technetium radiopharmaceuticals.

Additionally, modifications of the ligand periphery of tetradentate systems in many cases are not complicated compared to penta- or hexadentate ligands. This allows tuning of the chemical and physical properties of the complexes, and may explain the large number of technetium complexes with tetradentate systems, which are currently used in clinics [6] or are under consideration for new radiopharmaceuticals [91].

In the following section, the synthesis of some new tetradentate benzamidines and their complexes with rhenium and technetium are described. Such ligands can be synthesized by two alternative routes: reactions of R^1R^2bzm-Cl with diamines or with tridentate ligands having a NH_2 donor group (Scheme 3.19).

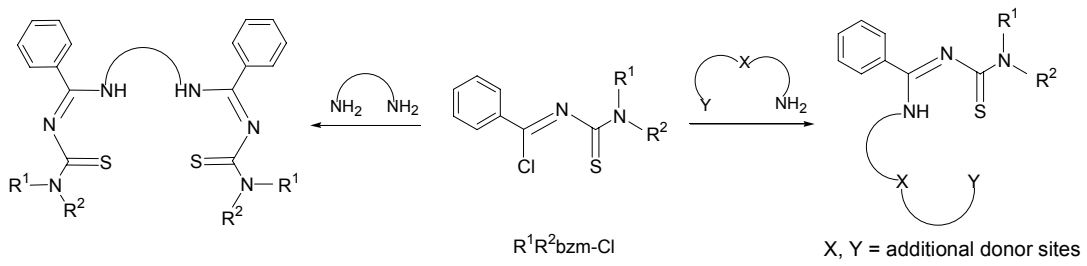

Scheme 3.19 The synthesis of tetradentate benzamidines.

3.2.1 Benzamidines Derived from o-Phenylenediamine (H_2L^6) and their Re and Tc Complexes

3.2.1.1 Synthesis of H_2L^6

Symmetric tetradentate benzamidine ligands (H_2L^6), which were synthesized from R^1R^2bzm-Cl and o-phenylenediamine in acetone, were previously reported by Beyer et al. [14]. However, the authors could not isolate pure products directly from the reaction mixtures. More pure compounds they obtained later by the decomposition of [NiL^6] complexes, which were prepared by template reactions from R^1R^2bzm-Cl, o-phenylenediamine and $[Ni(BF_4)_2]\cdot 6H_2O$ in MeOH [92].

Interestingly, R^1R^2bzm-Cl reacts with o-phenylenediamine in THF in a cleaner way and pure ligands H_2L^6 can be isolated with reasonable yields. The products were characterized by standard spectroscopic methods.

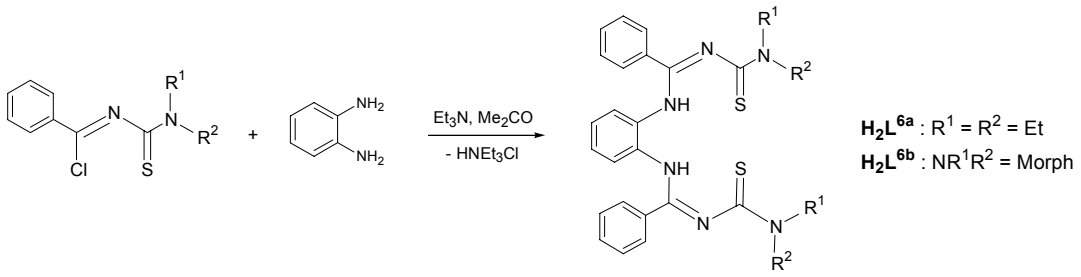

Scheme 3.20 The synthesis of H_2L^6.

IR spectra of H_2L^6 exhibit a medium absorption around 3250 cm^{-1} and a very strong band in the region of 1640 cm^{-1}, which are assigned to ν_{NH} and $\nu_{C=N}$ stretches respectively. ^1H NMR spectra confirm the symmetric structure of the products. Thus, the resonances of the aromatic protons of the o-phenylenediamine residue appear as two doublets at around 6.40 ppm and 6.80 ppm. Two series of signals corresponding to alkyl groups of the NR^1R^2 residues are also observed, but are less resolved, which reflects the hindered rotation of the thiourea moiety.

3.2.1.2 Re^VO Complexes with H_2L^6

Despite the fact that the ligand H_2L^6 was reported very early, its coordination chemistry is less explored, and only complexes of Ni^{2+} and Cu^{2+} are known [14,92]. The X-ray structures of these complexes reveal the coordinated H_2L^6 as planar tetradentate and double deprotonated N_2S_2-chelators [14].

H_2L^{6a} reacts with $(NBu_4)[ReOCl_4]$ in MeOH under formation of a red crystalline precipitate of the composition $[ReO(L^{6a})(ReO_4)]$ (**34**) (Scheme 3.21). The yield is only about 30 %, which can be explained by the rapid formation of the perrhenate unit. Such side-reactions are not very unusual [93] and were previously found as results of hydrolysis followed by disproportion of the anionic complex $[ReOCl_4]^-$ (to ReO_2 and ReO_4^- species) [33]. This finally results in low yields in the complex formation reactions.

The IR spectrum of **34** shows no band in the region above 3100 cm^{-1}, which could be assigned to an NH stretch, and the intense $\nu_{C=N}$ absorption is strongly shifted by 120 cm^{-1} to longer wavelengths. This indicates the expected double deprotonation and chelate formation of the ligand. While the terminal {Re=O} core is indicated by a medium absorption at 983 cm^{-1}, the presence of coordinated ReO_4^- is confirmed by a very strong absorption at 921 cm^{-1} corresponding to a hypsochromic shift of the Re=O absorption by about 15 cm^{-1} compared to that in the perrhenate anion [94]. The ^1H NMR spectrum of **34** reveals its symmetric structure, in which two benzamidine parts are magnetically equivalent and, thus, a planar coordination mode of $\{L^{6a}\}^{2-}$ is suggested. As the consequence of hindered rotation around the C-N bonds in the C(S)-NEt_2 moieties and the earlier discussed inflexible structure, two well resolved triplets of two ethyl groups and four multiplets corresponding to four methylene protons are observed. The FAB^+ MS spectrum of **34** does not show the molecular ion peak, but exposes the intense fragment $[ReO(L^{6a})]^+$ (m/z = 745) with an expected isotope distribution. This confirms the weakness of the bond to ReO_4^- and the ready dissociation of this ligand. In the FAB^- MS spectrum, a peak corresponding to the $[ReO_4]^-$ anion (m/z = 251) is observed.

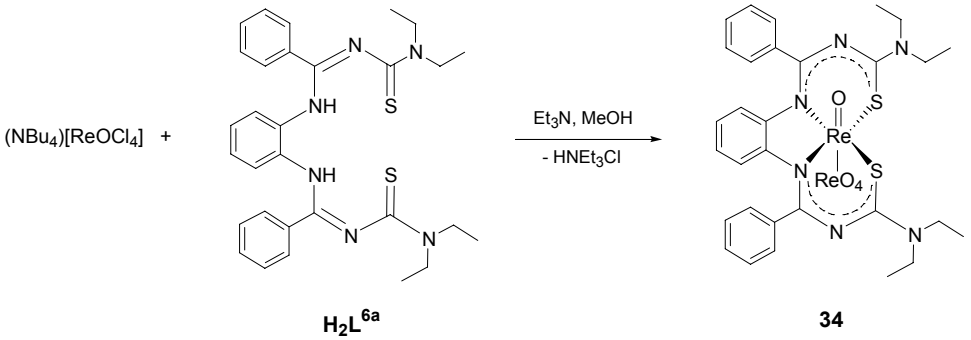

Scheme 3.21 Reaction of H_2L^{6a} with $(NBu_4)[ReOCl_4]$.

The spectroscopic analysis of **34** is additionally confirmed by the results of an X-ray structure determination. Figure 3.21 depicts the molecular structure of **34** and selected bond lengths and angles are presented in Table 3.19. The rhenium atom is coordinated in a distorted octahedral environment with a terminal oxo ligand and a perrhenato unit in axial positions. The $[L^{6a}]^{2-}$ is arranged in the equatorial plane and binds symmetrically to the rhenium atom as

a $\{N_2S_2\}$ tetradentate ligand. The Re atom is placed 0.422(4) Å above this plane towards the oxo ligand. In this arrangement, all phenyl rings are bent out of the equatorial plane.

While the Re1–O10 bond length of 1.692(8) Å falls within the range of rhenium-oxygen double bonds, the Re1–O20 distance of 2.327(9) Å is much longer than a typical rhenium-oxygen single bond and reflects only a weak interaction between the perrhenato ligand and the Re atom of the chelate. Consequently, the Re2–O20 distance is only a little longer than those of the other Re-O bonds in the perrhenato unit.

Table 3.19 Selected bond lengths and angles in [ReO(L^{6a})(ReO_4)] (**34**)

Bond lengths (Å)			
Re1–O10	1.692(8)	Re2–O20	1.682(9)
Re1–O20	2.327(9)	Re2–O30	1.65(2)
Re1–S1/S11	2.362(3) / 2.360(3)	Re2–O40	1.671(1)
Re1–N5/N15	2.032(9) / 2.015(9)	Re2–O50	1.65(3)
S1–C2/S11–C12	1.75(1) / 1.75(1)	C4–N5/C14–N15	1.36(1) / 1.37(1)
C2–N3/ C12–N13	1.35(1) / 1.36(1)	C2–N6/ C12–N16	1.31(1) / 1.30(1)
Angles (°)			
O10–Re1–S1/S11	100.5(3)/ 101.5(3)	O10–Re1–O20	178.9(4)
O10–Re1–N5/N15	100.5(4)/ 102.1(4)	Re1–O20–Re2	166.9(6)

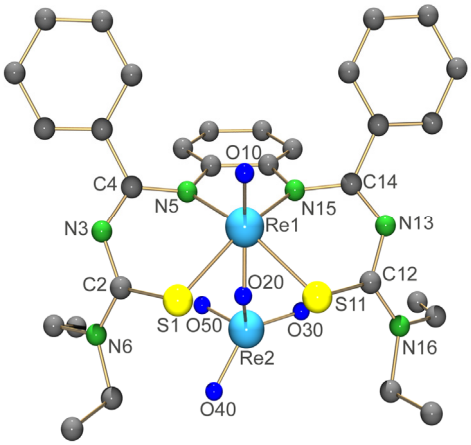

Figure 3.21 Molecular structure of [ReO(L^{6a})(ReO_4)] (**34**). Hydrogen atoms were omitted for clarity.

In order to prevent the undesired formation of $[ReO_4]^-$, the synthetic procedure was modified slightly. The supporting base was added just after refluxing the mixture of $(NBu_4)[ReOCl_4]$ and one equivalent of H_2L^{6b} in MeOH for a few minutes. A red solid of the composition $[\{ReOL^{6b}\}_2O]$ (**35**) precipitated directly from the reaction mixture and was isolated in high yield (Scheme 3.22).

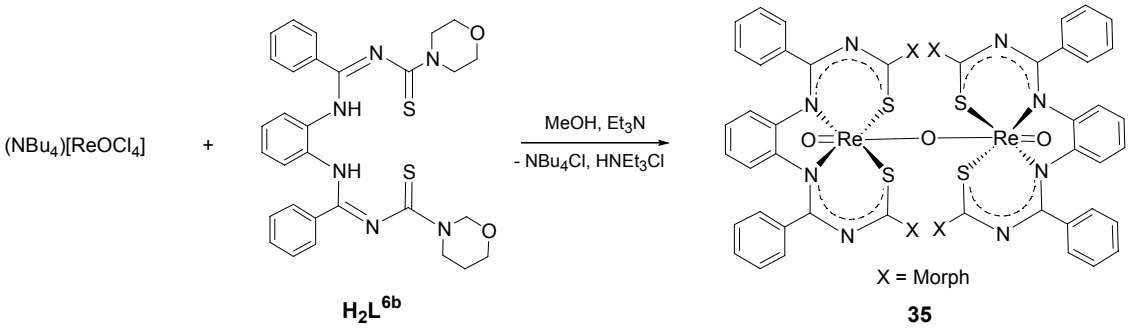

H_2L^{6b} **35**

Scheme 3.22 Reaction of H_2L^{6b} with $(NBu_4)[ReOCl_4]$.

The X-ray quality single crystals of **35** were obtained by slow evaporation of a CH_2Cl_2-Me_2CO solution. Figure 3.22 presents the dimeric structure of **35** and selected bond lengths and angles are listed in Table 3.20. In both units of the dimeric compound **35**, the Re atoms possess a distorted octahedral environment with the two oxo ligands in *trans* position to each other. The four positions in the equatorial plane are occupied by the donor atoms S1, N5, S11 and N15 of $(L^{6b})^{2-}$. The bridging oxygen atom is placed on a glide and the second unit of the molecule is symmetry generated. However, the two rhenium atoms and the bridging oxygen atom are not linear; the angle Re1-O20-Re2 is 175.5(8)°. Due to the interaction between the two units, the aromatic ring of the phenylendiamine unit is pulled far from the other unit and has less distortion from the equatorial plane than that in **34**. The Re-O20 bond distance of 1.921(1) Å is shorter than a normal rhenium-oxygen single bond reflecting some double bond character. This is due to the transfer of electron density from the terminal oxo ligand. This also agrees with the lengthening of the Re1-O10 bond by about 0.05 Å compared to the corresponding distance in **34** and brings the Re atom closer to the basal plane with a distance of 0.141(4) Å.

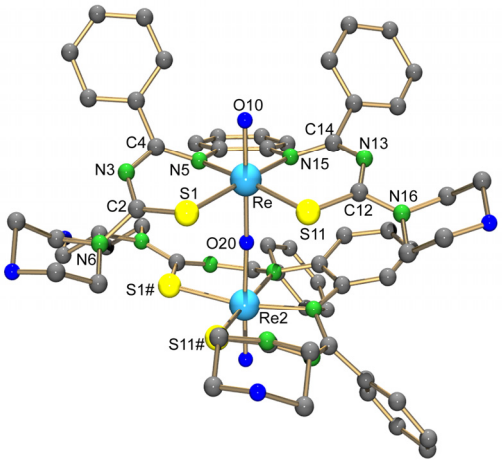

Figure 3.22 Molecular structure of $[\{ReO(L^{6b})\}_2O]$ (**35**). Hydrogen atoms were omitted for clarity.

Table 3.20 Selected bond lengths and angles in [{ReO(L^{6b})}$_2$O] (**35**)

Bond lengths (Å)			
Re1–O10	1.740(1)	S1–C2 / S11–C12	1.72(2) / 1.74(1)
Re1–O20	1.919(1)	N3–C4 / N13–C14	1.34(2) / 1.34(2)
Re1–S1/S11	2.378(4) / 2.375(4)	C4–N5 / C14–N15	1.35(2) / 1.33(2)
Re1–N5/N15	2.074(1) / 2.12(1)	C2–N6 / C12–N16	1.40(2) / 1.37(2)
Angles (°)			
O10–Re1–S1/S11	94.3(4) / 95.9(4)	O10–Re1–O20	177.1(5)
O10–Re1–N5/N15	92.7(5) / 91.5(4)	Re1–O20–Re2	175.5(8)

With such a high symmetric structure, the ^{1}H NMR spectrum of **35** should be simple, with resonances of half of the $(L^{6b})^{2-}$ ligand. However, such an expectation is not right. For instance, the CH_2 signals of the morpholine moieties appear as an overlapping complex array with very poor resolution and four different signals corresponding to the aromatic protons of the phenylendiamine residues are observed. This may be the result of the hindered rotation around the Re1-O20-Re2 bonds which makes two halfs of $(L^{6b})^{2-}$ in each monomer magnetically not equivalent. The FAB^+ MS spectrum does not show the molecular ion peak. However, a low intense peak corresponding to $[ReO_2(L^{6b})]^+$ can be found. The most intense peak was assigned tor the fragment cation $[ReO(L^{6b})]^+$.

3.2.1.3 Re^VN and Tc^VN Complexes with H_2L^6

The tetradenate H_2L^6 ligand which potentially forms two six-membered chelate rings together with one five-membered chelate ring can act as a doubly deprotonated ligand and prefers a planar coordination sphere. In this context, $\{L^6\}^{2-}$ can stabilize the $\{ReO\}^{3+}$ core in two different steps. The first is the formation of a square pyramidal cation, $[ReO(L^6)]^+$, which has not yet been isolated. Secondly, $[ReO(L^6)]^+$ can achieve a charge compensation by the formation of octahedral neutral compounds of the type $[ReOX(L^6)]$, where X is a single negative, monodentate ligand as in **34** or by the formation of dimeric complexes like **35**. With the $\{M^VN\}^{2+}$ (M = Re, Tc) cores, however, $\{L^6\}^{2-}$ should favorably form five-coordinate, neutral complexes. Square pyramid is the most common geometry in rhenium(V) and technetium(V) nitrido coordination chemistry due to the strong *trans* influence of the $\{N\}^{3-}$ ligand.

Reactions of H_2L^{6b} with rhenium or technetium nitrido starting materials such as $[M(N)Cl_2(PPh_3)_2]$ (M = Re, Tc) proceed very slowly in CH_2Cl_2 even under reflux. At room

temperature, however, the addition of a supporting base like Et_3N results in a fast consumption of the sparingly soluble precursors and the formation of clear red solutions from which red crystalline solids of the compositions [M(N)(L^{6b})] [where M = Re (**36**), Tc(**37**)] were isolated in high yields (Scheme 3.23).

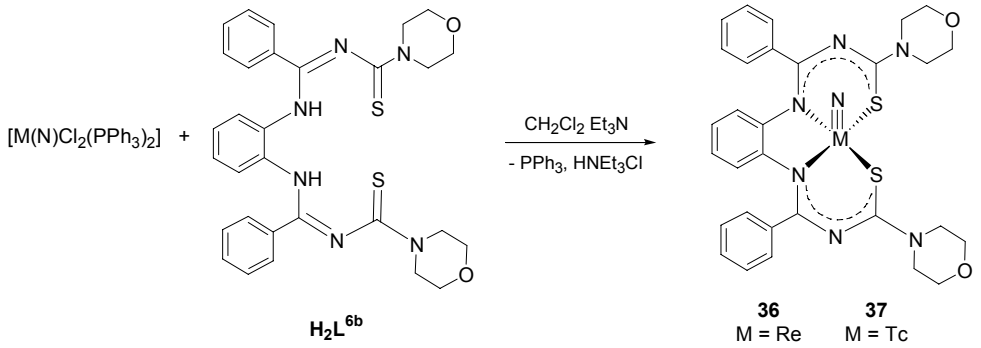

Scheme 3.23 Reactions of H_2L^{6b} with $[M(N)Cl_2(PPh_3)_2]$ (M = Re, Tc).

The double deprotonation of the coordinated ligand $\{L^{6b}\}^{2-}$ in **36** and **37** is indicated by the disappearance of absorptions above 3100 cm^{-1} corresponding to N-H stretches, and strong bathochromical shifts of the $\nu_{C=N}$ bands in the IR spectra. ^1H NMR spectra of these compounds confirm the expected symmetric arrangement of $\{L^{6b}\}^{2-}$. The resonances of the morpholinyl residue are less resolved and the signals of protons in the phenylenediamine moiety are slightly shifted to lower field compared to those in the spectrum of the oxo complex **34**. The ESI MS spectrum of **36** exhibits an intense molecular ion peak with the required isotopic pattern.

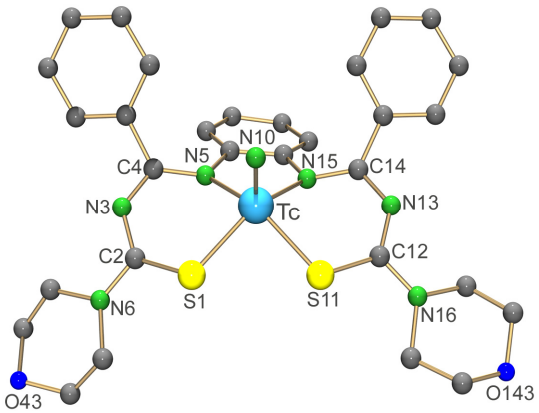

Figure 3.23 Molecular structure of [Tc(N)(L^{6b})] (**37**). Hydrogen atoms were omitted for clarity.

Single crystal X-ray diffraction studies additionally confirm the isostructures of **36** and **37**. Figure 3.23 illustrates the molecular structure of **37** as representative of the compounds. Selected bond lengths and angles of **36** and **37** are compared in Table 3.21. As expected, the metal atoms reveal a distorted square-pyramidal arrangement with a nitrido ligand in the apical position. The basal plane formed by the four donor atoms of $\{L^{6b}\}^{2-}$ is only slightly

distorted with a maximal deviation from the mean least-square plane by about 0.024 Å for S11. The metal atoms are situated 0.573(3) Å for **36** and 0.598(3) Å for **37** above this plane towards the nitrido ligand. The M-N10 bond lengths of 1.649(8) Å and 1.604(8) Å in **36** and **37**, respectively, fall in the expected range of rhenium-nitrogen and technetium-nitrogen triple bonds.

Table 3.20 Selected bond lengths and angles in [Tc(N)(L^{6b})] (**37**)

	36	**37**		**36**	**37**
Bond lengths (Å)					
M–N10	1.649(8)	1.604(8)	C2–N6	1.37(2)	1.34(1)
M–S1	2.349(2)	2.355(2)	C4–N5	1.35(1)	1.36(1)
M–S11	2.356(2)	2.361(2)	S11–C12	1.752(9)	1.72(1)
M–N5	2.077(6)	2.092(8)	C12–N16	1.35(1)	1.34(1)
M–N15	2.083(6)	2.053(8)	C14–N15	1.36(1)	1.35(1)
S1–C2	1.745(9)	1.74(1)			
Angles (°)					
N10–M–S1	104.1(3)	105.1(3)	N10–M–S11	104.2(3)	104.9(3)
N10–M–N5	104.8(3)	105.7(4)	N10–M–N15	107.2(3)	107.2(4)
S11–M–N5	150.8(2)	149.2(2)	S1–M–N15	148.6(2)	147.6(2)

3.2.2 Benzamidines Derived from o-Aminoacetophenon 4-Methylthiosemicarbazone (H_2L^7) and their Re and Tc Complexes

3.2.2.1 Synthesis of H_2L^7

The success of the rhenium and technetium chemistry with H_2L^5 ligands stimulated the designing of a tetradentate benzamidine containing thiosemicarbazone-type ligand. Thus, the reaction of benzimidoyl chloride and a tridentate thiosemicarbazone containing an additional amino donor group, like o-aminoacetophenon 4-methylthiosemicarbazone (**II**), was carried out.

In the synthesis of the benzamidines described above, acetone was frequently used as solvent. However, due to the reaction of aminoacetophenone and 4-methylthiosemicarbazide with H_2SO_4 as catalyst [95], compound **II** contains a small amount of its sulfate salt. This can catalyze the condensation between the amino group of **II** and acetone. In order to avoid this undesired side-reaction, dry EtOH was used instead of acetone for the preparation of the

ligand H_2L^7. Although $Et_3N{\cdot}HCl$ does not precipitate in this case, the progress of the reaction can easily be controlled by thin layer chromatography, and the ligand H_2L^7 precipitates directly from the reaction mixture as a pure yellow powder (Scheme 3.24).

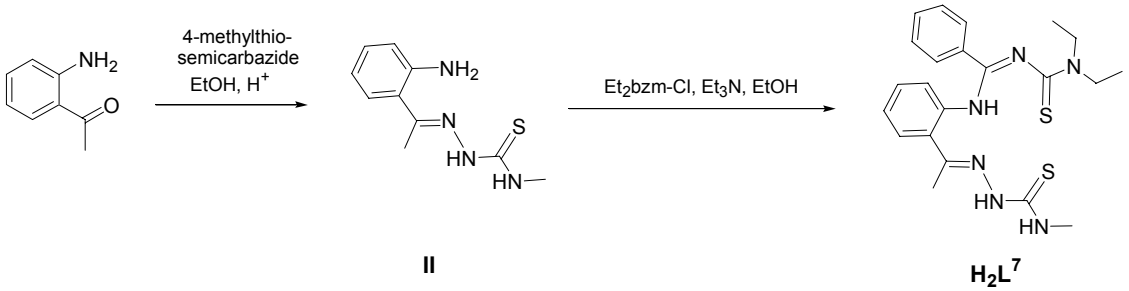

Scheme 3.24 Synthesis of H_2L^7.

The IR spectrum of H_2L^7 is characterized by broad bands of the N-H vibrations in the region around 3200 cm^{-1} and sharp, intense absorptions at 1717 cm^{-1} and 1686 cm^{-1} which are assigned to the C=N stretches. In the ^1H NMR spectrum, three different N-H resonances at 7.64 ppm, 8.41 ppm and 12.62 ppm can be observed. The hindered rotation around the C-NEt_2 bond is indicated by two well resolved signal sets of ethyl groups, while the similar C-NHMe bond of the thiosemicarbazone unit is flexible enough to give only one methyl signal at 3.08 ppm.

3.2.2.2 A Re^VO Complex with H_2L^7

Tetradentate ligands, especially with the N_2S_2 donor set, are among the most common chelators for rhenium(V) and technetium(V) oxo cores. In most of the cases, however, the S donor atoms belong to thiol groups. Hitherto, no rhenium and technetium complex with a tetradentate ligand containing an S donor site derived from a thiourea or a thiosemicarbazone moiety has been published.

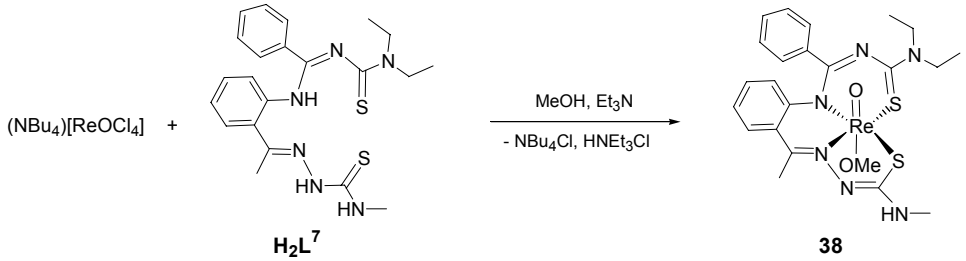

Scheme 3.25 Reaction of H_2L^7 with $(NBu_4)[ReOCl_4]$.

H_2L^7 reacts with $(NBu_4)[ReOCl_4]$ in MeOH in the presence of the supporting base Et_3N under formation of a red crystalline solid of the composition $[ReO(OMe)(L^7)]$ (**38**) in high

yields (Scheme 3.25). The reaction can be carried out at room temperature or under reflux without significant change in the yield.

In the IR spectrum of **38** remains a sharp medium absorption band of the N-H stretch at 3387 cm^{-1}. A strong bathochromical shift of $\nu_{C=N}$ reflects the expected chelate formation with a large delocalization of π-electron density. The strong absorption of the Re=O vibration appears at 941 cm^{-1}, which is within the typical range for *trans* oxo/alkoxo rhenium complexes [35]. In the ^{1}H NMR spectrum of **38,** the absence of two N-H resonances and a high field shift of the other N-H signal in the CS-NHMe moiety to 5.26 ppm are observed. This reflects that the organic ligand is coordinated to Re in the form $\{L^{7}\}^{2-}$. Furthermore, the chelate formation leads to a strong downfield shift of about 1.1 ppm of the Me-C=N signal. The presence of a methoxy group in **38** is clearly shown by an additional singlet at 3.04 ppm.

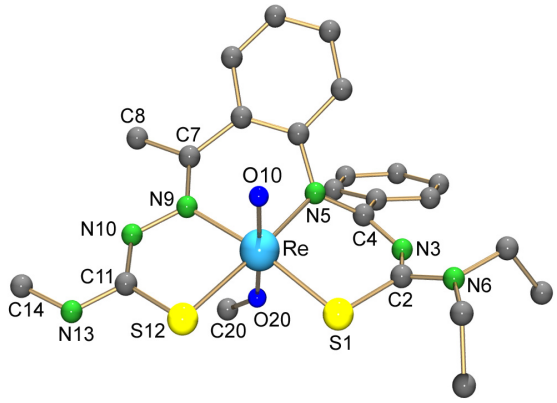

Figure 3.24 Molecular structure of [ReO(OMe)(L^{7})] (**38**). Hydrogen atoms were omitted for clarity.

Table 3.22 Selected bond lengths and angles in [ReO(OMe)(L^{7})] (**38**)

Bond lengths (Å)					
Re–O10	1.706(4)	Re–N9	2.128(4)	C2–N6	1.336(7)
Re–O20	1.918(4)	S1–C2	1.753(5)	C7–N9	1.309(7)
Re–S1	2.358(1)	C2–N3	1.335(7)	N9–N10	1.393(6)
Re–S12	2.379(1)	N3–C4	1.312(7)	N10–C11	1.311(7)
Re–N5	2.094(4)	C4–N5	1.348(6)	C11–S12	1.752(5)

Hydrogen bond				
D-H…A	d(D-H)	d(H…A)	d(D…A)	<(DHA)
N13-H13…S12#1	0.86	2.78	3.635(5)	173.1

Symmetry transformations used to generate equivalent atoms: #1 -x+2,-y+1,-z+1

The X-ray diffraction data of **38** are in a good agreement with the spectroscopic results. Figure 3.24 shows the molecular structure of **38**. Selected bond lengths and angles are given in Table 3.22. The environment of the Re atom is best described as a distorted octahedron

with an oxo and a methoxo ligand placed in axial positions. The $\{L^7\}^{2-}$ ligand is arranged in the equatorial plane and coordinates to rhenium via its N_2S_2 donor set as expected. The Re atom is located only 0.151(2) Å above the mean least-square plane formed by the four donor atoms of $\{L^7\}^{2-}$ towards the oxo ligand. The Re–O20 bond distance of 1.918(4) Å is shorter than a typical rhenium–oxygen single bond and reflects some double bond character. The required electron density is transferred from the double bond of the oxo ligand. Consequently, the Re-O10 bond distance of 1.706(4) Å is slightly longer than those in other octahedral rhenium oxo complexes. This is in a good agreement with the bathochromical shift of the $\nu_{Re=O}$ absorption in the IR spectrum.

3.2.2.3 Re^VN and Tc^VN Complexes with H_2L^7

The nitrido ligand $\{N^{3-}\}$ is isoelectronic with the oxo ligand $\{O^{2-}\}$. Its high negative charge makes the nitrido ligand to a much stronger π-donor than $\{O^{2-}\}$ and it perfectly stabilizes the oxidation state +V of rhenium and technetium. The strong donating nitrido ligand transfers electron density to the metal center, and consequently the $\{Re^VN\}^{2+}$ and $\{Tc^VN\}^{2+}$ cores prefer ligands with 'soft' donor atoms.

H_2L^7 reacts easily with $[ReNCl_2(PPh_3)_2]$ in boiling CH_2Cl_2. The resulting ligand exchange reaction gives a red solid of the composition $[ReN(L^7)]$ (**39**). The addition of a supporting base such as Et_3N allows the synthesis to be carried out at ambient temperature with a higher yield (Scheme 3.26). The product is less soluble in alcohols but good soluble in CH_2Cl_2 or $CHCl_3$ and can be recrystallized from a CH_2Cl_2-MeOH solution.

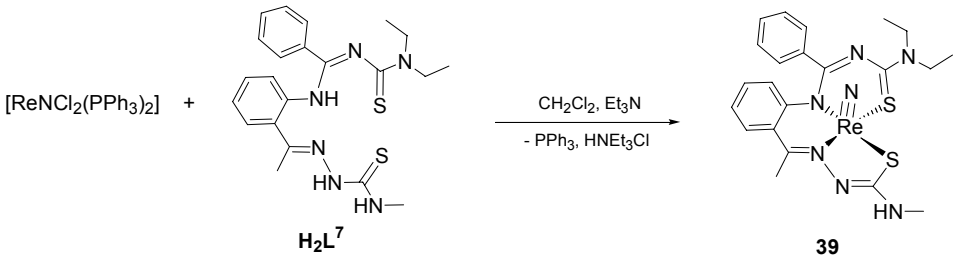

Scheme 3.26 Reaction of H_2L^7 with $[ReNCl_2(PPh_3)_2]$.

Like in the case of the oxo complex, the IR spectrum of the nitrido complex **39** reveals a moderate absorption at 3417 cm^{-1} which is assigned to the N-H stretch of the MeNH-CS group. The signals of the coordinated ligand are found with a strong bathochromic shift of $\nu_{C=N}$ of about 190 cm^{-1} with respect to the IR spectrum of H_2L^7. The ^1H NMR spectrum of **39** is characterized by four well resolved signals of four methylene protons with an ABX_3

coupling pattern, which results from the rigid structure of the tertiary amine nitrogen atom of the thiourea moieties. The resonance of the N-H proton appears as a broad singlet at 5.28 ppm. Again, the signal of the methyl group, which is directly bonded to the azomethine group is strongly shifted and appears as a singlet at 3.13 ppm.

Complex **39** was additionally studied by X-ray single crystal diffraction. The molecular structure is shown in Figure 3.25. Selected bond lengths and angles are listed in Table 3.23. The rhenium atom has a distorted square-pyramidal environment with the terminal nitrido ligand in apical position. The ligand $\{L_7\}^{2-}$ is equatorially coordinated via its N_2S_2 donor set. The N10-Re-X angles, where X is the donor atom in the basal plane, fall in the range between 100.9(2) and 110.3(1) °. The Re-N10 bond lengths of 1.668(4) Å is in the expected range for rhenium–nitrogen triple bonds [33].

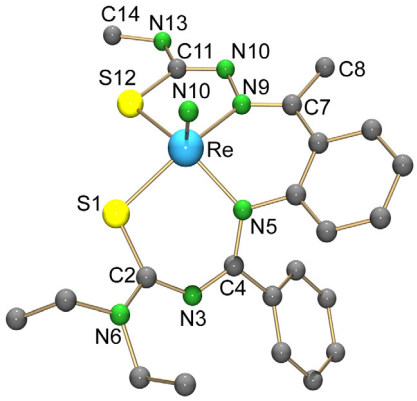

Figure 3.25 Molecular structure of [ReN(L^7)] (**39**). Hydrogen atoms were omitted for

Table 3.23 Selected bond lengths and angles in [ReN(L^7)] (**39**)

Bond lengths (Å)					
Re–N	1.668(4)	Re–N9	2.120(4)	C2–N6	1.327(6)
Re–S1	2.347(1)	S1–C2	1.745(5)	C7–N9	1.307(6)
Re–S12	2.340(1)	C2–N3	1.346(6)	N9–N10	1.406(5)
Re–N5	2.053(4)	N3–C4	1.305(5)	N10–C11	1.306(7)
		C4–N5	1.375(5)	C11–S12	1.756(5)
Angles (°)					
N10–Re–S1	105.7(1)		N10–Re–N5	106.7(2)	
N10–Re1–S2	110.3(1)		N10–Re–N9	100.9(2)	

The reaction of H_2L^7 with the analogous technetium precursor $[TcNCl_2(PPh_3)_2]$ is somewhat different. Beside the orange crystals of the technetium complex [TcN(L^7)] (**40**), which is analogous to **39**, an unexpected yellow crystalline complex of the composition $[TcN(PPh_3)(Et_2NC(S)NH)(L^{7b})]$ (**41**) is formed and can be isolated in moderate yields

(Scheme 3.27). Both **40** and **41** are sparingly soluble in MeOH and crystallize from the reaction mixture after the addition of MeOH as big crystals which can be separated mechanically.

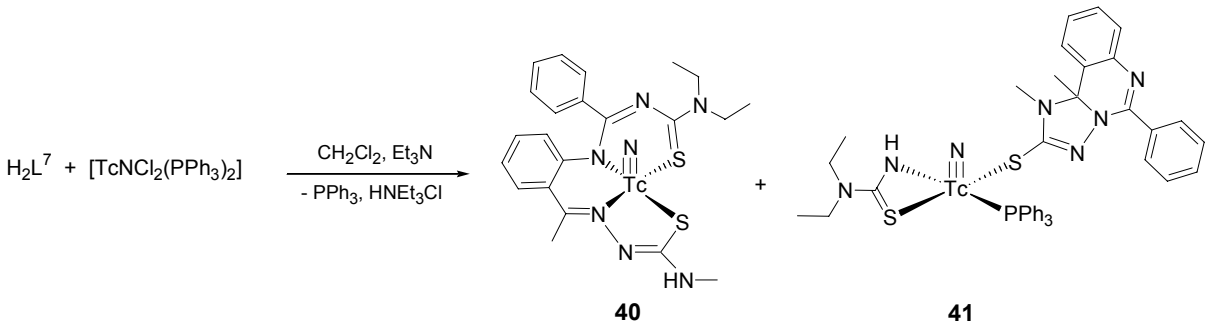

Scheme 3.27 Reaction of H_2L^7 with $[TcNCl_2(PPh_3)_2]$.

IR and ^1H NMR spectra of complex **40** mainly exhibit the same patterns as described for the rhenium complex **39.** The molecular structure of **40,** which is illustrated in Figure 3.26, confirms the analogous arrangement of the ligands. Selected bond lengths and angles are shown in Table 3.24. The technetium atom reveals a distorted square-pyramidal coordination sphere with an apical $\{N\}^{3-}$ ligand. All structural patterns discussed for the structure of **39** can also be applied to the technium complex **40**.

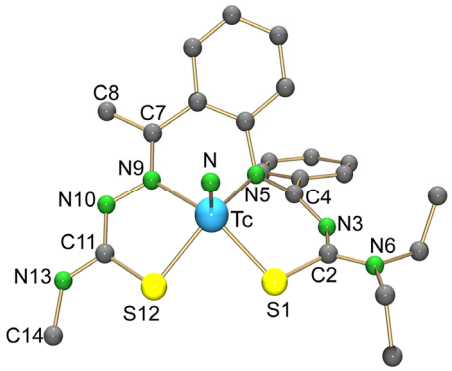

Figure 3.26 Molecular structure of $[TcN(L^7)]$ (**40**). Hydrogen atoms are omitted for clarity.

Table 3.24 Selected bond lengths and angles in $[TcN(L^7)]$ (**40**)

Bond lengths (Å)					
Tc–N	1.617(5)	Tc–N9	2.120(4)	C2–N6	1.330(7)
Tc–S1	2.359(1)	S1–C2	1.728(6)	C7–N9	1.315(6)
Tc–S12	2.347(1)	N3–C4	1.311(6)	N10–C11	1.315(6)
Tc–N5	2.057(4)	C4–N5	1.369(6)	C11–S12	1.748(5)
Angles (°)					
N–Tc–S1	105.2(1)		N–Tc–N5	107.7(2)	
N–Tc–S12	110.3(1)		N–Tc–N9	101.6(2)	

The IR spectrum of compound **41** is similar to that of **40** except that the N-H vibration band is sharp and long-wave shifted to 3363 cm^{-1}. The ^{1}H NMR spectra of the two compounds are completely different. In ^{1}H NMR spectrum of **41**, the ethyl resonances still reflect the rigid structure of the tertiary amine nitrogen atom of the thiourea group, but the observed signals are strongly high-field shifted. Despite the fact that in the ^{1}H NMR spectrum of **40**, the CH_3-NH signal of the thiosemicarbazone moiety appears as a doublet at 3.05 ppm (due to coupling with the adjacent proton N-H), the corresponding resonance of **41** is a singlet and is detected at 3.66 ppm. Another methyl signal in the NMR spectrum of compound **41**, appears at 1.41 ppm. This resonance is at an even higher field than that in the spectrum of the uncoordinated H_2L^7. From the ^{1}H NMR results we can conclude that the main skeleton of the organic ligand '$\{L^7\}^{2-}$' in **41** is not maintained. However, the structure of the compound can not be deduced. The ^{31}P NMR spectrum reveals a singlet at 48.86 ppm and, thus, indicates the presence of a PPh_3 ligand in the coordination sphere of the metal.

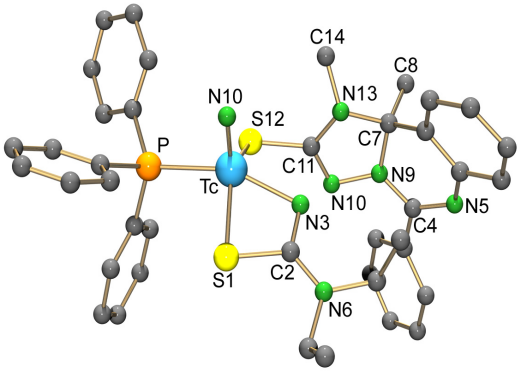

Figure 3.27 Molecular structure of $[TcN(PPh_3)(Et_2N(CS)NH)(L^{7b})]$ (**41**). Hydrogen atoms were omitted for clarity.

Figure 3.27 depicts the molecular structure of **41**. Selected bond lengths and angles are presented in Table 3.25. The X-ray structural study confirms the assumed decomposition of the ligand $\{L^7\}^{2-}$ from which the heterocyclic thiol/thione HL^{7b} and N,N-diethylthiourea are formed (also compare scheme 3.28). The coordination environment of the technetium atom is best described as a distorted square pyramid with an apical nitrido ligand. The basal plane, is occupied by the heterocyclic ligand $\{L^{7b}\}^-$, which binds to the Tc atom monodentate via its sulfur atom. N,N-Diethylthiourea deprotonates and acts as a bidentate thioureido ligand coordinated to Tc via a nitrogen atom and the sulfur atom. The last position in the basal plane is occupied by a triphenylphosphine ligand, which is arranged in *trans* position to the nitrogen donor atom of the N,N-diethylthioureido ligand. The bonding situation in the ligand $\{L^{7b}\}^-$ reveals the sp^2 hybridization of the carbon atoms C11 and C4. Although some delocalization of π–electron density is found in the skeleton of $\{L^{7b}\}^-$, the C4-N5 and C11-N10 bond lengths of 1.32(1) Å and

1.31(1) Å, respectively, are slightly shorter than the other carbon-nitrogen bonds and indicate more double bond character. The Tc-S12 distance of 2.373(2) Å is 0.03 Å shorter than the Tc-S1 bond length. Delocalization of the negative charge is also observed in the four-membered chelate ring of the N,N-diethylthioureido ligand and is reflected by the C2-N3 and C2-S1 bond lengths which fall between the values of carbon–nitrogen and carbon–sulfur single and double bonds.

Table 3.25 Selected bond lengths and angles in [TcN(PPh_3)($Et_2N(CS)NH$)(L^{7b})] (**41**)

Bond lengths (Å)					
Tc–N	1.617(8)	S1–C2	1.767(9)	N10–C11	1.32(1)
Tc–S1	2.403(3)	C2–N3	1.32(1)	C11–N13	1.39(1)
Tc–N3	2.097(7)	C2–N6	1.33(1)	C11–S12	1.742(9)
Tc–S12	2.373(2)	C4–N5	1.33(1)	C7–N13	1.48(1)
Tc–P	2.405(2)	C4–N9	1.34(1)	C7–N9	1.47(1)
Angles (°)					
N–Tc–S1	111.6(3)	N–Tc–N3	107.1(4)	N3–Tc–P	156.4(2)
N–Tc–S12	111.6(3)	N–Tc–P	94.9(3)	S1–Tc–S12	136.2(1)

The formation of **41** is reproducible and clearly a result of the decomposition of H_2L^7. However, it is worth to mention that a similar decomposition is not found in the synthesis of the analogous rhenium complex under the same conditions. More interestingly, the technetium complex **40**, which contains the coordinated ligand $\{L^7\}^{2-}$, is completely stable, even under reflux conditions in CH_2Cl_2 with and without the addition of a base. Additionally, the purity of the ligand H_2L^7 was confirmed by different spectroscopic methods as well as elemental analysis. These synthetic evidences suggest that the compounds **40** and **41** were formed independently and the decomposition of H_2L^7 should appear during the formation of the complex **41**. A mechanism for the formation of **41** is proposed in Scheme 3.28. The chloro ligand of [$TcNCl_2(PPh_3)_2$] is supposed to be firstly exchanged by the thiourea sulfur atom of H_2L^7. This is confirmed by a previously published reaction pattern of [$ReOCl_2(PPh_3)_3$] and a benzamidine derived from glycine ester, in which an intermediate S-thiourea monodentate product was successfully isolated [96]. Subsequently, a phosphine ligand is replaced either by the N5 or the N3 donor atom. The first situation results in the formation of a benzamidine chelate ring and consequently produces complex **40**. The second leads to an intermediate cationic complex **III** (Scheme 3.28a, in which the positive charge locates on the C4 atom. This allows a nucleophilic substitution/cyclization process and subsequently results in the decomposition of H_2L^7 and the formation of **41**. The ability of thiocarbonylbenzamidines to establish four-membered chelate rings as shown in the intermediate **III** is experimentally

proven, since this coordination mode could recently be found in the ruthenium complex $[Ru^{II}(H_2L^1)Cl_2(BDPB)]$ (**IV**), where BDPB is bis(diphenylphosphino)butane (Scheme 3.28b) [97].

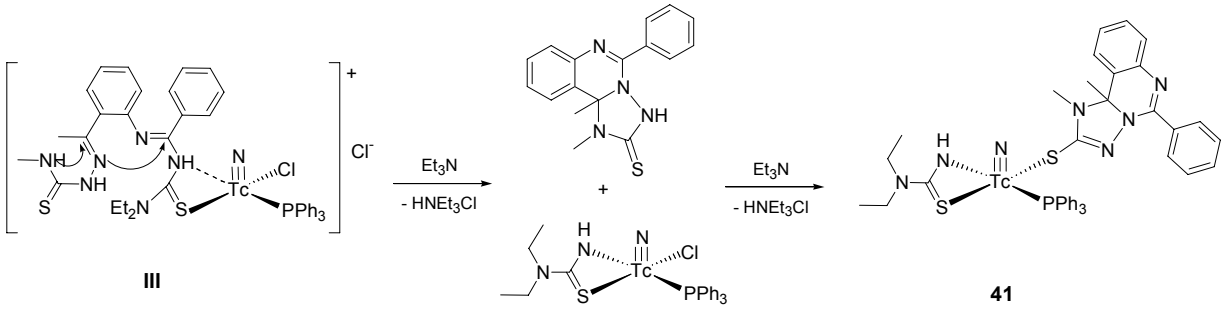

Scheme 3.28a Proposed formation of $[TcN(PPh_3)(Et_2tu)(L^{7b})]$ (**41**).

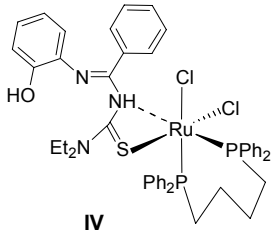

Scheme 3.28b Structure of $[Ru^{II}(H_2L^1)Cl_2(BDPB)]$, (**IV**).

3.2.3 Benzamidines Derived from o-Aminobenzylsalicylideneimine (H_2L^8) and their Re Complexes

3.2.3.1 Synthesis of H_2L^8

Azomethine compounds (Schiff bases) belong to the most common ligand systems due to their facile synthesis and convenience in the construction of various multidentate systems.

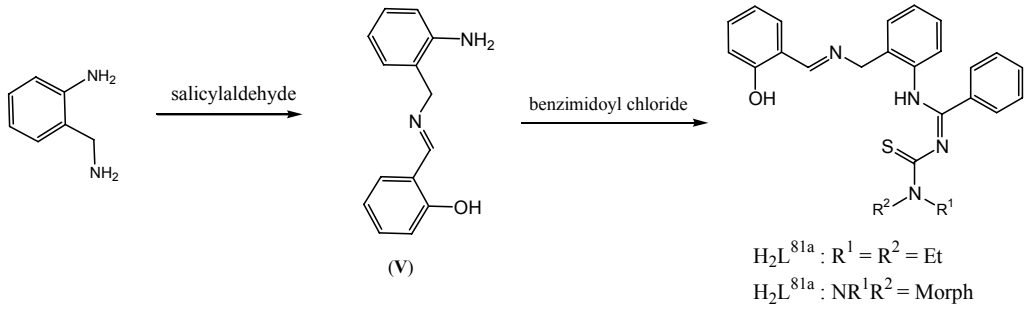

Scheme 3.29 Prospective synthesis of the tridentate ligand H_2L^{81}.

o-Aminobenzylamine was used as a starting material for the synthesis of a tetradentate benzamidine ligand containing an additional Schiff base. The benzylamine group of this asymmetric diamine can be selectively condensed with one equivalent of salicylaldehyde to

form the Schiff base **V** without protection of the aromatic amine [98]. The formation of **V** is proven by the ^{1}H-NMR spectrum which shows a typical singlet of the proton of the azomethine group at 8.40 ppm. Additionally, a singlet at 4.75 ppm, which is assigned to methylene protons, reveals that the imine bond is formed via the nitrogen of the benzylamine group.

Expectedly, the aromatic amine group of the Schiff base **V** can subsequently be reacted with benzimidoyl chlorides to give the ONNS tetradentate ligands H_2L^{81} as shown in Scheme 3.29. Thus, the reactions of benzimidoyl chlorides with **V** were carried out in dry acetone as mentioned in the standard procedure and pure yellow solids of the ligands could be isolated in high yields. Bright yellow crystals of the products were obtained by slow evaporation of dichloromethane methanol solutions.

The IR spectra of the compounds exhibit bands in the region above 3200 cm^{-1} which are expected for O-H and N-H vibrations. The very strong absorptions around 1620 cm^{-1} are assigned to C=N stretches. The ^{1}H NMR spectra of the compounds in $CDCl_3$ reveal poorly resolved patterns. In the ^{1}H NMR spectrum of H_2L^{81a} in $CDCl_3$, for instance, triplet signals of the methyl groups are observed at 1.04 ppm and 1.13 ppm, while a quartet at 3.80 ppm and a broad singlet at 3.57 belong to two methylene resonances. The broad singlet at 4.60 ppm region belongs to the methylene protons, which bind to the N atom of the azomethine group. A better resolved ^{1}H NMR spectrum was obtained in DMSO-d_6. Interestingly, the resonance of the methylene protons C=NC$\underline{H_2}$Ph appears at 4.60 ppm as a doublet with J = 5.5 Hz. Nevertheless, this coupling pattern can not be explained based on the structure of H_2L^{81} and indicates some unexpected reaction in this solvent.

For a better understanding of the molecular structure of this type of compounds, the X-ray single crystal structure of the diethyl derivative was studied. Figure 3.28 depicts the molecular structure of the compound which is clearly not the expected structure for H_2L^{81a}. In this structure (H_2L^{8a}), the benzamidine side does not connect to the aromatic amine but to the benzylamine and the azomethine bond is formed with the nitrogen atom of the aromatic amine. The C8-N9 bond distance of 1.287(2) Å, which is clearly within the range of carbon-nitrogen double bonds, additionally confirms the formation of an azomethine group with the aromatic amine. The C4-N3 bond length of 1.295(2) Å reflects more double bond character than the C4-N5 bond (1.352(2)Å). This bonding situation indicates the protonation on the N5 atom, which is in a agreement with the experimental finding of an intermolecular hydrogen bond between N5 and O67 of a neighbouring molecule. In solution, however, a proton

exchange between N5 and N3 atoms must be considered, which finally results in the broadening of the ^{1}H NMR signal of the protons on C7.

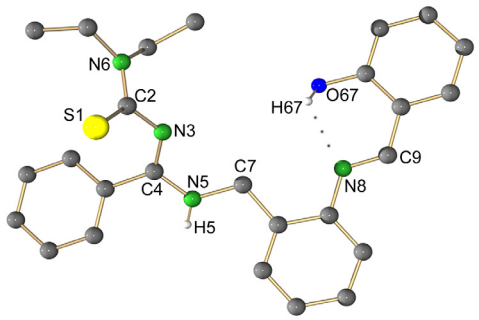

Figure 3.28 Molecular structure of H_2L^{8a}. Hydrogen atoms bonded to carbon atoms were omitted for clarity.

Table 3.26 Selected bond lengths and angles in H_2L^{8a}

Bond lengths (Å)					
S1–C2	1.686(1)	N3–C4	1.295(1)	N5–C7	1.451(1)
C2–N3	1.373(1)	C4–N5	1.352(1)	N8–C9	1.287(1)

Hydrogen bonds				
D-H…A	d(D-H)	d(H…A)	d(D…A)	<(DHA)
O67–H67…N8	0.82	2.17	2.5756(15)	110.7
N5–H5…O67#1	0.86	2.55	3.1878(16)	132.2

Symmetry transformations used to generate equivalent atoms: #1 -x,-y+2,-z1

The formation of H_2L^{8} can be understood by a tautomeric equilibrium between the Schiff base **V** and 1,2,3,4-tetrahydroquinazoline **VI** which is previously mentioned for these types of compounds [98,99]. Compound **VI** reacts with benzimidoyl chloride favorably at the nitrogen atom which belongs to the benzylamine and the product subsequently undergoes a ring opening (Scheme 3.30). A similar ring opening step is also observed when tetrahydroquinazolines of the type **VI** are treated with an additional equivalent of aldehyde or ketone to give the corresponding bis-imine products [98].

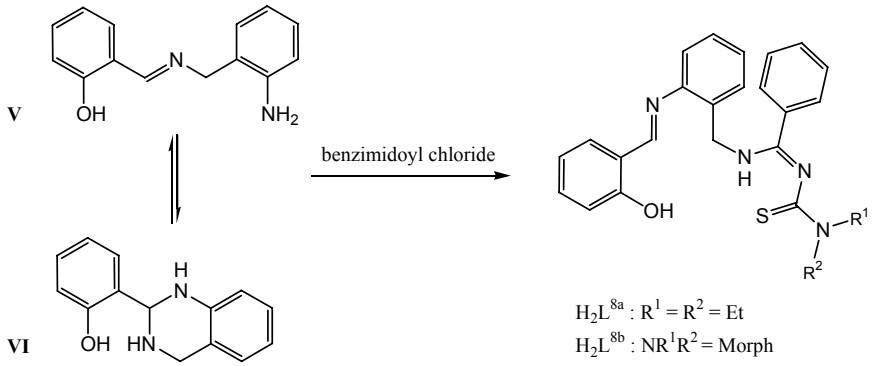

Scheme 3.30 Synthesis of the tridentate ligand H_2L^{8}.

3.2.3.2 A $Re^{V}O$ Complex with H_2L^{8}

Ligand H_2L^{8a} readily reacts with $(NBu_4)[ReOCl_4]$ in methanol without the addition of a supporting base under formation of a dark green solution from which a green precipitate of the composition $[ReOCl_2(HL^{8a})]$ (**42**) deposited within ten minutes (Scheme 3.31). The product is sparingly soluble in common solvents such as alcohols, CH_2Cl_2 or $CHCl_3$. In DMSO, the compound is well soluble, but decomposed by ligand exchange reactions with solvent molecules. This produces difficulties to elucidate its structure by NMR methods. The IR spectrum of **42** shows a broad medium absorption band at 3271 cm^{-1}, which can be assigned to N-H or O-H vibrations. Additionally, the $\nu_{C=N}$ absorption at 1600 cm^{-1} is much higher than those of corresponding stretches in other rhenium benzamidine complexes and indicates that the ligand is not completely coordinated or deprotonated. A strong absorption band at 968 cm^{-1} is typical for the $\nu_{Re=O}$ vibration.

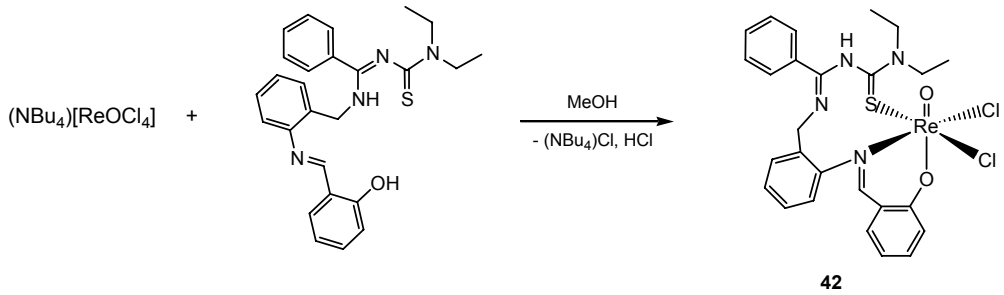

Scheme 3.31 Reaction of H_2L^{8a} with $(NBu_4)[ReOCl_4]$.

When the reaction is carried out in a highly diluted solution without stirring, the product slowly deposits as a crystalline solid. The X-ray single crystal diffraction of **42** was studied and the molecular structure of **42** is presented in Figure 3.29. Selected bond lengths and angles are listed in Table 3.27. The Re atom possesses a distorted octahedral coordination sphere with a terminal oxo ligand. The organic ligand is singly deprotonated and coordinates to the Re atom only via three donor atoms. The oxygen atom of the phenolate which is in *trans* position to the oxo ligand, the nitrogen atom of the azomethine and the sulfur atom of the thiourea group. The two remaining positions in the coordination sphere are occupied by two chloro ligands, which are in *cis* position to each other. The hydrogen atom of the benzamidine is refined at the atom N5 based on a suitable peak of electron density found in the final Fourier map and it is involved in the formation of the intermolecular hydrogen bond between N3 and O67. This is also in a good agreement with the bond length situation, in which the C4-N5 bond of 1.320(12) Å is longer than the C4-N3 bond length of 1.304(11) Å

and reflects less double bond character. The Re-S1 distance of 2.406 Å is longer than those of other rhenium benzamidine complexes but in the same range of those in rhenium complexes with monodentate neutral thioureas [100].

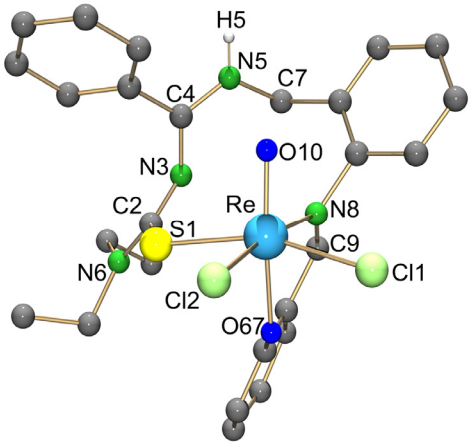

Figure 3.29 Molecular structure of $[ReOCl_2(HL^8)]$ (**42**). Hydrogen atoms bonded to carbon atoms were omitted for clarity.

Table 3.27 Selected bond lengths and angles in $[ReOCl_2(HL^8)]$ (**42**)

Bond lengths (Å)					
Re–O10	1.681(6)	Re–Cl1	2.405(2)	N3–C4	1.30(1)
Re–O67	2.019(6)	Re–Cl2	2.364(3)	C4–N5	1.32(1)
Re–S1	2.406(2)	S1–C2	1.760(9)	N5–C7	1.47(1)
Re–N8	2.179(8)	C2–N3	1.34(1)	N8–C9	1.25(1)
Angles (°)					
O10–Re–S1	97.6(2)	O10–Re–N8	87.1(3)	O10–Re–Cl1	99.8(2)
N8–Re–S1	102.2(2)	Cl1–Re–Cl2	85.2(1)	O10–Re–Cl2	99.9(3)
O10–Re–O67	168.4(3)	S1–Re–Cl1	159.6(1)	N8–Re–Cl2	171.7(2)

Hydrogen bond				
D-H…A	d(D-H)	d(H…A)	d(D…A)	<(DHA)
N5-H5…O67#1	0.86	2.10	2.944(10)	168.8

Symmetry transformations used to generate equivalent atoms: #1 x+1/2,-y+1/2,-z+2

3.2.3.3 A $Re^{V}N$ Complex with H_2L^8

In the presence of a supporting base like Et_3N, H_2L^8 slowly reacts with $[ReNCl_2(PPh_3)_2]$ in CH_2Cl_2 at ambient temperature under formation of a red crystalline complex of the composition $[ReN(PPh_3)(L^8)]$ (**43**). Heating of the reaction mixture leads to a fast

consumption of the sparingly soluble precursor but dramatically decreases the yield of the isolated product (Scheme 3.32). This may be the result of the dissociation/oxidation of the monodentate triphenylphosphine ligand, and/or a rapid competing solvolysis reaction after removal of chloro ligands by the formation of $Et_3N{\cdot}HCl$. The compound **43** is readily soluble in solvents such as $CHCl_3$ or CH_2Cl_2. Single crystals of **43** are obtained by recrystallization from a CH_2Cl_2 – MeOH mixture.

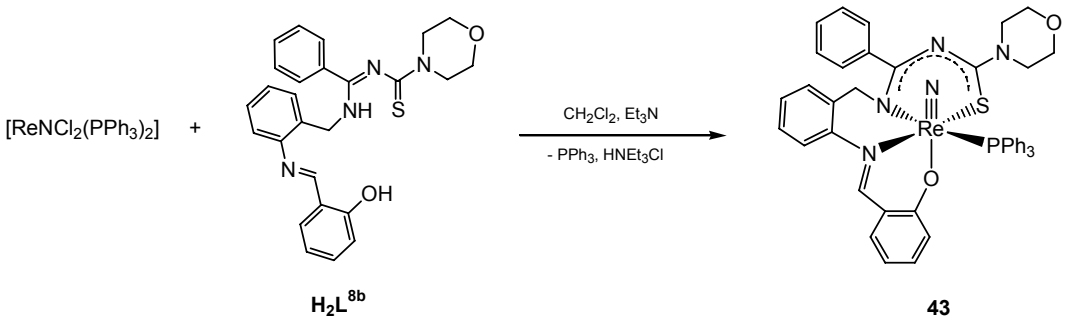

Scheme 3.32 Reaction of H_2L^{8b} with $[ReNCl_2(PPh_3)_2]$.

Figure 3.30 presents the molecular structure of **43**. Some important bond lengths and angles are listed in Table 3.28. The rhenium atom has a distorted octahedral environment with the nitrido ligand in the axial position. Unlike the situation in the complex **42**, in **43** we find a dianionic tetradentate organic ligand $\{L^8\}^{2-}$, which facially coordinates to the Re atom with an additional equatorial, six-membered chelate ring. The O atom of the phenolate group is placed *trans* to the nitrido ligand. The octahedral coordination sphere is completed by a triphenylphosphine ligand. It is obvious that the ligand $\{L^8\}^{2-}$, which comprises three six- membered rings is sufficiently flexible to adopt the facial coordination mode. However, it is unexpected that the phenolate oxygen atom is placed *trans* to the triple bonded nitrido

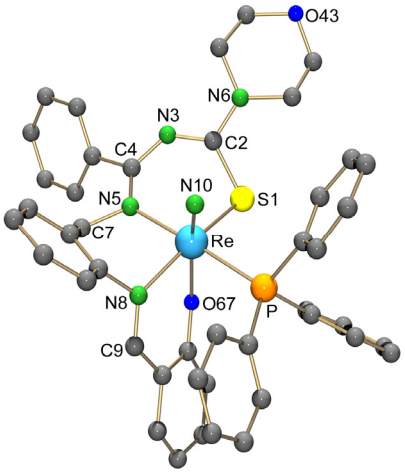

Figure 3.30 Molecular structure of $[ReN(PPh_3)(L^8)]$ (**43**). Hydrogen atoms were omitted for clarity.

ligand, which possesses a very strong *trans* influence and favourably forms square-pyramidal rhenium(V) complexes. This is reflected by the Re-O67 bond length of 2.196(4) Å, which issignificantly longer than that in the rhenium oxo complex **42** (2.019(6) Å) but slightly shorter than those in a few other octahedral rhenium nitrido complexes [101]. The Re-S1 bond length of 2.386(2) Å is about 0.02 Å shorter than the corresponding distance in **42**. The Re-N10 bond distance of 1.664(5) Å falls in the typical range of rhenium nitrogen triple bonds. The Re-N8 distance of 2.136(5) Å is in the same range of bonds between rhenium and azomethine nitrogen atoms in other rhenium Schiff base complexes [102]. With a length of 2.140(5) Å, the Re-N5 bond is much longer than those in other rhenium benzamidine complexes and reveals the *trans* influence of the phosphine ligand.

Table 3.28 Selected bond lengths and angles in [ReN(PPh_3)(L^8)] (**43**)

Bond lengths (Å)					
Re–N10	1.664(5)	Re–N8	2.136(5)	N3–C4	1.342(8)
Re–O67	2.196(4)	Re–P	2.453(2)	C4–N5	1.324(8)
Re–S1	2.386(2)	S1–C2	1.739(7)	N5–C7	1.479(7)
Re–N5	2.140(5)	C2–N3	1.315(8)	N8–C9	1.296(8)
Angles (°)					
N10–Re–S1	103.2(2)	N10–Re–N8	93.8(2)	N10–Re–N5	98.8(2)
N10–Re–O67	167.4(2)	N10–Re–P	84.3(2)	N5–Re–P	176.9(1)
N8–Re–S1	162.8(1)	S1–Re–N5	89.3(1)	N8–Re–N5	85.4(2)

3.2.4 A Benzamidine Derived from Triglycine Ester (H_3L^9) and Its Re^VO Complex

3.2.4.1 Synthesis of H_3L^9

Transition metal complexes with multidentate ligand systems on the basis of peptide frameworks attract much interest because they may mimic interactions between the metal ions and proteins under physiological conditions [103]. For coordination compounds used in drugs, in most of the cases, organic ligands must provide sufficient stability in order to exclude the ligand exchange with physiological proteins. A promising way for the synthesis of such stabilizing chelator systems, especially in rhenium and technetium chemistry, is the introduction of one or more ‘soft’ donor sites such as S or P to a small peptide framework [104]. With this approach, the affinity of the modified peptide to rhenium and technetium is

significantly increased. In the following subsection, a new way for the modification of a small peptide is introduced. Triglycine ethyl ester is attached to a thiocarbonylbenzamidine as described above for many examples. Expectedly, this will give access to a new class of chelators with the opportunity to construct of skeletons based on the variety of peptides.

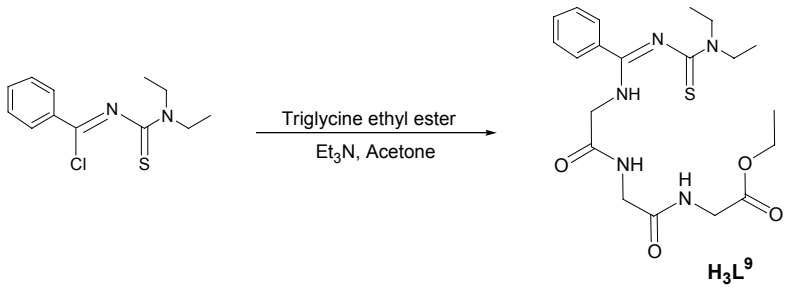

Scheme 3.33 Synthesis of the ligand H_3L^9.

Triglycine ethyl ester reacts with N,N-diethylaminethiocarbonyl benzimidoyl chloride in a clean reaction under formation of H_3L^9 in high yields (Scheme 3.33). The IR spectrum of H_3L^9 shows a strong, broad absorption at 3320 cm^{-1} and a very strong absorption band in the 1700 cm^{-1} region corresponding to the $\nu_{C=O}$ vibrations. In the ^1H NMR spectrum of H_3L^9, two well separated signal sets of ethyl groups of the CS-NEt_2 moiety are observed. The resonances of the C$\underline{H_2}$NH protons of the triglycine ester unit appear as three doublets at 3.97 ppm, 4.01 ppm and 4.15 ppm. Three broad singlets at 6.64 ppm, 7.15 ppm and 7.67 ppm can be assigned for NH resonances.

3.2.4.2 A Re^VO Complex with H_3L^9

Planar tetradentate chelating peptides which contain additional 'soft' donors are of interest for technetium(V) and rhenium(V) monooxo cores due to their formation of very stable complexes. They should possess a reasonable hydrophilicity which is useful for radiopharmaceutical applications [105]. Some ^{99m}Tc complexes with these types of ligands are used as routine pharmaceuticals for diagnostics of kidneys such as [$Tc^{99m}O$(MAG3)] (MAG = mercaptoacetyltriglycine) [6].

H_3L^9 reacts with (NBu_4)[$ReOCl_4$] in methanol in the presence of a supporting base such as Et_3N under formation of a red clear solution, from which an orange-red solid of the composition [$ReO(L^9)$] (**44)** can be precipitated by slow addition of H_2O (Scheme 3.34). The product is readily soluble in MeOH and even slightly soluble in water. A crystalline product can be obtained by recrystallization from a MeOH – H_2O mixture.

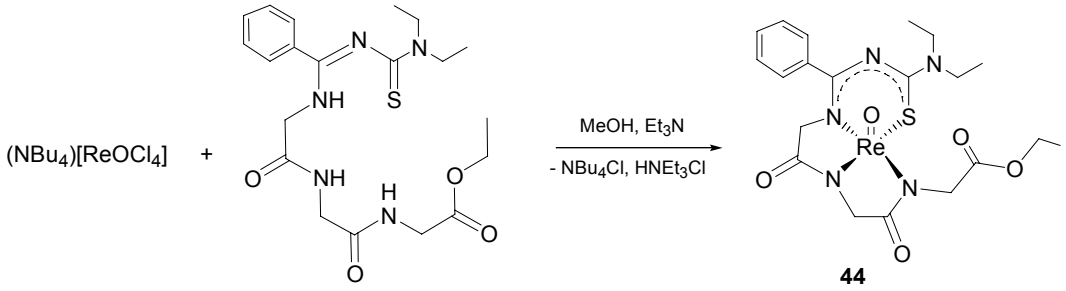

Scheme 3.34 Reaction of H_2L^9 with $(NBu_4)[ReOCl_4]$.

The IR spectrum of **44** does not show any absorptions in the region above 3100 cm^{-1} which is typical for the ν_{NH} stretch in the free ligand. This reflects the triple deprotonation of the ligand during the complex formation. A strong bathochromic shift (about 120 cm^{-1}) of the absorption corresponding to the $\nu_{C=N}$ vibration is also observed. The absorption of the $\nu_{C=O}$ stretches is only slightly shifted to lower wave number by about 10 cm^{-1}. The ^1H NMR spectrum of **44** is distinguished from that of the free ligand by four double doublets at 3.81, 3.98, 4.19 and 4.30 ppm with geminal coupling constants (16.0 Hz) which belong to the C$\underline{H_2}$NH protons in the chelate rings.

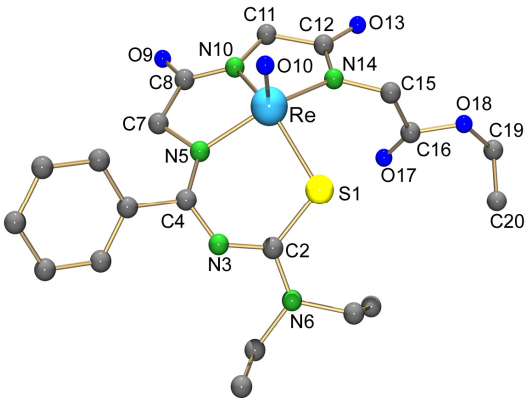

Figure 3.31 Molecular structure of [ReO(L^9)] (**44**). Hydrogen atoms were omitted for clarity.

Figure 3.31 depicts the molecular structure of **44**. Selected bond lengths and angles are listed in Table 3.29. Complex **44** is a neutral compound and the rhenium atom has adopted a square-pyramidal coordination sphere with an oxo ligand in the apical position. Four donor atoms of the ligand H_3L^9 are situated in the equatorial plane and the Re atom places about 0.655(2) Å above this basal plane, toward the oxo ligand. Consequently, all O10-Re-X angles, where X is a donor atom of the basal plane, fall in the range between 106 and 111°. The Re-O10 bond distance of 1.674(4) Å represents a typical rhenium-oxygen double bond. The distances from Re to the nitrogen atoms are not equal in this compound. The shortest distance of 1.971(4) is observed for N10, the nitrogen donor site sharing two five-membered chelate rings and the longest bond of 2.040(4) Å is found for N14, the donor atom contributing to

only one chelate ring. A similar observation is also found in the square-pyramidal rhenium(V) complex with the mercaptoacetyltriglycine ligand [6].

Table 3.29 Selected bond lengths and angles in [ReO(L^9)] (**44**)

Bond Lengths (Å)					
Re–O10	1.674(4)	C2–N3	1.338(6)	N10–C11	1.460(6)
Re–S1	2.306(1)	N3–C4	1.315(6)	C12–O13	1.232(6)
Re–N5	1.999(4)	C4–N5	1.350(6)	C12–N14	1.348(7)
Re–N10	1.971(4)	N5–C7	1.477(6)	N14–C15	1.455(6)
Re–N14	2.040(4)	C8–O9	1.216(6)	C16–O17	1.192(8)
S1–C2	1.754(6)	C8–N10	1.357(6)	C16–O18	1.31(1)
Angles (°)					
O10–Re–S1	106.9(1)	O10–Re–N5	107.6(2)	O10–Re–N10	111.3(2)
O10–Re–N14	108.3(2)	S1–Re–N10	141.7(1)	N5–Re–N14	142.5(2)

3.2.5 Summary and Conclusions

Tetradentate benzamidine-type ligands with a wide structure variety, ranging from symmetric ligands like H_2L^6 to ligands derived from thiosemicarbazones, Schiff bases or peptides can be conveniently prepared. Such ligands stabilize rhenium(V) and technetium(V) complexes with both monooxo and nitrido cores. While the ligands $\{L^6\}^{2-}$, $\{L^7\}^{2-}$ and $\{L^9\}^{3-}$ favorably bind meridionally to the metal cores, $\{L^8\}^{2-}$ which comprises three six-membered chelate rings prefers the formation of a facial complex.

Complex formation strongly depends on the nature of ligands and the charge compensation. Dianionic ligands such as $\{L^6\}^{2-}$ and $\{L^7\}^{2-}$ tend to stabilize rhenium(V) oxo and technetium(V) oxo cores in an octahedral environment and neutral complexes are formed either by incorporation of a monoanionic monodentate ligand such as ReO_4^- in **34**, MeO^- in **38** or via dimerization in **35**, while $\{L^9\}^{3-}$ can form a neutral square-pyramidal rhenium(V) oxo complex (**44**). The dianionic ligands $\{L^6\}^{2-}$ and $\{L^7\}^{2-}$ are suitable for the formation of neutral, square-pyramidal complexes with rhenium(V) nitrido and technetium(V) nitrido cores. Due to the flexibility of its skeleton, however, $\{L^8\}^{2-}$ can also form a neutral octahedral complex with the nitrido rhenium(V) core (**43**).

3.3 Rhenium and Technetium Complexes with Pentadentate Benzamidines

Pentadentate ligands which can complete the coordination spheres around monoxorhenium(V) and monoxotechnetium(V) cores are expected to be ideal chelator system for the formation of thermodynamically stable complexes with such cores. Up to now, however, only a few oxorhenium(V) and oxotechnetium(V) complexes with such ligands were published [106].

The synthesis of pentadentate systems via reactions of benzimidoyl chlorides and tetradentate amines seems to be a very facile approach. Additionally, the convenient variation especially of the periphery of the thiourea moiety as outlined in the previous sections is interesting for fine tuning of the chemical and physical properties of such pentadentate benzamidine ligands.

3.3.1 Pentadentate N'-substituted Benzamidines

3.3.1.1 N-Dialkylaminothiocarbonyl-N'-{2-methylene(phenyliminodiacetic)} Benzamidine (H_3L^{10})

The title compound can be prepared from an asymmetric amine such as 2-aminobenzyl amine in a multistep synthesis as shown in the Scheme 3.35. First, the aliphatic amine in 2-aminobenzylamine is selectively protected by reaction with di-tert.butyl dicarbonate to form o-$NH_2C_6H_4CH_2NHBOC$ (**VII**). Then, the aromatic amine **VII** is converted to the iminodi(ethylacetate) **XIII** by treatment with an excess amount of $BrCH_2COOEt$ in the presence of a supporting base. The reaction of **XII** with $BrCH_2COOEt$ proceeds very slowly. With MeCN as solvent, K_2CO_3 as supporting base and a 6 equivalents of $BrCH_2COOEt$, a mixture of **XIII** (60%) and mono-substituted product (40%) was obtained after refluxing the reaction mixture for 6 days. However, with the use of toluene as the solvent and a homogenous supporting base such as Pr_2EtN the formation of **XIII** is almost quantitatively even with 3 equivalents of $BrCH_2COOEt$ and a reflux period of 3 days. Hydrolysis of the ester **XIII** with NaOH in MeOH at room temperature gives the carboxylic acid **IX**, the aliphatic amine of which is then deprotected by CF_3COOH/CH_2Cl_2 (1:1). This gives the amine compound **X** in form of a salt. Because of the poor solubility of **X** in acetone, the synthesis of the corresponding benzamidine H_3L^{10} is carried out in dry EtOH with a modified workup procedure as stated in the experimental section.

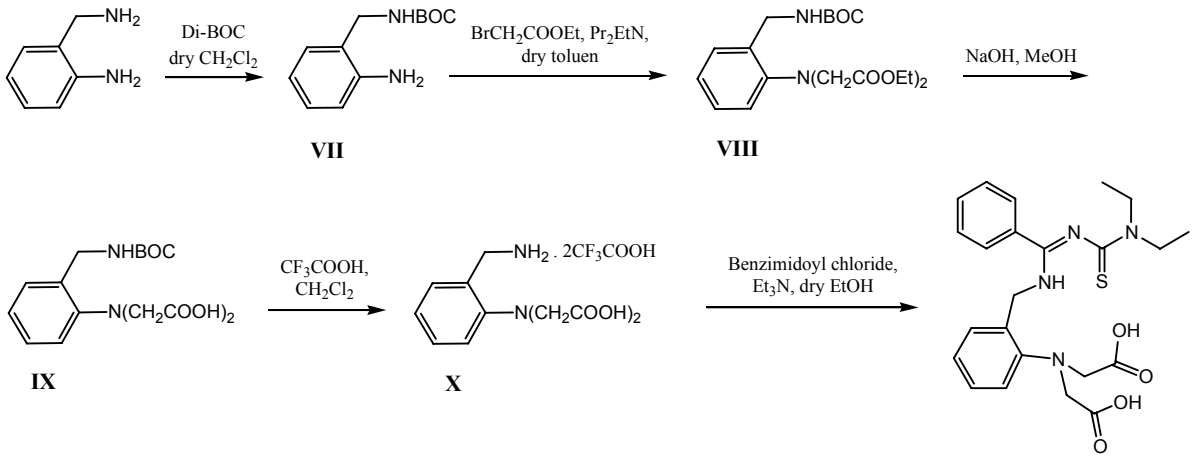

Scheme 3.35 The synthesis of the pentadentate ligand H_3L^{10}.

The ligand H_3L^{10} is obtained as a light yellow powder. The IR spectrum of H_3L^{10} exhibits very strong broad bands in the region between 3500 cm^{-1} and 2400 cm^{-1} which is characteristic for the ν_{OH} stretches of the free carboxylic groups. The corresponding $\nu_{C=O}$ vibrations appear as a very strong, broad absorption at 1720 cm^{-1} and are overlapped with a strong absorption of the $\nu_{C=N}$ stretch at 1631 cm^{-1}.

The ^1H NMR spectrum of H_3L^{10} shows two well separated signal sets of ethyl protons due to the hindered rotation of the C-NEt_2 moiety. While a singlet at 3.99 ppm is assigned to the methylene protons of $\underline{CH_2}CO$, a doublet at 4.64 with J = 5.2 Hz is typical for the methylene protons of $\underline{CH_2}NH$. The chemical shifts of the protons belonging to the aminobenzylamine appear in the range from 6.8 ppm to 7.0 ppm, which is at higher field compared to those of other aromatic protons. Broad singlets at 8.35 ppm and 12.67 ppm are assigned to the NH and COOH resonances.

3.3.1.2 N-Dialkylaminothiocarbonyl-N'-{phenylene-(2-methyliminodiacetic)} Benzamidine (H_3L^{11})

The pentadenate ligand H_3L^{11} is another, slightly modified derivative of 2-aminobenzyl-amine. The protons of the aliphatic amine are substituted by carboxylmethyl groups and the aromatic amine is reacted with benzimidoyl chloride. For this purpose, a synthesis starting from 2-nitrobenzylamine was chosen. A reaction with bromoacetic acid ethyl ester in dry MeCN gives diester **XI** in high yields. The reduction of nitro group in **XI**, which gives the amine **XII**, was performed by hydrogen gas with a Pd/C catalyst in methanol - ethyl acetate. The course of the reduction was controlled by ^1H-NMR spectroscopy and the reaction was quenched after 5h to minimize the impurity, which is formed by a slow cleavage of the

N-benzyl bond under the same conditions. The amine compound **XII** was purified by column chromatography using ethyl acetate/n-hexane (1:1) as elutant. Hydrolysis of compound **XII** with NaOH in MeOH gives the bis-carboxylic acid **XIII**. The final step, the reaction of **XIII** with benzimidoyl chloride to form the pentadentate H_3L^{11}, was done under similar conditions described for H_3L^{10}.

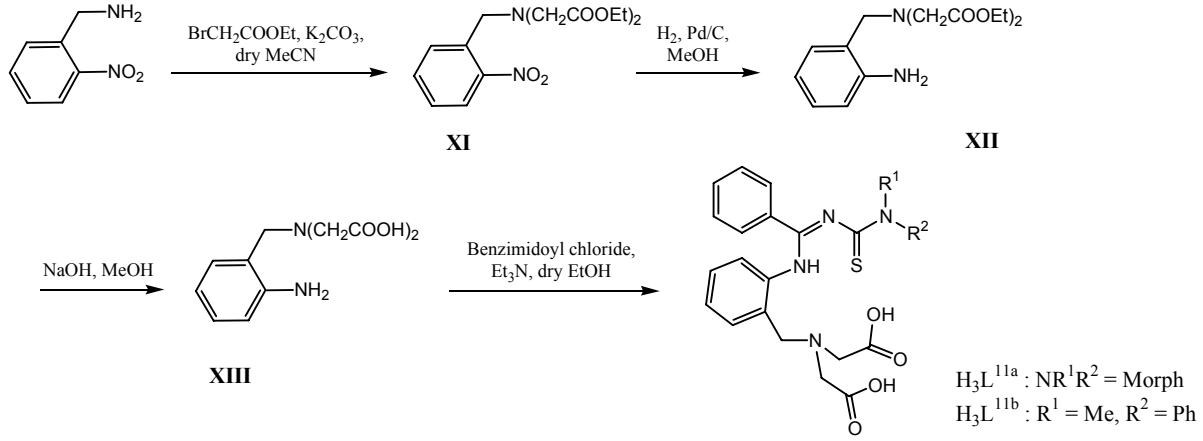

Scheme 3.36 The synthesis of the pentadentate ligand H_3L^{11}.

In the IR spectra of H_3L^{11}, ν_{OH} stretches of the free carboxylic groups show very broad, strong absorption bands in the region between 3500 cm^{-1} and 2500 cm^{-1}. Very strong absorptions around 1720 cm^{-1} are assigned to $\nu_{C=O}$ vibration bands which are overlapped with strong absorptions of $\nu_{C=N}$ stretches in the 1670 cm^{-1} region.

The ^1H NMR spectrum of H_3L^{11a} is characterized by two singlets at 3.89 and 3.95 ppm, which are assigned to the methylene protons of $\underline{CH_2}CO$ and $Ph\underline{CH_2}N$, respectively. The chemical shifts of protons belonging to the aminobenzylamine moiety are also found in the range from 6.7 ppm to 7.0 ppm. Broad singlets at 9.42 ppm and 11.46 ppm belong to NH and COOH resonances. The hindered rotation around the CS-NR^1R^2 bonds is also observed for H_3L^{11a} as well as H_3L^{11a}. Especially, in the case of H_3L^{11b}, which contains the asymmetric substituted residues R^1 and R^2, the hindered rotation results in the formation of E/Z isomers. The chemical shift exchange between them, however, is fast enough to obtain broadened signals.

3.3.2 Re^VO and Tc^VO Complexes with H_3L^{10}

The ligand H_3L^{10} reacts with $(NBu_4)[MOCl_4]$ (M = Tc, Re) precursors in MeOH with the addition of the supporting base Et_3N under formation of complexes of the composition

[MO(L^{10})] [M = Re (**45**), Tc (**46**)]. While the rhenium complex is slowly formed in refluxing methanol as a violet-purple powder, the technetium compound is readily precipitated from the reaction mixture at an ambient temperature as a green microcrystalline solid. The compounds **45** and **46** are very stable in the solid state and in solution. Interestingly, reactions of H_3L^{10} with different precursors (different cores and oxidation states) such as $[Re^{V}NCl_2(PPh_3)_2]$, $[Re^{V}(NPh)Cl_3(PPh_3)_2]$ or $[Re^{III}Cl_3(MeCN)(PPh_3)_2]$ under aerobic conditions, always end with the formation of complex **45**. This reveals that complexes of H_3L^{10} with the oxo core are much more thermodynamically stable than the corresponding complexes of $\{MN\}^{2+}$, $\{MNPh\}^{3+}$ or $\{M\}^{3+}$ (M = Re, Tc) cores.

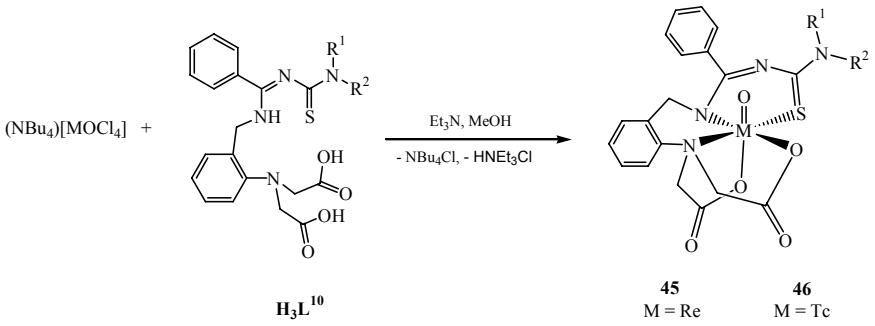

Scheme 3.37 Reactions of H_3L^{10} with $(NBu_4)[MOCl_4]$.

In the IR spectra of the complexes **45** and **46,** no absorptions in the region above 3100 cm^{-1} which correspond to ν_{N-H} and ν_{O-H} stretches in the free ligand are observed. This is a strong hint for the triply deprotonated ligand. While the $\nu_{C=O}$ bands of two nonequivalent carboxylate groups in **45** appear at 1720 cm^{-1} and 1666 cm^{-1}, the corresponding stretches in **46** reveal a broad band at 1715 cm^{-1}. The formation of a benzamidinate chelate, which is normally accompanied with a large delocalization of π electrons, is indicated by a strong bathochromical shift of the $\nu_{C=N}$ to the 1500 cm^{-1} region for both compounds. The medium absorption bands at 964 cm^{-1} and 951 cm^{-1} are assigned to the $\nu_{Re=O}$ and $\nu_{Tc=O}$ stretches, respectively. The ^{1}H NMR spectra of **45** and **46** in $CDCl_3$ show no signals of O-H or N-H protons. The spectra reflect the rigid arrangement around the tertiary nitrogen atoms of the (CS)-NEt_2 moieties, which results in magnetic nonequivalence of its four methylene protons. This is indicated by four separated signals with ABX_3 splitting patterns as previously mentioned. More important, the signals of the four methylene protons of N$\underline{CH_2}$CO appear in two pairs of doublets at 4.53/5.68 ppm, 4.83/5.06 ppm for **45** and 4.50/5.65 ppm, 4.85/5.08 ppm for **46** with typical geminal spin coupling constants (14.0 - 15.5 Hz). This observation indicates that the two carboxylates and the tertiary aromatic nitrogen atom coordinate to the metal centers to form two five-membered chelate rings. Two methylene protons in each ring

are magnetically not equivalent due to their up and down position with respect to the ring plane. Due to the dissociation of the protons of the neighbouring nitrogen atoms, the resonances of the methylene protons of the benzylamine groups are high-field shifted by about 0.8 ppm and appear as singlets at about 3.90 ppm. Interestingly, in the ^{1}H NMR spectrum of **45,** which is measured in DMSO-d_6, this singlet is splitted into two doublets at 4.10 ppm and 4.40 ppm (J = 18.2 Hz). This can only be explained by a restricted equilibrium between the chair and the boat conformations of the six-membered chelate ring in DMSO.

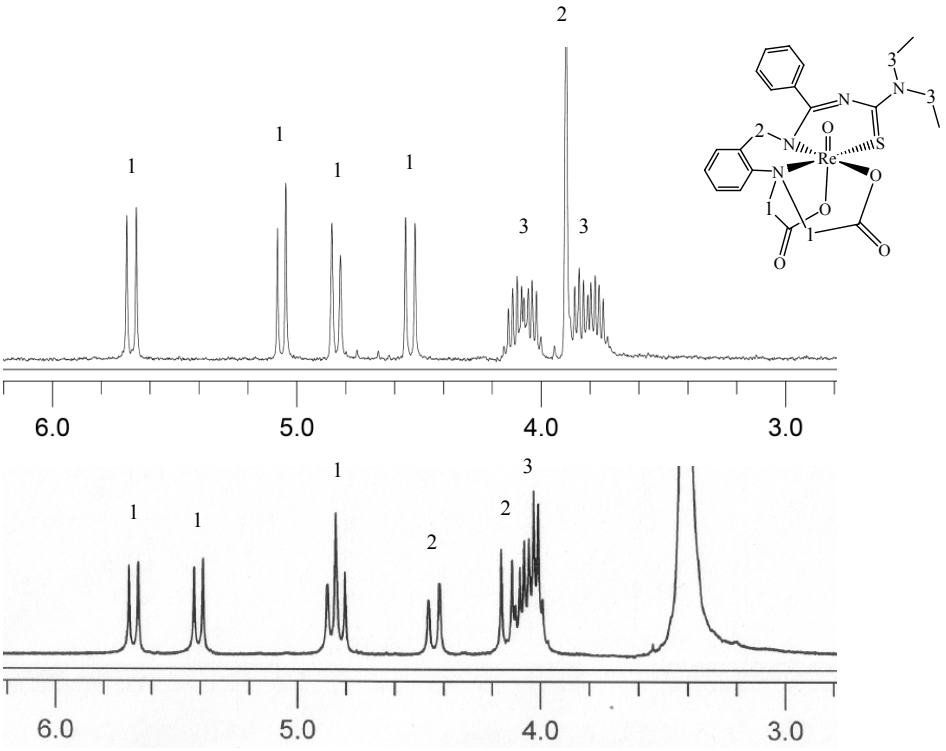

Figure 3.32 ^{1}H NMR Spectrum of [ReO(L^{10})] a: in $CDCl_3$, b: in DMSO-d_6

Single crystal X-ray diffraction of **45** and **46** confirm the conclusions drawn from spectroscopic studies. The molecular structure of **46** is depicted in Figure 3.33. The equivalent molecular structure of the rhenium complex **45** is not presented as an extra Figure. However, selected bond lengths and angles of both compounds are compared in Table 3.30. The metal atoms reveal a distorted octahedral coordination environment with terminal oxo ligands. The remaining five coordination positions are occupied by the donor atoms of $\{L^{10}\}^{3-}$. One carboxylate oxygen atom is in *trans* position to the oxo ligand. The distance from the metal atoms to the oxygen atoms *trans* to the oxo ligands is slightly shorter than the distances to the oxygen atoms in the equatorial planes. However, these distances fall in the range of rhenium-oxygen and technetium-oxygen single bonds found in some other carboxylate complexes [33,41]. The M-N bond to the tertiary nitrogen atoms N8 are longer by about 0.25 Å than those of M-N5. Nevertheless, the M-N5 bond lengths are in the same range of those in other

benzamidine complexes. The M-O10 bond lengths of 1.662(6) Å in **45** and 1.659(3) Å in **46** are in the expected range of rhenium-oxygen and technetium-oxygen double bonds.

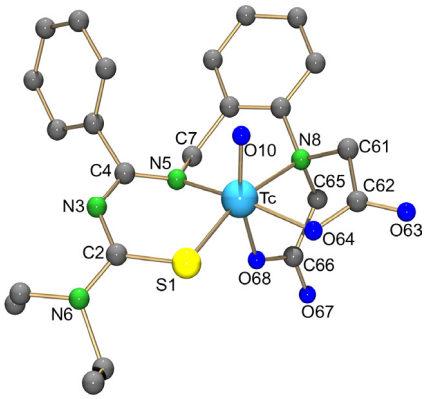

Figure 3.33 Molecular structure of [TcO(L^{10}) (**46**). Hydrogen atoms were omitted for clarity.

Table 3.30 Selected bond lengths and angles in [ReO(L^{10})] (**45**) and [TcO(L^{10})] (**46**)

	45	**46**		**45**	**46**
Bond lengths (Å)					
M–O10	1.662(6)	1.659(3)	S1–C2	1.75(1)	1.746(5)
M–S1	2.290(2)	2.296(1)	C4–N5	1.35(1)	1.349(6)
M–N5	2.022(7)	2.000(4)	C62–O63	1.22(1)	1.222(6)
M–N8	2.253(6)	2.253(4)	C62–O64	1.309(9)	1.285(6)
M–O64	2.078(6)	2.063(4)	C66–O67	1.20(1)	1.220(6)
M–O68	2.030(7)	2.031(3)	C66–O68	1.31(1)	1.292(6)
Angles (°)					
O10–M– S1	104.1(2)	104.5(1)	O10–M–O68	162.5(2)	162.4(1)
O10–M–N5	97.5(3)	97.0(1)	S1–M–N8	166.2(2)	165.5(1)
O10–M–N8	86.8(3)	87.2(1)	N5–M–O64	166.7(3)	167.8(1)
O10–M–O64	93.6(3)	93.7(1)	S1–M–N5	93.1(2)	92.8(1)

3.3.3 Rhenium Complexes with H_3L^{11}

3.3.3.1 $Re^{V}O$ Complexes with H_3L^{11a}

The ligand H_3L^{11a}, which is structurally similar to H_3L^{10}, reacts slowly with $(NBu_4)[ReOCl_4]$ in MeOH at ambient temperature and forms a red crystalline solid of the composition [ReO(L^{11a})] (**47a**) in high yields (Scheme 3.38). Addition of a supporting base such as Et_3N and heating the reaction mixture under reflux accelerates the reaction. The

product is well soluble in DMSO or DMF, but only less soluble in CH_2Cl_2 or $CHCl_3$ and almost insoluble in alcohols.

The IR spectrum of **47a** shows no absorption bands of OH or NH stretches which reflects the triply deprotonated form of the ligand. Additionally, the shift of the band corresponding to $\nu_{C=N}$ to 1535 cm^{-1} indicates the formation of a benzamidinate chelate ring. Two different absorptions of $\nu_{C=O}$ stretches are observed at 1713 cm^{-1} and 1696 cm^{-1}, which can be assigned to two nonequivalent carboxylate groups as previously obtained in the case of **45** and **46**.

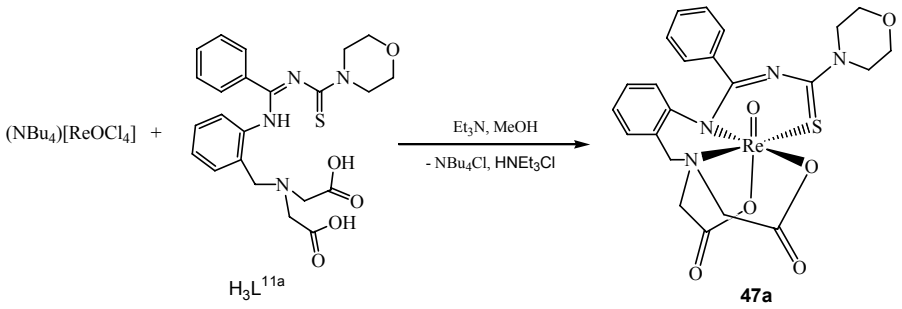

Scheme 3.38 Reaction of H_3L^{11a} with $(NBu_4)[ReOCl_4]$.

The ^1H NMR spectra of **47a** in $CDCl_3$ and DMSO have the same patterns which are characterized by three pairs of doublets with geminal coupling constants corresponding to the methylene protons of the chelate rings. While two $PhCH_2N$ protons resonate at 3.47 ppm and 3.71 ppm, the resonances of the four $COCH_2N$ protons appear in the range between 4.6 ppm to 5.6 ppm. The rigid structure of the morpholinyl residue is not clearly observed**.**

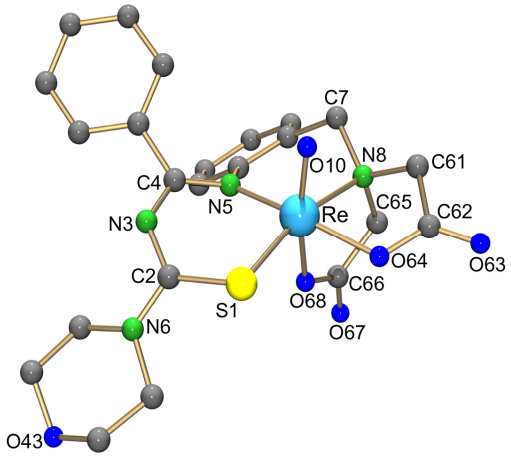

Figure 3.34 Molecular structure of $[ReO(L^{11a})]$ (**47a**). Hydrogen atoms are omitted for clarity.

Table 3.31 Selected bond lengths (Å) and angles (deg) in [ReOL^{11}] (**47a**)

Bond lengths (Å)					
Re–O10	1.672(7)	Re–O64	2.055(7)	C62–O63	1.20(1)
Re–S1	2.309(2)	Re–O68	2.040(7)	C62–O64	1.32(1)
Re–N5	2.037(8)	S1–C2	1.76(1)	C66–O67	1.22(1)
Re–N8	2.207(7)	C4–N5	1.35(1)	C66–O68	1.29(1)
Angles (°)					
O10–Re– S1	103.4(2)	O10–Re–O64	94.8(3)	N5–Re–O64	166.2(3)
O10–Re–N5	95.8(3)	O10–Re–O68	164.4(3)	S1–Re–N5	94.6(2)
O10–Re–N8	88.2(3)	S1–Re–N8	165.4(2)	N8–Re–N5	93.0(3)

X-ray quality single crystals of **47a** were obtained by slow evaporation of a CH_2Cl_2 – MeOH solution. Figure 3.34 depicts the molecular structure of **47a**. Selected bond lengths and angles are summarized in Table 3.31. The rhenium atom has adopted a distorted octahedral coordination environment, in which five positions in the coordination sphere are occupied by the donor atoms of the ligand $\{L^{11}\}^{3-}$ similarly to the above discussed compounds **45** and **46**, and the remaining position is occupied by a terminal oxo ligand. Again, the Re-O68 bond length, where O68 is *trans* to the oxo ligand, is slightly shorter than the Re-O64 distance, reflecting some transfer of electron density from the rhenium oxygen double bond to this bond. The most remarkable difference between the structures of **47a** and those of **45** and **46** is that the two phenyl rings in **47a** come closer to each other. This makes the six-memberred chelate ring belonging to aminobenzylamine unit more rigid and is the reason for the ^{1}H-NMR splitting pattern in this compound.

3.3.3.2 Re^V(NPh) Complexes with H_3L^{11}

Also the rhenium(V) phenylimido core, which is isoelectronic with the rhenium(V) oxo core, is expectedly stabilized by the H_3L^{11} chelator system. However, even reactions of H_3L^{11} with [Re(NPh)$Cl_3(PPh_3)_2$] in CH_2Cl_2 at room temperature with the addition of a supporting base result in side-products. Typically, such reaction mixtures form the phenylimido complex [Re(NPh)(L^{11})] (**48**) as the main product, but contain impurities of the oxo complex **47** and other (phosphine containing) side products. Heating the reaction mixture for a long period results in a complete hydrolysis of **48** and the formation of **47**. Nevertheless, pure complexes **48** can be isolated by chromatography on silica gel using $CHCl_3$ as elutant.

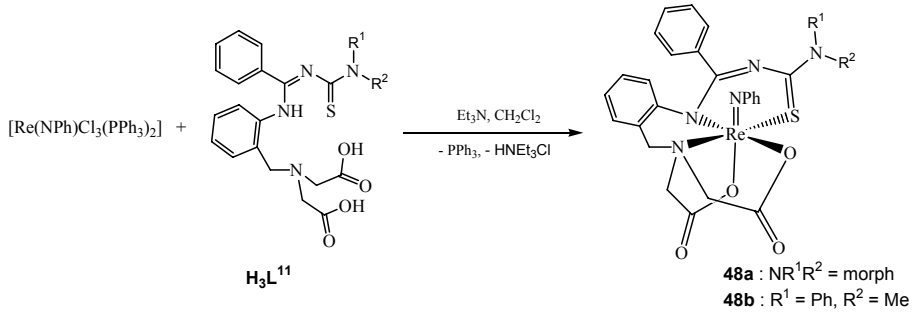

Scheme 3.39 Reactions of H_3L^{11} with $[Re(NPh)Cl_3(PPh_3)_2]$.

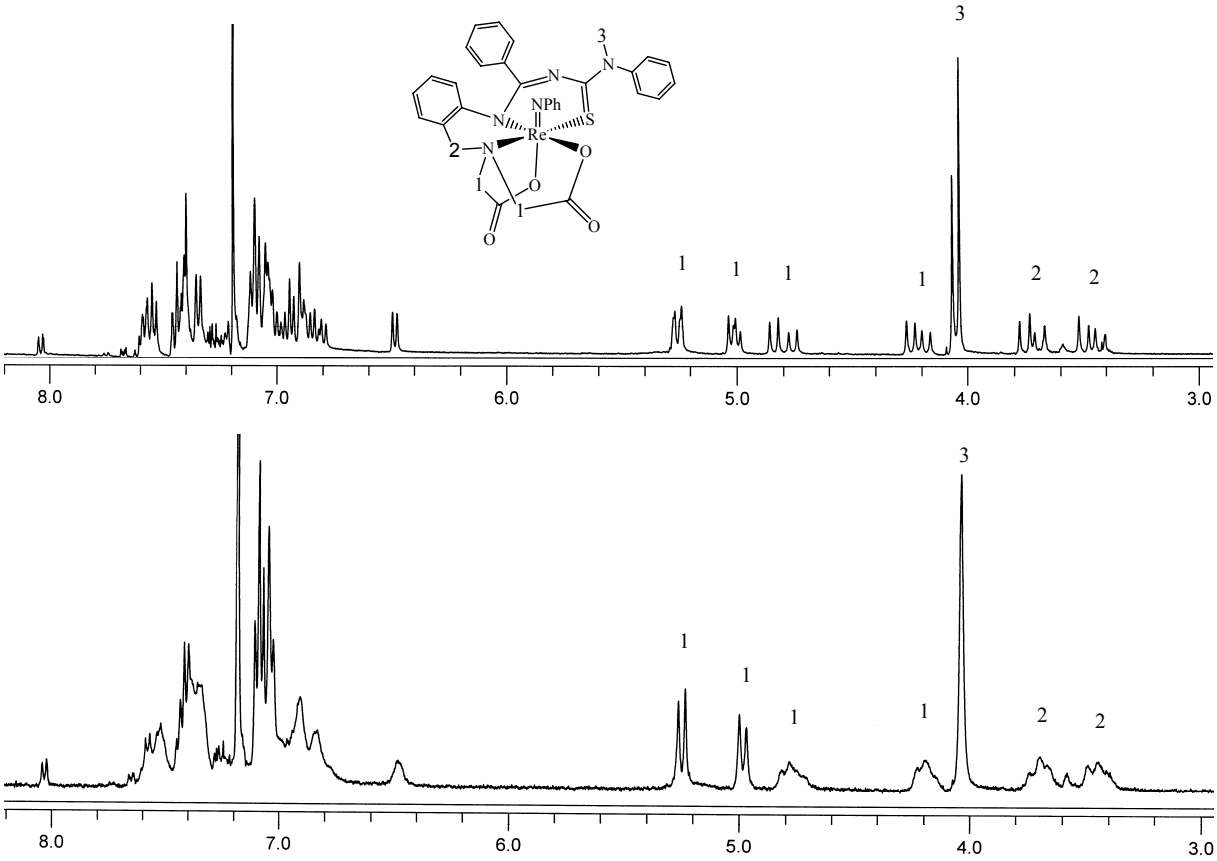

Figure3.35 ^{1}H NMR spectrum of [ReNPh(L^{11b})] (**48b**) in $CDCl_3$. a: at room temperature, b: at 50 ^{o}C.

The IR spectra of the compounds **48** are characterized by very strong, broad absorptions at 1700 cm^{-1} which are typically due to coordinated carboxylate groups. A strong bathochromic shift of the $\nu_{C=N}$ is also observed. The ^{1}H NMR spectrum of **48a** has principally the same pattern as that of **47a** except the additional aromatic signals, which come from the phenylimido ligand. In compound **48b**, which contains an asymmetric residue in the thiourea moiety, the hindered rotation around the MePhN-C bond leads to two E/Z isomers in solution. This is indicated by two sets of signals with the ratio of 0.55: 0.45 in the ^{1}H NMR spectrum of **48b** (measured in $CDCl_3$ at room temperature, Figure 3.35a). When the measurement is carried out at 50 ^{o}C, the rotation is much faster. Thus, only one set of signals some of which are broadened and less resolved can be observed (Figure 3.35b).

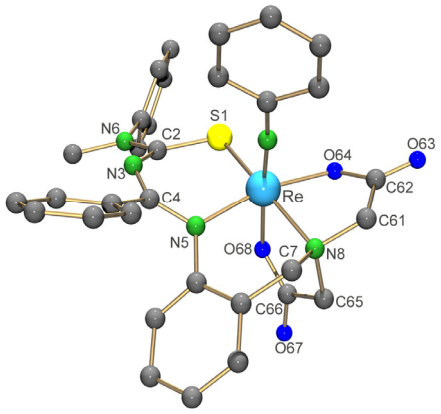

Figure 3.36 Molecular structure of [ReNPh(L^{11b}) (**48**). Hydrogen atoms are omitted for clarity.

Table 3.32 Selected bond lengths and angles in [Re(NPh)L^{11a}] (**48a**) and [Re(NPh)L^{11b}] (**48b**)

	48a	**48b**		**48a**	**48b**
Bond lengths (Å)					
Re–N10	1.69(1)	1.73(1)	Re–O64	2.090(7)	2.08(1)
Re–S1	2.339(3)	2.334(4)	Re–O68	2.03(1)	2.05(1)
Re–N5	2.05(1)	2.06(1)	S1–C2	1.73(1)	1.71(1)
Re–N8	2.16(1)	2.17(1)	C4–N5	1.34(1)	1.35(1)
Angles (°)					
N10–Re– S1	97.8(4)	98.6(4)	N10–Re–O68	168.6(4)	173.2(5)
N10–Re–N5	101.3(4)	95.1(6)	Re –N10–C71	167.3(9)	174.0(1)
N10–Re–N8	94.4(4)	94.5(5)	S1–Re–N8	165.1(3)	164.9(3)
N10–Re–O64	88.9(4)	95.2(5)	N5–Re–O64	166.2(4)	166.0(4)

Single crystals of **48** suitable for X-ray studies were obtained by slow evaporation of CH_2Cl_2/n-hexane mixtures. Figure 3.36 illustrates the molecular structure of **48b** as representative for this class of compounds. The analogous structure of **48a** is not shown in an extra Figure. Selected bond lengths and angles of both complexes are compared in Table 3.32. The structures reveal distorted octahedral environments around the rhenium atoms containing coordinated $\{L^{11}\}^{3-}$ as triply deprotonated, pentadentate ligands as is discussed for **47a**. The remaining positions in these octahedral spheres are occupied by phenylimido ligands which are *trans* to one of the carboxylate groups. The phenylimido ligands are almost linear with Re–N10–C61 angles in the range between 167 ° and 174 °. The Re-N10 bond lengths of 1.695 Å in **4a** and 1.727(12) Å **4b** are in the expected range of rhenium-nitrogen double bonds. The bonding situation inside the ligand $\{L^{11}\}^{3-}$ of the complexes **48** is generally similar to that of compound **47**.

3.3.4 Steps Toward Bioconjugation

One of the major challenges in both diagnostic and therapeutic radiopharmacy is to get a better control of the drug distribution. This means, to deliver the radioactive compound more efficiently to the target organs. A possible solution of this major problem is the development of a new generation of rhenium and technetium radiopharmaceuticals, in which a metal chelate couples to a bioactive molecule such as a receptor-binding organic compound or a protein via a spacer. This modern trend is called bifunctional (or bioconjugate) approach [10,107].

The labeling of such targeting molecules entails the question of a tight bonding of the metal center to the biologically active molecule without affecting its physiological properties. This means that the metal ion in its particular oxidation state needs to be stabilized and covalently linked to the vector. The connecting functionality to the biomolecule is commonly a carboxylate or an amine group that can conveniently be activated with standard strategies of organic chemistry. Labeling of the targeting molecules requires a chelator that is strong enough:

(i) to coordinate to technetium or rhenium at low concentrations

(ii) to give a single product in high yields

(iii) to stabilize the metal under *in vivo* conditions.

The chelator should form a biologically inactive metal complex. That means it must not influence the biological properties of the conjugate.

Most of the hitherto explored bioconjugated technetium and rhenium compounds base on tetradentate ligand systems with amine or amide nitrogen and thiolato sulphur atoms [108] or mixed-ligand approaches [109]. Pentadentate ligands, which can complete the octahedral coordination sphere around the metal oxo core and fully wrap the metallic centre, are expected to form more thermodynamically stable and kinetically inert complexes. However, due to difficulties in the synthesis of such types of chelators, no rhenium or technetium complexes containing pentadentate ligands have been previously introduced to a bifunctional labelling approach. In the following subsection, the potential of rhenium and technetium complexes with the pentadentate ligands of the type of H_3L^{10} for bioconjugation is discussed.

3.3.4.1 Modification of H_3L^{10}

For the use of ligands of the type H_3L^{10} or H_3L^{11} in bioconjugation, an additional anchor like a carboxylic or an amino group should be introduced to the periphery of the ligands. Generally, the ligand skeleton of H_3L^{10} can be modified at three different positions, at the phenyl group of the benzamidine, at the aromatic ring of aminobenzylamine or at the thiourea (CS)-NR^1R^2 moiety. The latter choice selection is the most convenient one and demonstrates the ready variation of the R^1, R^2 substituents which is mentioned in the previous sections. The desired pentadentate ligand H_3L^{10}-COOEt can be obtained by a multistep synthesis as is shown in Scheme 3.40. The synthesis of the benzoylthiourea **XV** and its nickel complex **XV**, which contains an ester group, was carried out similar to the standard procedure [15], except using the secondary amine **XIV** which was prepared from 4-aminobenzoic ethyl ester [110]. Due to the poor solubility of the nickel complex **XVI** in CCl_4, dry CH_2Cl_2 was used as the solvent for the synthesis of the corresponding benzimidoyl chloride **XVII**. The reaction of **XVII** with amine **X** was carried out in dry EtOH in the presence of Et_3N, which gave ligand H_3L^{10}-COOEt in high yields.

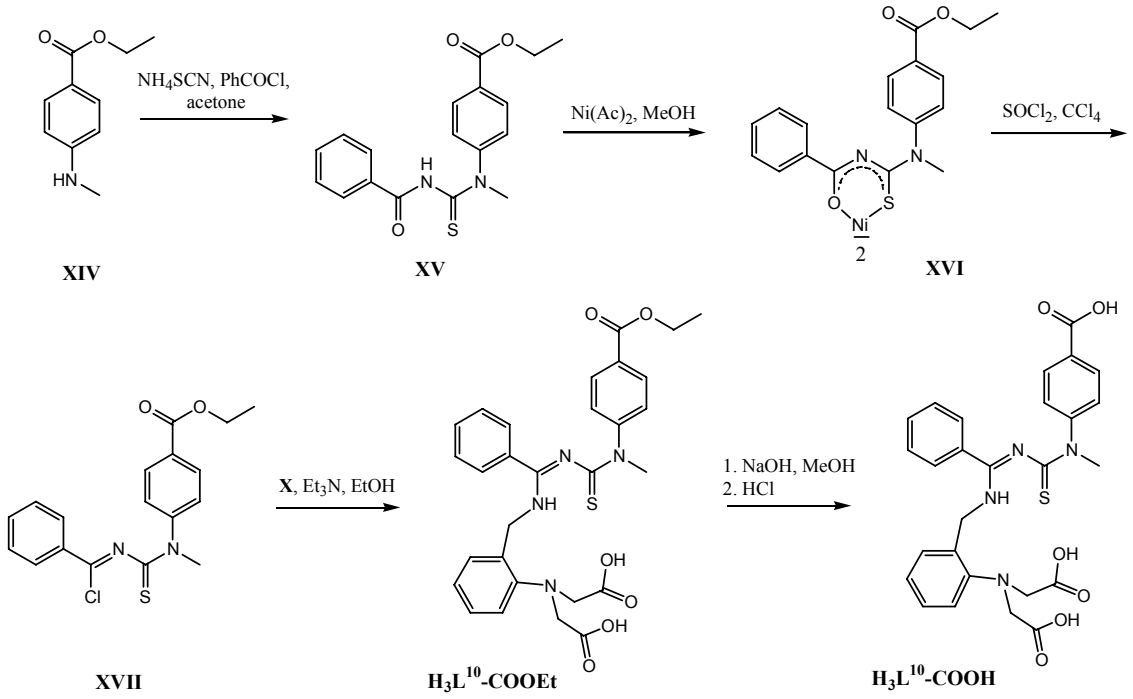

Scheme 3.40 The synthesis of H_3L^{10}-COOEt and H_3L^{10}-COOH.

The IR spectrum of H_3L^{10}-COOEt is characterized by a very broad strong absorption ranging from 3450 to 2500 cm^{-1} which is related to the carboxylic OH stretches. The $\nu_{C=O}$ stretches of protonated carboxylic acid groups appear as a broad strong band at 1713 cm^{-1}. Another strong absorption band at 1605 cm^{-1} is assigned to the $\nu_{C=N}$ vibration, which is typical

for benzamidine-type compounds. The ^{1}H NMR spectrum of H_3L^{10}-COOEt shows the expected signal pattern. A triplet at 1.41 ppm and a quartet at 4.37 ppm, respectively, belong to the resonances of the methyl and methylene protons of the ethyl ester. No hindered rotation effects, which are normally discussed for thiourea moieties, are observed. This is reflected by a sharp singlet at 3.56 ppm corresponding to the resonance of the N-Me protons. The signals corresponding to the methylene groups of N$\underline{CH_2}$CO and N$\underline{CH_2}$Ph are found as singlets at 3.83 ppm and 4.49 ppm, respectively. Two broad signals at 8.67 ppm and 12.13 ppm can be assigned to the NH and COOH resonances.

Hydrolysis of the ester H_3L^{10}-COOEt in an NaOH/MeOH solution gives the salt form $Na_3(L^{10}$-COO) which is subsequently treated with citric acid to obtain the acidic form H_3L^{10}-COOH of the ligand. The yield of the hydrolysis of H_3L^{10}-COOEt is almost quantitative and no side-reactions are detected. The IR spectrum of H_3L^{10}-COOH is similar to that discussed for H_3L^{10}-COOEt except a slight bathochromic shift of about 5 cm^{-1} for the absorption band of the C=O vibrations. In the ^{1}H NMR spectrum of H_3L^{10}-COOH, the absence of resonances of the ethyl ester group is observed. The other signals appear in the same region as those in the spectrum of H_3L^{10}-COOEt.

3.3.4.2 Re^{V}O and Tc^{V}O Complexes with H_3L^{10}-COOEt and H_3L^{10}-COOH

H_3L^{10}-COOEt readily reacts with $(NBu_4)[MOCl_4]$ (M = Re, Tc) precursors in refluxing MeOH with the addition of base under formation of a purple solid of the composition $[ReO(L^{10}$-COOEt)] (**49**) or the green technetium analogue $[TcO(L^{10}$-COOEt)] (**50**). Both compounds are isolated as pure crystalline solids in high yields. .

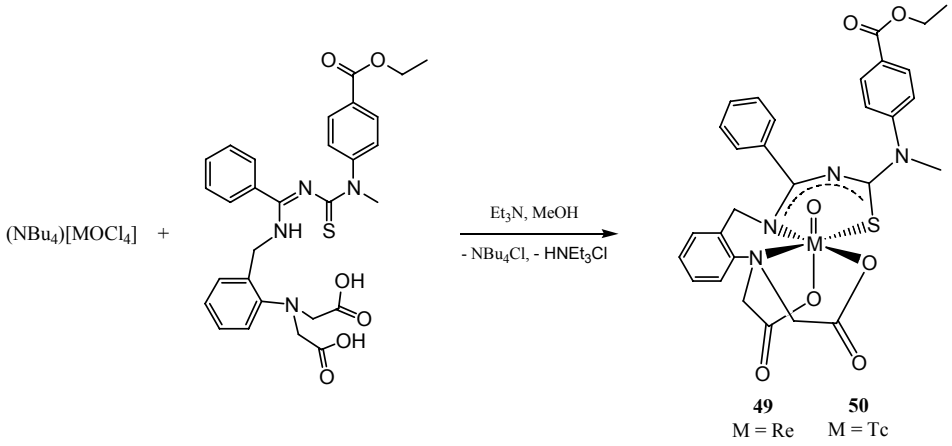

Scheme 3.41 Reactions of H_3L^{10}-COOEt with $(NBu_4)[MOCl_4]$

In the IR spectra of **49** and **50**, the absence of the broad strong absorptions of the OH vibrations confirms the coordination and the consequent deprotonation of the two carboxylic groups. The formation of benzamidine chelate rings is indicated by the strong bathochromatic shifts of the $\nu_{C=N}$ absorptions, which appear in the range between 1527 cm^{-1} and 1530 cm^{-1}. The absorption bands of the $\nu_{C=O}$ stretches are almost not shifted with respect to those in the uncoordinated ligand, but appear as two sharp peaks at 1717 and 1701 cm^{-1}. The better resolved $\nu_{C=O}$ absorptions may be a consequence of the strongly shifted $\nu_{C=N}$ band and the well defined, coordinated carboxylates. Medium absorption bands in the region of 980 cm^{-1} are assigned for $\nu_{Re=O}$ and $\nu_{Tc=O}$ vibrations. Like the ^{1}H NMR spectrum of the uncoordinated ligand, those of **49** and **50** do not reveal a hindered rotation around the (CS)-NMe(*p*-C_6H_4COOEt) bonds. This is indicated by only one set of well-resolved signals corresponding to protons of the NMe(*p*-C_6H_4COOEt) moiety. The absence of NH and COOH resonances suggests $\{L^{10}$-COOEt$\}^{3-}$ being coordinated as a triply deprotonated ligand. The coordination of the ligand $\{L^{10}$-COOEt$\}^{3-}$ in the expected fashion is also clearly confirmed by the appearance of six doublet signals with geminal coupling patterns belonging to the six methylene protons as previously discussed.

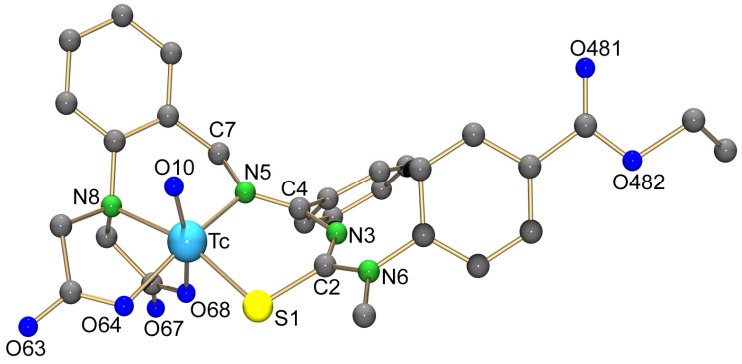

Figure 3.37 Molecular structure of [TcO(L^{10}-COOEt)] (**50**). Hydrogen atoms were omitted for clarity.

X-ray quality single crystals of **49** and **50** are obtained by recrystallization of the complexes from DMSO solutions. Figure 3.37 illustrates the molecular structure of **50**. The structure of the analogous rhenium complex is virtually the same and is not shown in an extra figure. Selected bond lengths and angles of both compounds are compared in Table 3.33. The metal atoms have adopted distorted octahedral environments, in which each one position is taken by a terminal oxo ligand and the five remaining positions are occupied by the donor atoms of $\{L^{10}$-COOEt$\}^{3-}$. The resulting molecular structures are very similar to those of **45** and **46** with minor differences in the substituted group of the thiourea moiety.

Table 3.33 Selected bond lengths and angles in of [MO(L^{10}-COOEt)] (**49** : M =Re, **50** : M =Tc)

	49	**50**		**49**	**50**
Bond lengths (Å)					
M–O10	1.651(8)	1.65(1)	M–O64	2.059(6)	2.05(1)
M–S1	2.294(2)	2.303(4)	M–O68	2.065(6)	2.08(1)
M–N5	2.047(7)	2.04(1)	S1–C2	1.76(1)	1.74(1)
M–N8	2.219(7)	2.25(1)	C4–N5	1.32(1)	1.34(1)
Angles (°)					
O10–M– S1	105.0(3)	105.2(4)	O10–M–O68	163.4(3)	162.4(4)
O10–M–N5	96.9(3)	97.4(5)	S1–M–N8	163.7(2)	163.7(3)
O10–M–N8	87.8(3)	87.8(5)	N5–M–O64	163.4(3)	163.2(5)
O10–M–O64	98.3(3)	98.6(5)	S1–M–N5	95.1(2)	94.7(3)

Like the H_3L^{10}-COOEt ligand, H_3L^{10}-COOH readily reacts with $(NBu_4)[ReOCl_4]$ in MeOH after addition of Et_3N. This is indicated by an immediate change of the color of the reaction mixture from which a violet solid of the composition [ReO(L^{10}-COOH)] (**51**) is isolated directly. The amount of base, which is added, must not exceed 3 eq of $(NBu_4)[ReOCl_4]$, in order to minimize the formation of the anion $[ReO(L^{13})]^-$ which is good soluble in MeOH. Many attempts to obtain good quality single crystals of **51** for an X-ray structure study have failed. However, the molecular structure of **51** is expected to be similar to that of **49** except the ethyl ester in **49** is replaced by a free carboxylic group. Obviously, this change can be proven by a spectroscopic analysis.

A very broad band between 3450 and 2500 cm^{-1} remains in the IR spectrum of **51,** but is much less intense than that of the uncoordinated ligand and confirms the existence of the free carboxylic group of the thiourea side. Besides the strong absorption band at 1705 cm^{-1} of the $\nu_{C=O}$ vibration in the coordinated carboxylate, an intense absorption at 1655 cm^{-1} is observed and can be assigned to the $\nu_{C=O}$ stretch of the free carboxylic group. The absorption related to $\nu_{C=N}$ of the benzamidine skeleton is strongly shifted and appears in the same region as in **49**. In compound **51**, the $\nu_{Re=O}$ stretch is observed at 984 cm^{-1}. The ^1H NMR spectra of **49** and **51** are compared in Figure 3.38. The ^1H NMR spectrum of **51** does not show the signals of the ethyl ester protons but reveals a broad signal at 13.24 ppm which is typical for OH protons of carboxylic groups. The other resonances of **51** have almost the same chemical shifts as those in **49**. This strongly confirms the analogous structures of the two compounds.

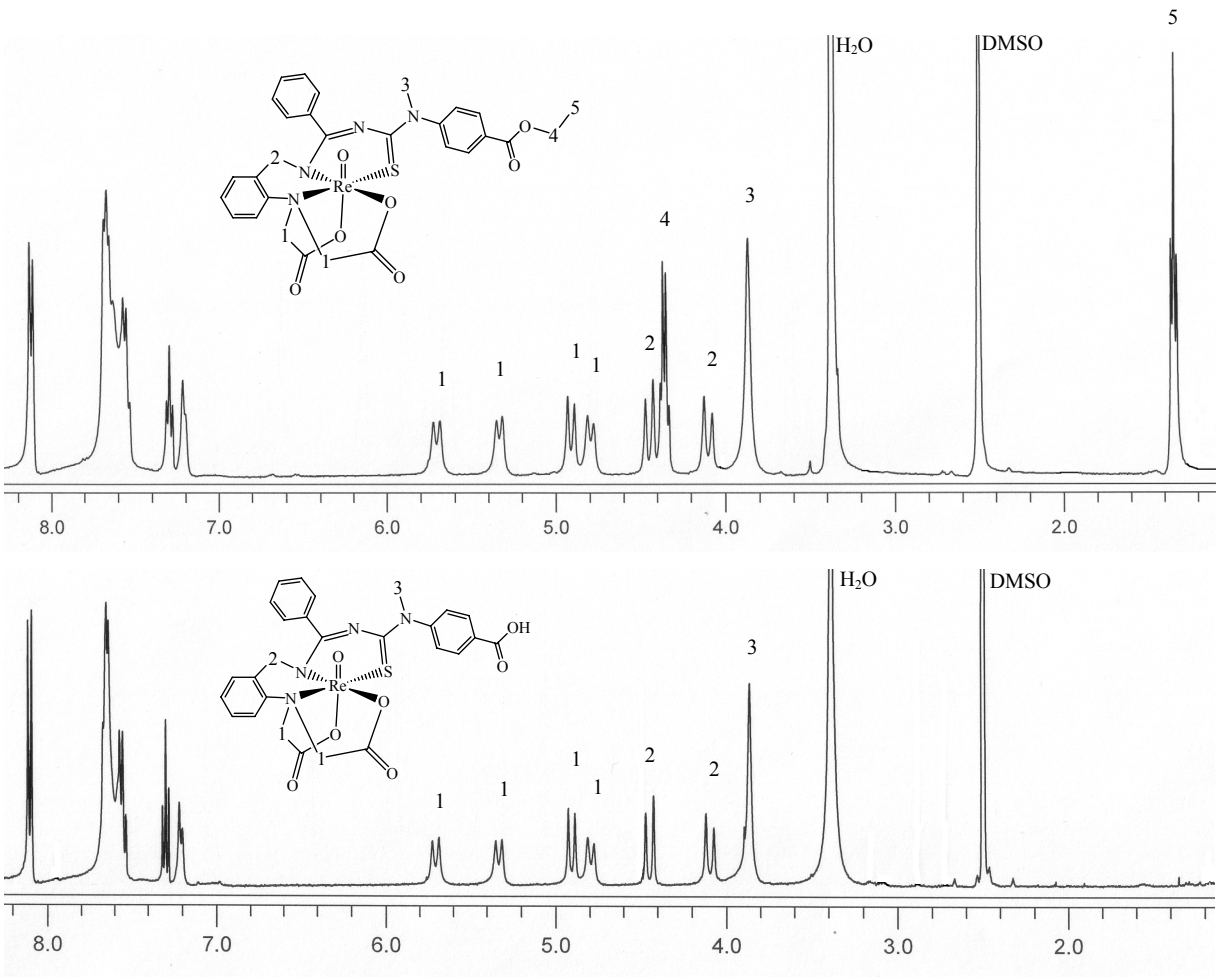

Figure 3.38 ^{1}H NMR spectrum of a: [ReO(L^{10}-COOEt)] (**49)** b: [ReO(L^{10}-COOH)] (**51**).

3.3.4.3 Bioconjugation with a Small Peptide

The additional carboxylic group in the periphery of ligand H_3L^{10}-COOH is intended to act as a linker in order to couple the complex to a peptide. For this purpose, we can consider two alternative routes. In the first approach, the free ligand is coupled to a targeting compound before being treated with a rhenium or technetium precursor. This approach is not recommended since no selective coupling at the carboxylic group of the thiourea moiety can be obtained. In the second approach, the metal complex **51** is firstly synthesized. In this case, the iminodiacetic moiety is blocked via the coordination bonds and the remaining carboxylic group can selectively react with peptides. Thus, the reaction of **51** with a small peptide such as triglycine ethyl ester was done in dry DMF at room temperature with the addition of a slightly excess of DCC (N,N'-dicyclohexylcarbodiimide) and HOBT (N-hydroxybenzotriazole) to give the coupling product [ReO(L^{10}-CON-TriGlyCOOEt)] (**52**) with yields of over 95%.

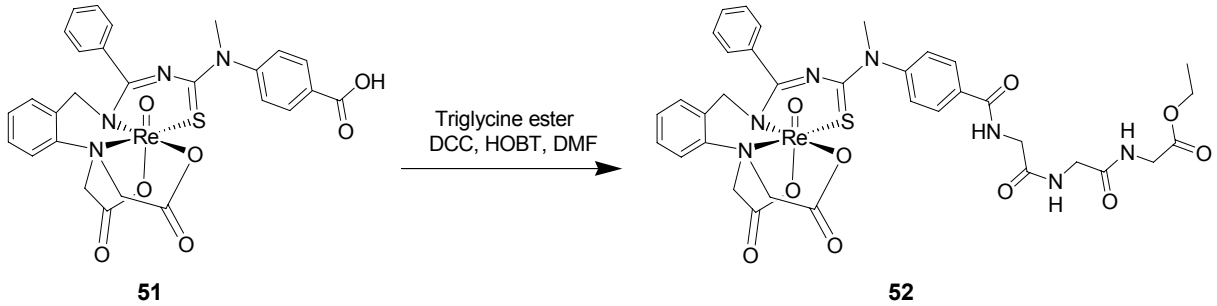

Scheme 3.42 Coupling reaction of [ReO(L^{10}-COOH)] (**51**) with triglycine ethyl ester.

Compound **52** is sparingly soluble in alcohol, CH_2Cl_2 or $CHCl_3$, but good soluble and stable in DMF or DMSO solutions. Good quality single crystals of **52** could not be obtained even after several attempts. Nevertheless, the structure of **52** is clearly proven by means of spectroscopic methods.

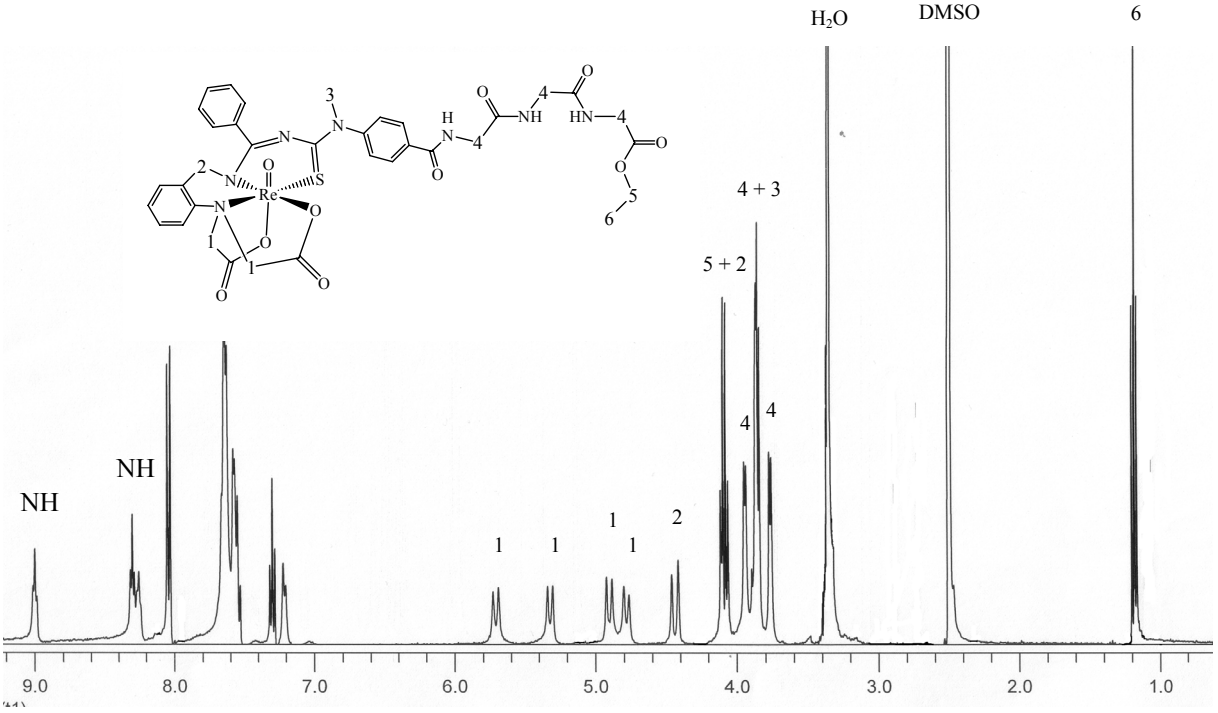

Figure3.39 ^{1}H NMR spectrum of [ReO(L^{10}-CON-TriGlyCOOEt)] (**52**).

The IR spectrum of **52** exhibits a strong absorption at 3325 cm^{-1} corresponding to the NH stretches of the triglycine residue. The absence of the broad strong OH band reflects the deprotonation of the carboxylic groups. The C=O stretches appear as a very broad strong band between 1600 cm^{-1} and 1750 cm^{-1}. While the absorption of the $\nu_{C=N}$ vibration is detected at the same position like in the IR spectrum of **51**, the absorption corresponding to $\nu_{Re=O}$ is bathochomically shifted by 5 cm^{-1}. The ^{1}H NMR spectrum of **52** additionally confirms the complex formation (Figure 3.39). The presence of the triglycine ethyl ester is characterized by

a triplet at 1.17 ppm and a quartet at 4.07 ppm belonging to ethyl ester protons, three doublets at 3.75 ppm, 3.84 ppm, and 3.93 ppm and three triplets at 8.24 ppm, 8.29 ppm, and 8.99 ppm correspond to the CH_2 and NH resonances, respectively. Moreover, the complex formation is clearly indicated by the presence of six doublets of CH_2 protons in the chelate ring which are presented at 4.06 ppm (overlapped with OCH_2 of the ethyl ester group), 4.43 ppm, 4.77 ppm, 4.89 ppm, 5.27 ppm and 5.71 ppm characterized by a geminal coupling pattern. The mass spectrum of **52** show only intense peaks at 956.2118 and 972.1876 corresponding to ions $[M + Na]^+$ (calcd., 956.1699) and $[M + K]^+$ (calcd., 972.1439).

3.3.5 Summary and Conclusions

The pentadentate thiocarbonylbenzamidines H_3L^{10} and H_3L^{11} are very suitable chelator systems to form thermodynamically stable complexes with oxo as well as phenylimido rhenium(V) and technetium(V) cores. In all complexes, the metal cores exhibit octahedral coordination spheres and are completely wrapped by the organic ligands.

Moreover, H_3L^{10} can be modified by the use of benzimidoyl chloride **XII,** which gives ligand H_3L^{10}-COOEt. The compound H_3L^{10}-COOEt was hydrolyzed to form a bifunctional ligand such as H_3L^{10}-COOH which subsequently reacts with $(NBu_4)[ReOCl_4]$ under formation of the complex $[ReO(L^{10}\text{-}COOH)]$ (**51**) in high yield. Compound **51** can be successfully labeled by a small peptide (triglycine ethyl ester).